Novel Dry Particle Layering for Drug Delivery to the Lungs

OLAITAN OLUWAYEMISI ABIONA

Doctor of Philosophy

ASTON UNIVERSITY

September 2021

Aston University

Novel Dry Particle Layering for Drug Delivery to the Lungs

Olaitan Oluwayemisi Abiona

Doctor of Philosophy

Thesis Summary

Formulation of dry powder based delivery system using existing technologies such as high shear blending and TURBULA® mixing lacks predictability, scalability and involves extensive trial and improvement to achieve uniform powder blends. This challenge is compounded when dealing with drugs that are heat and moisture sensitive, fracture during blending, which requires extensive modifications such as temperature jackets and product quarantine respectively. Following the successful development of a novel aerosolized and isothermal dry particle coating device (iDPC) for the formation of composite particles by a previous work in this research group, this work aimed to develop a mechanistic understanding of the iDPC and explore its use in the formulation of dry powders for inhalation. There are three main sub-divisions in this work; the mechanistic understanding of the novel iDPC device, to develop a scientific rationale for its processes, determination of changes to carrier surface properties by particle surface characterisation techniques, and a Quality by design approach based on the mechanistic understanding obtained to develop dry powders for inhalation for pulmonary drug delivery.

The capability of the novel iDPC device to produce composite particles were directly linked to its centrifugal force and micro fluidization technique, which provide the blending energy input. The stages of dry particle coating as already established in literature i.e. deagglomeration, dispersion and redistribution were identified in the novel iDPC device along with the periods at which they commence. The use of the micro fluidization technique was found to hasten these processes, although they still occurred in its absence.

Carrier particle properties such as particle size, powder flow, thermal and surface properties, determined by a range of characterisation techniques such as laser diffraction, FFC, SEM, CLSM, BET SSA, DSC, XRD and IGC show that most carrier properties are retained post-processing in the iDPC. Changes in surface energy were observed especially when different inert gases were used to achieve micro fluidization. The observed changes particularly in the acid-base component of the surface energy was attributed to changes in the orientation of lactose water of crystallisation post blending. More evidence to support this was later obtained.

The established method of incorporating fine lactose to a coarse lactose based DPI formulation was investigated using the iDPC. Similar to optimal fines concentration of 10% reported in literature, the addition of 9.4% fine lactose was optimal to DPI formulation performance. In the same chapter, the possibility of a fines-free formulation with the added advantage of better flow, which is beneficial for formulation preparation, handling and dosing, was also explored, through pre-conditioning the lactose carrier in the iDPC. This approach also increased FPF although, to a lesser extent than the fines-coarse carrier system.

Surface interaction dynamics were determined through surface energy measurements of the lactose carrier, using inert gases of different densities i.e. helium, nitrogen and argon to generate the air blade for micro fluidization. Processing induced differences especially in the specific surface energy component of lactose surface energetics were revealed. Reduced acid-base surface energy observed was attributed to possible reorientation of the molecules of lactose water of crystallisation, increasing interaction between polar probes and particle

surface, and resulting in increased polar surface energy, corroborating findings from chapter 3.

In conclusion, the findings from this work is an advancement towards using scientific rationale of dry coating device mechanistic understanding, a quality by design approach and carrier selection to leverage particle interaction dynamics for early formulation prediction of product performance.

Key words: *Isothermal dry particle coating (iDPC) device, mechanistic understanding, quality by design, dry powders for inhalation*.

Dedication

To the memory of my dad, thank you for all you did for us while you were here

To my mum, for all your sacrifices over the years

To my siblings, for being the best support system

To my husband, for the joy that sharing our lives bring

To my daughter, for being my daughter

Acknowledgements

I would first like to thank God for seeing me through my PhD journey, I would never have been able to do it without You Lord, thank you for fulfilling your word.

I would like to deeply appreciate my supervisor Professor Afzal Mohammed, for the opportunity to do this PhD, and for the opportunity to work with Aston Particle Technologies during the course of my PhD. His enthusiasm for this work, and his understanding, support and confidence in me helped me to successfully complete my PhD. I could not have asked for a better supervisor. I would also like to thank my associate supervisor Dr Ali Al-Kahttawi for his support.

I would like to thank Dr David Wyatt and Jasdip Koner for always willing to give advice, suggestions and feedback on my work, I appreciate your time. Also, I would like to thank Shital Lungare and Rhys Jones for helping out with laboratory instrumentation whenever necessary. I also would like to thank my colleagues and technical staff in the MB328 research laboratory.

I would like to use this opportunity to acknowledge Aston University for their financial support towards my PhD.

To my husband, Omotayo, thank you so much for always being there to encourage, support, cheer and pray with me throughout this journey. You are the best and I love and appreciate you dearly. To my daughter, Olivia EriifeOluwa, I cannot describe the joy that you have brought to my life, thank you for coming at this time and for being such an amazing child.

To my mum, you have been such a pillar of support in every way, words fail me to express the depth of my appreciation to you mum, I am grateful to God for blessing me and my siblings with you.

To my siblings, your faith in me is part of what has brought me this far, thank you for believing in me and supporting my dreams, I do not take you all for granted, you are the best siblings I could ever have, and this PhD is for “us”.

List of contents

List of Abbreviations

ACI	Anderson Cascade Impactor
AFM	Atomic force microscopy
ANOVA	Analysis of variance
API	Active pharmaceutical ingredient
CFC	Chlorofluorocarbon
CLSM	Confocal laser scanning microscopy
COPD	Chronic obstructive pulmonary disease
DoE	Design of experiments
DPI	Dry powder inhaler
DSC	Differential scanning calorimetry
FCA	Force control agent
FP	Fluticasone propionate
G-force	Centrifugal force
ICH	International Counsel of Harmonisation
iDPC	Isothermal dry particle coating
IGC	Inverse gas chromatography
IGL	Inhalation grade lactose
MgSt	Magnesium stearate
MMAD	Mass median aerodynamic diameter
NGI	Next generation impactor
PMDI	Pressurised metered dose inhaler
QbD	Quality by design
SEM	Scanning electron microscopy
USP	United States Pharmacopoeia
VMD	Volume mean diameter
αLM	Alpha – lactose monohydrate

List of tables

List of figures

1. Chapter One

Introduction and Literature review

1.1 Pulmonary drug delivery

Pulmonary drug delivery has been used to deliver drugs for local action, in the treatment of pulmonary diseases such as asthma, chronic obstructive pulmonary disease (COPD), lung cancer and cystic fibrosis through direct drug administration to the site of drug action. Targeted drug delivery to the site of action, lowers the effective dose required, reduces systemic side effects and resultant adverse drug reactions. Drugs meant for systemic action have also been delivered through the pulmonary route, by leveraging the rich blood supply to the lungs, high permeability and its large surface area for high absorption. The ability of the pulmonary route to evade first pass metabolism and absorption limitations in the gastrointestinal tract (GIT) particularly makes it a valid non-invasive alternative for administration of drugs with limited oral bioavailability (Hoppentocht et al., 2014, Pilcer and Amighi, 2010, Sou and Bergström, 2021).

1.2 Dry Powder Inhalers

Dry powder inhalers (DPIs) are devices that deliver dry powder formulations to the lungs for either local or systemic action (Islam and Gladki, 2008). They are the most recent devices developed for pulmonary drug delivery, after nebulisers and pressured metered dose inhalers (pMDIs). Although pMDIS are still the most commonly used, DPIs are fast gaining more popularity due to their advantages. Particularly, the absence in DPIs of propellants such as CFCs, which are used in pMDIs. The environmental implications of CFCs is causing a gradual but inevitable move from pMDIs to DPIs. In addition, DPIs have the added advantages of formulation stability, better API deposition in the lungs, and the ability for breath actuation of the device, which eliminates the need for patient – device coordination (Pilcer and Amighi, 2010, Labiris and Dolovich, 2003).

1.2.1 Dry Powder Inhaler formulations

Micron sized particles between 1 – 5 microns are required for adequate drug delivery to the lungs. Micronisation, a top bottom approach is used to reduce drug particle size to the desired range. However, as particle size is reduced, the particle weight becomes less than the inter-particulate force between them. This results in a high inter-particulate force/weight ratio i.e. bond number which causes cohesion. The high bond number and drag force (i.e. air resistance / force opposing particle motion), resist particle motion in bulk powder and cause such fine particles to form agglomerates and consequently flow poorly. The resulting cohesiveness makes it difficult to handle and formulate fine particles (Castellanos, 2005, Yang et al., 2005). Coarse carrier particles with mean particle size between 50μm -150μm are used to improve formulation, handling, flow and dispersion of the micronized API. During formulation, the drug particles attach to the surface of the carrier in an interactive mixture, but the API particles are expected to detach from the carrier upon aerosolization and then be effectively dispersed to reach the deep region of the lungs (Pilcer et al., 2012). The pulmonary route is most commonly used to deliver very potent medications that require very small doses, up to a few micrograms. The predominant limitation in formulating more medicines for pulmonary delivery is due to the higher dose that may be required for instance in the case of antibiotics. Formulating higher doses implies that a larger quantity of the API powders will be needed. This will potentially complicate the formulation process, since the influence of the physico-chemical drug properties on the behaviour of the powder blend will increase with the dose of the API required (Hoppentocht et al., 2014).

Figure 1.1 shows an illustration of a carrier – based DPI formulation, where the API and carrier are blended in an interactive mixture, but just strong enough that the API is able to detach from the carrier during aerosolization to release the API.

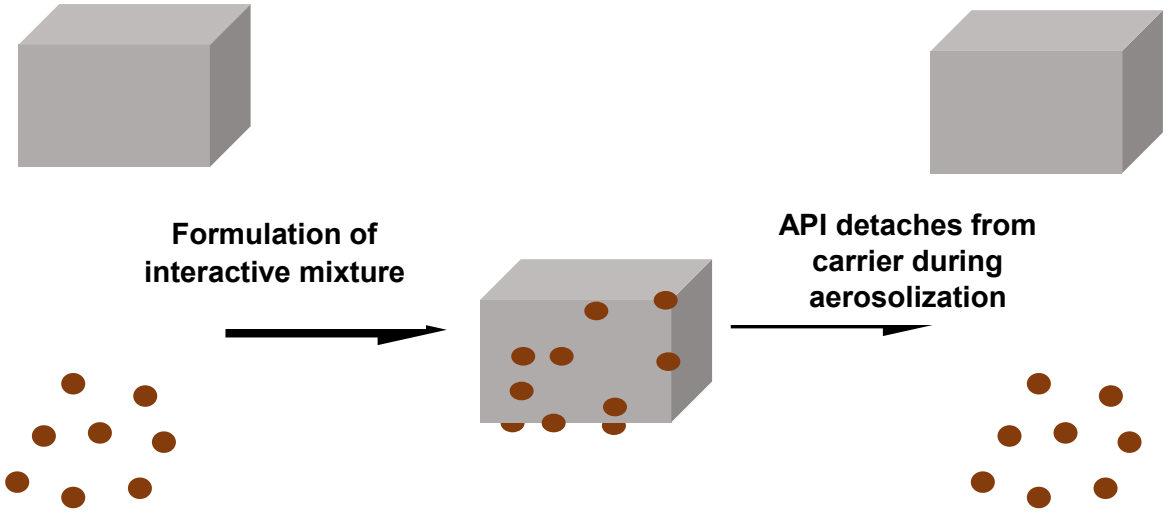

Figure 1.1 Figure illustrating the attachment of API to carrier surface in an interactive mixture during DPI formulation. API and carrier are blended in an interactive mixture, but just strong enough that the API detaches from the carrier during aerosolization to release the API.

Dry powder inhaler formulations are designed to facilitate delivery of powder-based therapeutic agents to the lungs. They are formulated as either loose clusters (carrier –free) comprising only the active pharmaceutical ingredient (API) or as a carrier – based formulation (Islam and Gladki, 2008, Daniher and Zhu, 2008). This work focuses on carrier – based DPI formulations, which generally comprise an interactive mixture of an API and a carrier, delivered through an appropriate passive inhalation device. In such carrier-based DPI formulations, since the carrier is often the main component, the aerosol performance of the formulation is largely dependent on the carrier characteristics such as particle size distribution, shape and surface properties. Therefore, carrier selection is crucial in determining the aerosolization of the drug particles and their presentation for drug deposition in the lungs, due to interparticulate forces between carrier and the respirable particles themselves (Peng et al., 2016). Alpha lactose monohydrate (αLM) is the most commonly used carrier in DPI formulation due to its ready availability, proven safety in inhalation products, its physicochemical properties, broad

compatibility with most APIs, its stability and easy clearance from the body (Pilcer and Amighi, 2010).

1.3 Lactose and its properties

Lactose is a disaccharide comprising galactose and glucose linked by a 1-4-glycosidic bond. It exists in both crystalline and amorphous forms. Crystalline lactose can be prepared either as Alpha-(α) lactose monohydrate (O-β-D-galactopyranosyl-(1-4)-α-D-glucopyranose) or anhydrous beta- (β) lactose (O-β-D-galactopyranosyl-(1-4)-β-D-glucopyranose), which contains about 70-80% anhydrous β-lactose and 20-30% anhydrous α-lactose depending on the temperature of crystallization (Rowe et al., 2009).

Alpha lactose monohydrate is prepared by crystallizing a supersaturated solution of lactose at temperatures below 93.5^0C. The predominant crystalline shape depends on the conditions of crystallization, with prisms, pyramids and tomahawk shapes being the most common ones (Gänzle et al., 2008).

β-anhydrous lactose is a reducing sugar prepared by crystallizing at temperatures above 93.5^0C. Unlike α-lactose monohydrate, which is more thermodynamically stable, β-anhydrous lactose has a tendency for moisture uptake and reaction with primary and secondary amines when stored under conditions of high temperature and relative humidity. Due to mutarotation of one anomer to the other, both α and β crystal forms of lactose coexist in equilibrium in solution regardless of the crystal form that is used in preparing the solution (Ganzle et al., 2008; Rowe et al., 2009).

Amorphous lactose, which is the most reactive form of lactose, is produced when a solution of lactose is dried rapidly such that crystallization cannot occur. It contains equal amounts of α and β lactose and is more readily reactive with primary and secondary amines than the crystalline forms (Ganzle et al., 2008; Rowe et al., 2009).

Anomeric variations and differences in moisture content may critically impact interacting surfaces. In fact, a study by Traini et al., (2008) shows significant variations in the aerosolization performance of different polymorphic forms of lactose of similar size fraction.

The observed difference in aerosolization performance was attributed to the differences in surface chemistry of the different forms of lactose, which influenced their surface free energies and adhesion behaviour with salbutamol sulphate.

1.3.1 Inhalation grade lactose

Inhalation grade lactose (IGL) could be either α-lactose monohydrate or anhydrous β-lactose. It is usually prepared from pharmaceutical grade lactose under stricter manufacturing conditions for its specific application. Spray drying is also used to produce inhalation grade lactose, spray-dried lactose contains up to 20% amorphous lactose. Although the amount of lactose ingested from a DPI formulation is safe in lactose intolerant people, contamination with milk protein can cause anaphylactic reactions in those who have severe milk allergies. Hence, to eliminate the risk of anaphylaxis, IGL is subjected to broader microbiology specifications compared to other grades, such as endotoxin levels (Nowak-Wegrzyn et al., 2004, Pilcer and Amighi, 2010, Rowe et al., 2009)

Different particle size fractions are generated by milling, sieving or air classification depending on specific requirements. These different production and processing methods coupled with batch-to-batch variation contribute to the history of the lactose particles. This history informs the lactose surface properties, most importantly its surface energetics, which influences particle-particle interactions with different APIs and ultimately affect DPI formulation performance. The size and morphology of α-lactose monohydrate crystals have been shown to vary based on the level of supersaturation of the solution used in the preparation (Parimaladevi and Srinivasan, 2014). In addition, several studies reveal the effects of batch and technological variations on lactose surface properties. Patera et al. (2012) studied the surface energies of α- lactose monohydrate, produced by milling and sieving and spray-dried amorphous lactose, both sourced from two different manufacturers. The results showed significant differences in surface energy for the same type of lactose from different manufacturers. Newell et al. (2001) also studied the difference in surface energies of crystalline lactose, spray-dried lactose, milled lactose and a 99:1 physical mixture of crystalline

and amorphous lactose. In addition to significant differences in surface energy values based on the grade of lactose, there was also a wide variation in the surface energy values of amorphous spray-dried lactose of the same batch, which was attributed to different surface orientations of the lactose molecules in the amorphous grade. In addition, Ticehurst et al. (1996) found that four batches of α-lactose monohydrate obtained from the same source exhibited different specific surface energy and different processing performance, which was attributed to variations in crystallinity or purity. Therefore, the presence of amorphous regions, surface impurities and the composite nature of the different lactose grades means that there are continuous inconsistencies to handle with lactose carriers.

Furthermore, some studies show the resultant effects of variations in lactose properties on DPI formulation performance. In a study carried out by Steckel et al. (2004) IGL was prepared from five different batches of the same grade of lactose (Lactochem® crystals), which varied in mean diameter, and had agglomerate and fines content more than usually present in batch-to-batch variations. They found significant differences in the efficacy of DPI formulations produced using IGL obtained from the different batches of Lactochem®, especially in DPI formulation blends containing low API concentration. Likewise, Larhrib et al. (1999) examined the effects of using five different lactose grades with similar VMD and found substantial differences in the efficiency of delivery of salbutamol sulphate from DPI formulations prepared using the different lactose carriers. In addition, Pitchayajittipong et al. (2010) report an increase in fine particle dose as fluidization energy of the lactose carrier used increases. Therefore, the preparation history determines the surface properties of the lactose particles and most importantly the surface energetics, which influence particle-particle interactions between the carrier particles themselves and any respirable API particles, ultimately affecting the performance of the DPI formulation. Despite the significance of carriers in DPI formulation performance, relatively little work has been reported on the use of having a readily measurable carrier particle property that will be useful in optimising and predicting DPI formulation performance through experimental design.

1.4 Lactose – based DPI formulations

1.4.1 Challenges associated with carrier (lactose) – based DPI formulations

Micronized APIs are notoriously difficult to handle due to their cohesive force, which is usually greater than the dispersion force generated during aerosolization (Nokhodchi and Martin, 2015). For this reason the use of carriers generally in DPI formulation eases pharmaceutical handling, formulation and production of the micro fine particles of the active materials. The use of carriers is however not a panacea. Indeed, DPI formulation carriers affect the delivery of APIs to the lungs, as incomplete detachment from carrier particles leads to sub-optimal delivery of administered drugs (Daniher and Zhu, 2008). It is also important to have a balance between the drug-carrier adhesion and the force needed for deaggregation, such that the API-carrier system does not separate during handling, dispensing and transportation, and still allow optimal separation of API from carrier during aerosolization (de Boer et al., 2012).

Complete detachment of drug from carrier, which is difficult to achieve, would be required to maximise the formulation performance. Ultimately, the detachment of API is dependent on the cohesive-adhesive balance of the drug-carrier mixture, which determines the strength of the interactive mixture and ease of drug detachment from carrier when required (Begat et al., 2004, Hooton et al., 2006, Jones et al., 2008, Mangal et al., 2016).

The predominant physical forces on particle surface are Van der Waal's interaction, electrostatic force from charge separation, capillary forces determined primarily by environmental moisture and forces associated with mechanical interlocking. These forces control the interaction between the drug and carrier particles. Van der Waal's interactions is a result of transient dipolar attraction between the surfaces of the particles, when they are in close proximity to each other. Capillary forces occur due to the formation of condensed vapour at the interface of two lyophilic particles that are in contact with each other, electrostatic attractive interactions occur when two oppositely charged particles encounter each other, while mechanical interlocking can result from lock and key conformation between particles due to surface irregularities (Pilcer et al., 2012, Zeng et al., 2000).

Since the interaction between drug particles and lactose particles are based on surface forces, the physicochemical and surface properties of lactose are capable of influencing this interaction. For example, the conditions of manufacturing process such as temperature of crystallization, absolute concentration of supersaturated lactose solution, presence of impurities, nucleation event(s) and cooling profile all influence the size, shape, surface amorphous content and energy distribution of the lactose carrier (Paterson, 2017, Pilcer et al., 2012). The rugosity (surface roughness or surface smoothness) and shape of lactose particles influence the surface area of contact for particle interaction and the strength of adhesion force between the drug and carrier particles. Similarly, the surface characteristics of the lactose carrier used will also affect compatibility with API and the stability of DPI formulation (Traini et al., 2012, Pilcer et al., 2012, Kou et al., 2012). Active pharmaceutical ingredients delivered by DPIs are often highly potent and must be delivered in very low quantity hence, the carrier makes up the bulk of the formulation. The carrier properties are therefore critical to the overall DPI formulation performance, and any change in carrier properties will have a pronounced effect on the delivery of the API (Zeng et al., 1998, Peng et al., 2016). Due to these variations, with resultant differing physicochemical properties of the carrier, for guided carrier selection and optimal DPI performance, it has been important to study the effects of different carrier properties on DPI performance. Specific lactose properties such as size, shape, and surface morphology have been investigated extensively, and their effects on DPI formulation performance are summarised in section 1.5. However, the interactive effects of carrier properties on DPI formulation performance make it difficult to establish a direct cause and effect relationship between a single carrier property and its effect on the performance of a DPI formulation. Alpha lactose monohydrate remains the most widely used carrier for DPI formulations. The physicochemical properties of α-lactose monohydrate particles, such as particle size, shape and solid form, are profoundly influenced by the method of production. Therefore, wide variations in these properties are inevitable. In this chapter, the role of surface energetics in the optimisation of dry powder inhaler formulations is considered in lactose carrier selection. Several useful lactose particle modification methods are discussed as well

as the use of fine lactose and of force control agents in DPI formulation development. It is concluded that where these have been investigated, the empirical nature of the studies, do not permit early formulation prediction of product performance; but only allow the evaluation of the final formulation quality. The potential to leverage particle interaction dynamics through the use of experimental design utilising quantifiable lactose particle properties, critical quality attributes is explored particularly in respect of when a Quality by Design (QbD) approach has been used in optimisation.

1.4.2 Mechanisms of API detachment from carrier

Given the difficulty of studying the effect of lactose physicochemical properties in isolation, it is important to consider how several factors may simultaneously affect API aerosolization. There are two major mechanisms by which API particles are believed to detach from carrier particles, viz: detachment by airflow stream or fluid forces and detachment by transfer of momentum caused by impaction when carrier particles collide with the inhaler or capsule wall (Donovan and Smyth, 2010).

Airflow stream is generated when the powder bed is aerosolized upon inhalation. For detachment of API particles to occur through this mechanism, it is essential that the carrier surface has minimal asperities, which allows for a clear path for the airflow to access and remove the API particles (de Boer et al., 2003a, Donovan and Smyth, 2010).

Mechanical forces on the other hand are generated when carrier particles impact the inhaler wall, leading to momentum transfer from the carrier to API particles, which then generates detachment force. The detachment force generated is proportional to the amount of momentum transferred, which is in turn dependent on the mass of the carrier particle, assuming constant velocity of the different carrier sizes in the formulation (Donovan and Smyth, 2010).

Equation 1-1

$$\rho = mv$$

$$\text{Where } \rho = \text{momentum}$$

$$\text{m} = \text{particle mass}$$

$$\text{v} = \text{particle velocity}$$

Although detachment by mechanical forces may not obstructed by surface asperities as much as detachment by flow, the detachment force generated must be greater than the adhesive force between API and carrier and the position of the particle must favour removal of the API particles (Xu et al., 2010, Donovan and Smyth, 2010).

Although the airflow stream generated is dependent on patient inspiratory flow rate, some devices are designed to release a DPI dose only when a minimum inspiratory flow threshold is produced. In other devices that do not have the aforementioned mechanism, majority of patients are able to achieve the minimum flow rates necessary to deagglomerate the DPI formulations. For the remaining very young and very old, who lack the cognitive ability and strength to properly use a DPI, nebulisers remain the preferred option (Buttini et al., 2016; Weers and Clark, 2016).

Fine API particles attached to fine carriers are more likely to be detached by the airflow stream generated during aerosolization than API particles attached to coarse carriers. API particles on larger carriers are more likely to be detached by mechanical forces due to impaction. This difference is due to a combination effect of carrier size and surface morphology. With smaller carriers that have smoother surfaces, APIs can be easily detached, since the API particles are freely exposed to the airflow stream. With larger carriers that have more surface asperities, drug particles may be shielded from airflow during aerosolization of the powder bed. This results in the likelihood of the API being aerosolized through detachment via mechanical force and momentum transfer. Additionally, since momentum transfer is directly proportional to the mass of carrier particle, larger carriers will transfer more momentum required for drug particle detachment (Donovan and Smyth, 2010, Xu et al., 2010). It is important to note that this may

result in deposition of drug in inhaler/delivery device (undelivered dose) if the position of the particle is not favourable. This was the case in a study by Steckel and Müller (1997) in which undelivered dose from an interactive mixture of budesonide and α-lactose monohydrate of different sieve fractions increased as the carrier particle size increased.

Additionally, as API particle size decreases, the force required for detachment increases, the same applies to API particles attached to high-energy sites, due to higher adhesive forces between API and carrier particles. While larger API particles, either fine drug agglomerates or large primary particles, have a higher surface area and better aerodynamic profile to interact with the airflow stream and be detached through the airflow stream, smaller primary drug particles require greater detachment force usually by mechanical detachment. This influences the respirable fraction of the formulation, with detachment by momentum transfer generating more primary particles than detachment by airflow stream, in which predominantly either aggregates or larger primary particles are detached (Donovan and Smyth, 2010). This was evident in a study by Kaialy et al. (2012a), in which although lactose carrier particles with overall smaller VMD increased fine particle fraction (FPF), there was a concurrent increase in deposition of budesonide in the throat region, which increases the potential for side effects

1.4.3 API deposition mechanism in the respiratory tract – The significance of particle aerodynamic diameter

Particle aerodynamic diameter is defined as the diameter of a sphere of unit density that attains the same velocity as a non-spherical particle of random density in the airflow generated upon aerosolization (Chow et al., 2007). The effectiveness of a DPI formulation is determined by the region in the respiratory tract where it is deposited. Particles with aerodynamic diameter between 0.5 – 5 μm can reach the deep lung region, while particles greater than 5 μm settle in the oropharynx region and are eventually swallowed. Particles less than 0.5 μm are mostly exhaled and do not deposit in the airways (Pilcer and Amighi, 2010, Yang et al., 2014). Therefore, the purpose of the DPI formulation therapy should guide the airways region targeted for drug delivery. Studies have shown that particles deposited in the upper airways

are cleared within 2 to 4 hours, while those that reach the deep lung region can stay up to 3 days. For the local treatment of respiratory diseases such as asthma and COPD, which is the focus of this work, drug delivery must be targeted to the deep lung region. This will ensure sufficient local concentration of the drug and minimise systemic side effects (Sou and Bergström, 2021). In order to achieve particles with aerodynamic diameter between 0.5 – 5 µm, respirable particles with particle size between 1 - 5 µm must be produced, and different mechanisms of particle deposition in the airways i.e. impaction, sedimentation and diffusion are adopted depending on particle size. These mechanisms are illustrated in figure 1.2.

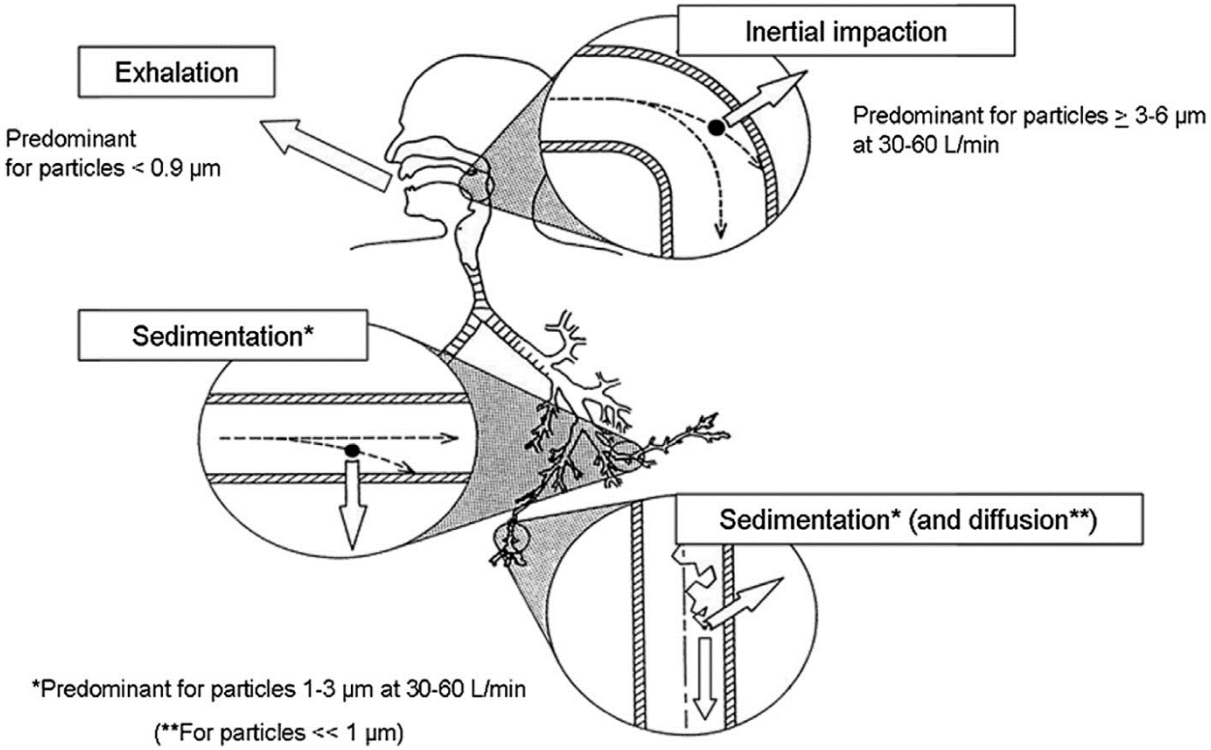

Figure 1.2 Figure illustrating the mechanisms of particle deposition in the airways. Aerosolized particles > 5µm settle passively in the upper airways, due to high speed of inhaled air and branching of the airways. They are eventually swallowed and do not contribute to the delivered dose of the API. Aerosolized particles with aerodynamic diameter between 0.5-5µm settle by gravitational force and reach the bronchioles and alveoli i.e. the deep lung region, which is desirable for adequate local drug concentration required in treatment of local respiratory diseases such as asthma and COPD. Aerosolized particles < 0.5µm collide with air molecules and are either deposited in the deep lung region by diffusion or predominantly exhaled. Image source: Demoly et al. (2014).

1.5 Carrier factors affecting performance of DPI formulations

1.5.1 Effect of carrier particle size

The consensus on the effect of carrier particle size on drug aerosolization is that smaller carriers are more favourable for drug dispersion (Steckel and Müller, 1997, Louey et al., 2003, Islam et al., 2004, Kaialy et al., 2012a). However, it is difficult to examine the effects of individual physicochemical properties of carrier on DPI performance in isolation. This is because of the interdependence of physicochemical properties, as such, changing one property e.g. particle size, may generate other variable(s) e.g. particle shape, surface roughness, surface area or surface property. Therefore, several variables may be present while only one is being examined. In order to overcome this challenge, Ooi et al. (2011) used a series of model polystyrene spheres to examine how carrier size, independent of other variables as much as possible, affects aerosol performance. They investigated the aerosolization of salbutamol sulphate from model polystyrene carrier particles of three different particle sizes. These model carrier particles were deliberately prepared to have similar density, shape, surface roughness and chemistry, thereby reducing the number of between observations. This study shows that, in isolation of other variables, as carrier size decreases, a concurrent increase in drug aerosolization performance occurs. The significant increase in aerosol performance was primarily attributed to more frictional and rotational collisions between particles of the smaller carrier in the powder bed, facilitating API detachment from carrier during aerosolization. Although this model carrier is not typical of an ideal drug-carrier system, it provides useful data to evaluate potential similarities or differences in ideal drug-carrier systems where multiple variables may be present simultaneously (Ooi et al., 2011).

Earlier research to investigate the effect of lactose size on *in-vitro* deposition of salmeterol xinafoate reported similar findings as above, where FPF increased with low carrier particle size < 32 μm (Steckel and Müller, 1997). Ideally, as particle size increases, surface area and surface energy decreases. It is expected that this should reduce drug-carrier adhesion and facilitate drug dispersion. However, the opposite trends observed were attributed to the higher

impact that larger carriers have on the inhaler wall during aerosolization of the powder bed, which results in more undelivered dose. This is aggravated by the fixed drug: carrier mass ratio, which results in a higher drug to carrier surface area ratio with larger carriers, in which there will be more drug particles per carrier with the use of larger carriers, since the number of carrier particles reduce with larger carriers (Steckel and Müller, 1997, Ooi et al., 2011). This observation is consistent with that of (Ooi et al., 2011), where one of the other factors thought to facilitate drug dispersion from smaller carriers is the lower drug: carrier surface area ratio along with increased number of carrier particles, which promote more frictional and rotational collisions between particles. These explanations link drug dispersion directly to the innate volume mean diameter (VMD) of the carrier, which is not the case with more recent studies.

More recently, studies have attributed the improved dispersion observed with smaller lactose carriers to the fine content rather than inherent particle size. This is a more plausible explanation considering that the presence of fine and coarse carrier fractions will favour the two main mechanisms of drug detachment described in section 1.4.2. Consequently, the API particles attached to both fine and coarse carrier fractions are able to detach producing a higher fine particle fraction. Islam et al. (2004) investigated the direct effect of six different grades of lactose on the dispersion behaviour of salmeterol xinafoate (SX). They found that as the VMD of lactose decreased, the FPF of SX increased. They speculated that this could either be due to the distinct ability of decreasing lactose particle size to improve dispersion, or a function of the fine lactose content in the carrier, which increases as VMD decreases. The removal of fine lactose by wet decantation from two of the six lactose grades used in this study and subsequent decline in SX dispersion supported the latter claim (Islam et al., 2004). Similarly, in a study by Guenette et al. (2009), different size fractions of lactose were mixed in different proportions based on experimental design to produce ten lactose carrier blends with D_{50} between 29.74μm – 89.54 μm. These lactose blends were used to investigate the aerosolization performance of salbutamol sulphate (SS). The formulations containing the highest amount of ultrafine (<10 μm) and fine lactose (10 μm - 40 μm) produced the highest FPF, this was also attributed to the fine lactose content. Similar observations have been found

in other studies, although, the fine lactose content desirable in improving dispersion needs to be balanced to avoid undesirable effects such as poorer flow, less homogeneity and increased possibility of carrier deposition in lower airways (Steckel and Müller, 1997, Kaialy et al., 2012a). Other recent studies have directly investigated the effect of extrinsic lactose fines on aerosolization behaviour of DPIs. This is considered later on in section 1.7 as a means of lactose surface modification rather than as an effect solely down to carrier particle size, due to the other different factors (such as change in surface roughness, surface energy, and potential reduction in high energy sites) that come into play to impact drug aerosolization.

1.5.2 Effect of carrier particle shape and surface morphology

Particle shape and morphology can be characterised using several descriptors, which are elongation ratio (ER), flatness ratio (FR), roundness (RO), shape factor (F_{shape}) and surface factor ($F_{surface}$). ER and FR are the basic parameters hence, referred to as first order descriptors. In simple terms, ER is the ratio of particle length to width, while FR is the ratio of width to thickness. With reference to perfect cubes and spheres which have ER and FR of 1, more elongated particles have ER > 1 while flatter particles have FR > 1(Kuo et al., 1998, Kaialy et al., 2012a) . RO is a measure of both particle geometric shape and surface smoothness, a sphere with a smooth surface has a roundness value of 1, while a sphere with rough surface and other shapes have a roundness value greater than 1. Therefore, the higher the roundness value, the more irregularly shaped and/or the rougher the surface of the particle is (Larhrib et al., 1999). F_{shape} is a second order descriptor, given that it is a measure of particle shape irregularity based on particle orientation and contact area, but independent of actual particle dimensions. F_{shape} values range from -1 to 1, with more irregularly shaped particles having smaller values. While ER, FR, RO and F_{shape} define particle shape, RO and $F_{surface}$ characterise particle surface texture or morphology. Thus, $F_{surface}$ is referred to as a third order descriptor. Regular particles with smooth surfaces have $F_{surface}$ value of 1, while a decrease in $F_{surface}$ value indicates rougher surfaces (Kaialy et al., 2012b).

Kaialy et al. (2011), using ER (values between 1.62±0.04 to 5.89±0.2) and roundness (values between 1.36±0.13 to 6.49±2.91) as the descriptor of carrier shape, investigated the effect of five different carrier shapes on salbutamol sulphate. Although they discovered that the higher the ER of the carrier particle, the higher the deposition of salbutamol sulphate to the lower airway regions, it is important to note that there were significant variations of other physicochemical properties. To support the estimations obtained by shape factor descriptors, scanning electron microscopy (SEM) micrographs and particle size distribution revealed the extent of variation in particle size, shape, surface morphology, degree of surface roughness/smoothness, surface asperities and even the amount of intrinsic carrier fines, while the effect of particle shape was the only focus of this study. It is interesting to note that carrier particles with higher ER (acetone crystallised mannitol ER = 4.83±0.18 and ethanol crystallised mannitol ER = 5.89±0.19) were the same ones with smoother surface, they also had a smaller VMD and a higher amount of intrinsic fines up to 8.6%. These observations further highlight the difficulty of investigating one physicochemical property in isolation, as the additional factors that were not in consideration may well have influenced the overall conclusions.

With respect to lactose as a carrier, Kaialy et al. (2012b)carried out a comprehensive study, which acknowledged a consolidation of multiple lactose shape components on DPI performance. In contrast to the above study, variation in particle size was eliminated. All lactose carriers used had similar VMD between 81.6±2.6 μm to 84.9±1.3 μm; and the same amount of fine lactose, less than 1% of fine (< 10 μm) lactose fraction. As in the above study, the lactose carrier with the highest ER deposited the highest amount of salbutamol sulphate to the lower airway regions. However, the better aerodynamic performance was attributed to co-effects of high surface roughness and shape irregularity of the lactose carrier.

Another comprehensive study by Larhrib et al. (1999) emphasises the co-effects of different lactose carrier physicochemical properties. Five different grades of lactose carrier were investigated for their effects on DPI performance, in which ER and roundness were the only quantitative descriptors of lactose carrier shape. Interestingly, the fine particle dose and FPF

more than doubled significantly, when an amorphous lactose grade was used, which in addition had the lowest ER. In addition to considerable particle size variations, several variations revealed by SEM micrographs, such as surface roughness and asperities, were higher in the crystalline lactose grade. Amorphous lactose had a considerably higher amount of fine lactose content (23% < 10 μm and 12% < 5 μm), which was the main reason given for its efficient delivery of salbutamol sulphate.

Also using different grades of lactose carriers, Kho and Hadinoto (2013) investigated the effect of three different lactose carrier shapes (tomahawk - CL, needle - NL and pollen shaped - PL) at two differing size fractions i.e. 50 – 70 μm and 14 – 20 μm on the delivery of amorphous ciprofloxacin nanoparticles. The aerosolization efficiency of the API – carrier particle blends were compared with that of the carrier-free inhalable aggregates of ciprofloxacin nanoparticles. For the smaller lactose size fraction (14 – 20 μm), they reported no significant increase in emitted dose and FPF using NL lactose carrier compared to the carrier free formulation. This was despite NL having the highest ER of 4.1 compared to 1.5 and 1 for CL and PL respectively. This is likely due to the poorer flow linked to formulations with carriers that have high ER, as well as higher potential for drug loss and drug deposition in throat region, which reduces emitted dose and FPF (Kho and Hadinoto, 2013). In contrast to NL, CL and PL lactose were able to double the FPF to 17±1% and 16±1% respectively from 8±2% for the carrier free formulation. Although, mass median aerodynamic diameter (MMAD) for all formulations was similar to that of the carrier free formulation (between 5.5 – 6.0 μm), suggesting that the drug particles were deposited as aggregates of ciprofloxacin nanoparticles. This was confirmed by the NGI deposition pattern of the ciprofloxacin nanoparticles, which mainly deposited in stage 1, with average aggregate size greater than 6 μm. The drug detachment mechanism supports this observation, since the small carrier size used favours API detachment by the airflow stream, which is more likely to release large drug particles or fine drug agglomerates (Donovan and Smyth, 2010). MMAD is defined as the median aerodynamic diameter of the fine particle dose by mass. Lower MMAD values imply

the delivery of smaller API particles, which have a greater tendency of reaching the deep lung (Hassanpour Aghdam et al., 2016).

For the larger CL, NL and PL, (50 – 70 μm) all three were able to increase emitted dose to 70 – 80% from 52% for the carrier free formulation, this was attributed to the ability of larger carriers to reduce drug aggregates. This increase in emitted dose did not produce a corresponding increase in FPF for the formulation prepared with PL which remained at 8±2%. This was attributed to poor drug detachment from the crevices on the PL carrier surface. Rationally, undetached API from carrier surface does not negatively affect the emitted dose, as it potentially deposits in the earlier stages of the NGI with the carrier particles, which also contributes to emitted dose but not FPF. The NL and CL carriers however increased FPF to 17±2% and had similar deposition patterns. Overall, this study showed that there was no superiority of carrier particle performance despite the difference in shape (Kho and Hadinoto, 2013).

1.6 The Mixing Process

Fan et al. (1970) describe solid mixing as the process of randomly dispersing two or more particulate solids amongst each other by the random movement of the particle. The primary purpose of solid mixing is to achieve blend homogeneity; the components of a homogenous mixture are uniform throughout the whole blend, and random samples, which are expected to be representative of the whole mixture, are analysed to determine blend homogeneity (Bridgwater, 2012, Fan et al., 1970). The mixing process of powders used in DPIs and other pharmaceutical formulations is vital to the quality and performance of the product. The need for blend homogeneity in DPI blends cannot be over-emphasised, as this directly affects drug content uniformity, the lack of which may result in over dosing of API, dangerous side effects and potential death and the under dosing of API of which may result in poor therapeutic effect and deterioration of patient disease and health.

Despite being an age-old process, powder mixing still very much lacks a uniform scientific approach, and is commonly treated as an art based on previous experience and trial and error,

similarly in the food industry where mixing is also critical (Cuq et al., 2013). In addition, the wide range of particle size, size distribution, shape, density and chemical composition of materials in DPI formulation creates a barrier to process development, as there is no one size fits all. For instance, the challenges posed by free flowing materials (segregation) differ from those encountered when mixing fine or poor flowing materials (agglomeration) (Bridgwater, 2012). It is critical to understand the nature of materials to be mixed, and the mixing mechanisms of different mixers/blenders, in order to select the most appropriate type of blender to achieve a homogenous mixture (Fan et al., 1970). The three major mixing mechanisms are described as follows.

1.6.1 Mixing mechanisms

1.6.1.1 Convection

This describes the movement of a group of particles within the powder bed from one part of the mixing vessel to another. This movement is usually as a result of a rotating blade or paddle. As the impeller moves, it moves the particles alongside, increasing surface contact between the particles and homogenising the mixture (Bridgwater, 2012, Fan et al., 1970).

1.6.1.2 Diffusion

In diffusion, the movement of the impeller causes movement of individual particles relative to one another. Over time, there is a reshuffling between the particles; as they are spread over new surfaces as a result of their random motion. This causes new particle-particle interactions to occur which facilitate homogenous mixing (Bridgwater, 2012, Fan et al., 1970).

1.6.1.3 Shear

In convective mixing, narrow zones of high velocity exist between groups of particles referred to as slip zones. The high velocity coupled with the narrow size of these slip zones allows shearing to occur. As agglomerated particles move through these zones, they are forcefully compressed against mixing vessel walls and broken up hence; this mechanism is also

reported to cause deagglomeration of cohesive powder (Alonso and Alguacil, 1999, Bridgwater, 2012).

An understanding of these mixing mechanisms helps when selecting the mixer for a specific purpose. For example, in DPI formulations, where fine APIs are mixed with large carrier particles, the deagglomeration of fines (API) is critical to the process. Therefore, it will be important to select a mixer that is able to break up agglomerates (de Boer et al., 2012). While mixers that predominantly operate by the convective and shear mechanism work better to break up agglomerates, those that operate predominantly by diffusion require longer mixing times to do the same. Increased mixing times however can increase the potential for unintended segregation i.e. demixing and be detrimental to blend homogeneity (Zheng, 2009). However, the increased particle-particle interaction created during diffusive mixing is highly favourable in achieving a uniform drug-carrier blend caused by particle redispersion. Apart from the desired blend quality, there are other factors that need to be considered in designing a mixing process, such as drug:carrier ratio in terms of size and quantity, batch size, sensitivity of materials to heat or moisture, adhesiveness of materials onto mixer surfaces, potential for contamination, potential for unwanted particle size reduction and triboelectrification (Bridgwater, 2012). Triboelectrification is a process through which contact between the same or different particle surfaces or contact with mixing vessel surface causes charge generation. Triboelectrification has a significant impact in the processing of pharmaceutical powders when mixing APIs with excipients, as the tendency of electrostatic charge generation on particle surface increases (Ghori et al., 2015).

The most commonly used mixers in DPIs are low shear mixers like TURBULA® mixers and high-shear mixers like the Turbo Rapid Variable (TRV) Mixer. Low shear mixers have been predominantly developed for powder mixing whereas high shear blenders have a heritage of mixing liquids and solids. High shear mixers utilise all three mixing mechanisms of operation (diffusion, shear and convection) which ought to deliver the best conditions for the deagglomeration of fine API and subsequent homogeneous dispersion of the API on the carrier particles (Koner et al., 2017). However, with DPI formulations, beyond creating a good

quality homogeneous mixture, which is able to withstand agitation during handling, packaging, transportation, storage etc. up until the point of use, it is critical to create a balance between drug-carrier adhesion and subsequent drug detachment, which is essential for API delivery to the lungs. The drug-carrier adhesive force determines the formulation homogeneity and ability to withstand agitation, while this adhesive force needs to be overcome for optimal DPI formulation dispersion and performance. Recent developments in mixing technology specifically isothermal dry particle coating (iDPC), holds out the prospect of predictive and science driven mixing and coating rather than black art (Dahmash et al., 2018; Koner et al., 2017).

1.7 Optimisation of DPI formulation dispersion by carrier surface modification

Different methods have been explored to modify carrier surface properties in order to control DPI dispersion behaviours. These methods have been reviewed extensively by different authors and are summarised in table 1.1.

Table 1.1 Major literature reviews on optimisation of carrier-based DPI formulation performance

Title of article and Author(s)	Focus of review article
The Influence of Fine Excipient Particles on the Performance of Carrier-Based Dry Powder Inhalation Formulations **Jones and Price (2006)**	Active site and agglomerate theories to explain effect of lactose fines
Particle Engineering for Pulmonary Drug Delivery **Chow et al., 2007**	Surface morphology and dispersion behaviour in relation to asperities
Formulation strategy and use of excipients in pulmonary drug delivery **Pilcer and Amighi (2010)**	Hydrophobic lubricants Carrier free formulations
Lactose as a carrier for inhalation products: breathing new life into an old carrier **Marriot and Frijlink (2012)**	Impact of lactose physicochemical properties such as size, size distribution, shape and surface roughness of the particle, the presence of moisture, impurities or performance
A critical view on lactose-based drug formulation and device studies for dry powder inhalation: Which are relevant and what interactions to expect **de Boer et al. (2012)**	Carrier surface properties and role in drug-carrier interaction in relation to active sites on carrier surface Role of amorphous spots and carrier fines in drug-carrier interactions The need for balance between cohesive and adhesive forces in DPI formulations and forces required for dispersion during inhalation and how this balance relies on the control of interparticulate force

	Relationship between active sites and high surface energy
Physico-chemical aspects of lactose for inhalation **Kou et al. (2012)**	Physicochemical properties of lactose that affect DPI performance including carrier size, distribution and shape; surface roughness; polymorphic form of carrier; flow properties and electrostatic charge
Drug–lactose binding aspects in adhesive mixtures: Controlling performance in dry powder inhaler formulations by altering lactose carrier surfaces **Zhou and Morton (2012)**	Engineering of lactose surface morphology through surface smoothness, surface roughness, solvent based coating and mechanical dry coating Characterisation of coating quality
Technological and practical challenges of dry powder inhalers and formulations **Hoppentocht et al. (2014)**	Briefly mentions the use of crystalline and sieved lactose fraction as carriers in DPIs and passivation of active sites on carriers by ball milling, wet smoothing and use of FCAs
A proposed definition of the 'activity' of surface sites on lactose carriers for dry powder inhalation **Grasmeijer et al. (2014)**	Relationship between carrier surface activity and the energy with which they bind APIs Preferential occupation of active sites and retaining of drug particles on active sites during drug dispersion
Formulation Design of Dry Powders for Inhalation **Weers and Miller (2015)**	Improving dispersion by lactose fines and FCAs; effects of lactose size, shape and morphology in dispersion Preferential attachment of lactose fines to high energy sites which occur as a result of clefts, amorphous domains, different crystalline orientations or other surface defects related to moisture, charge or contamination on lactose surface

From single excipients to dual excipient platforms in dry powder inhaler products **Shur et al. (2016)**	The use of lactose as a single excipient platform in DPI formulations and introduction of a functional additive (Mg stearate used a lubricant, FCA, stabiliser, water barrier and chemical stabiliser) to form a dual excipient platform for DPIs
A review of factors affecting electrostatic charging of and adhesive mixtures for inhalation **Kaialy (2016)**	General review on the impact of electrostatics on Dpi formulations Influence of polymorphic form and size distribution of lactose on electrostatic charge, and how surface charge on carrier and drug can affect the dry coating or mixing process and Dpi aerosolization
Influence of physical properties of carrier on the performance of dry powder inhalers **Peng et al. (2016)**	Impact of carrier properties on aerosolization including carrier particle size (size distribution), shape, morphology (surface roughness), density and geometric diameter. Role of fine carrier and associated theories (active site, agglomeration, fluidization theory, buffer hypothesis)
Modelling the performance of carrier-based dry powder inhalation formulations: Where are we, and how to get there? **Elsayed and Shalash (2018)**	More general carrier-based review, focused on the key performance determinants of DPI formulations Carrier size and size distribution, concentration and size of fine carrier, carrier surface roughness and porosity and carrier shape were identified as carrier components that affect DPI performance

1.7.1 Addition of fine lactose particles

The incorporation of fine lactose particles in a carrier-based DPI formulation has been investigated considerably. Supported by two major theories, it is established that the inclusion of lactose fines enhances formulation performance (Kinnunen et al., 2014, Le et al., 2012, Zeng et al., 1999, Zeng et al., 1998). The first is the “active site” theory, which explains that fine lactose particles attach to potential drug binding sites, leaving the drug particles to attach to less active sites on the coarse lactose carrier surface from which they are more easily detached on inhalation. Surface active sites on lactose particles have been described based on surface morphology, rugosity, irregularity, presence of impurities, surface energy and chemical properties. Surface crevices, which are larger than drug particles and reduce the tendency for drug detachment are presumed to be active sites. Also are sites with higher surface energy, related to polar or dispersive forces, increased surface interaction forces e.g. van der Waals or capillary forces; and sites which are charged or chemically contaminated (de Boer et al., 2003b, Zhou and Morton, 2012). There is however, no evidence of preferential binding of lactose fines over drug particles or vice-versa at such “active sites”; thus, lactose fines before drug particles blending order is important for improved DPI formulation performance based on this theory (Zeng et al., 2000, Zeng et al., 1998).

The second is the “agglomerate theory”, which was put forward based on contrasting evidence where blending order did not influence the formulation performance (Louey and Stewart, 2002, Lucas et al., 1998). This theory states that the dominant mechanism affecting attachment is that fine lactose particles preferentially form agglomerates with the fine drug particles rather than simply blocking active sites on coarse lactose. Upon inhalation, the fine drug particles are more easily detached from the fine lactose surface due to smoother carrier surface, or the carrier-drug agglomerates may be small enough to be delivered as part of the respirable dose. There is also the possibility of easier detachment of the drug-carrier agglomerates, since greater mass of the aggregated particles allows for greater effect of fluid forces for drug detachment by the airflow stream (Jones et al., 2008, Jones and Price, 2006, Lucas et al.,

1998, Shur et al., 2008). The mechanisms of drug detachment from carrier particles as described in section 1.3 provide further support to the agglomerates theory.

1.7.2 Use of force control agents

To mask the “active sites” on coarse lactose, force control agents (FCAs), which are generally materials thought to reduce cohesion and adhesion have also been used to modify carrier surface and facilitate dispersion. Most commonly used are magnesium stearate and L-leucine, since the unproven toxicological profile of potential anti-adherents restricts the choice of material for delivery to the lung (Zhou and Morton, 2012). Some studies have also explored polymers as potential surface coating agents for lactose (Traini et al., 2012).

(Kumon et al., 2006) investigated the effect of coating three different lactose carriers of mean diameter 10 μm, 60 μm and 150 μm with magnesium stearate and sucrose stearate, on the surface properties of the carriers, and how this impacts the aerosolization behaviour of a particular but unnamed drug. Generally, they found that formulations containing lactose coated with magnesium stearate (MgSt) and sucrose stearate deliver higher FPF with correspondingly increased deposition of the drug in the lower stages of an Anderson Cascade Impactor (ACI), when compared to the performance of formulations of an uncoated carrier. This was attributed to the ability of the FCAs to reduce adhesion between the drug and lactose carrier. This was also supported by the fact that more of the drug dose remained undelivered due to retention in the inhaler device, which was attributed to reduced drug-carrier adhesion. There was also a dose independent increase in FPF with magnesium stearate and sucrose stearate, which was due to weak drug-carrier adhesion, even at high-energy binding sites, because of the force controlling effects. Likewise, a recent study carried out by Benke et al. (2020), compares the aerodynamic properties of micronized meloxicam potassium in a carrier free formulation, lactose – based formulation and surface modified lactose (with MgSt) carrier-based formulation, with spray-dried meloxicam potassium in the three formulations. The authors report better lung deposition for the surface modified lactose carrier-based formulations in the two categories of micronized and spray-dried meloxicam potassium.

There is also the potential to use FCAs in carrier-free formulations, since they primarily reduce interparticulate forces, whether adhesive or cohesive as would be the case in a pure drug formulation. Begat et al. (2009) investigated the effects of MgSt, leucine and lecithin on the performance of salbutamol sulphate and budesonide in a carrier-free system. All three FCAs produced a significant increase in FPF and corresponding reduction in MMAD of the aerosolized drug. These authors suggested that this was due to the FCAs' ability to reduce interfacial free energy between the drug particles, hence, reduce cohesion and facilitate deagglomeration.

Other methods such as carrier surface smoothing have also been used to facilitate DPI aerosolization, by evening out crevices where drug particles would otherwise be trapped as highlighted in table 1.2. However, contrasting evidences show that carrier surface roughening likewise enhanced DPI performance. It is suggested that these conflicting data are the result of diversity in terms of blending equipment, inhaler device, nature of drug particles etc., which complicate the direct cohesive-adhesive interaction between lactose surface morphology and DPI performance (Zhou and Morton, 2012).

Table 1.2 Notable strategies for enhancing DPI formulation performance

DPI enhancing strategies	Rationale	References
Use of fine carrier particles as performance modulators	Active sites theory, Agglomerate theory	(Kinnunen et al., 2014, Le et al., 2012, Zeng et al., 1999, Zeng et al., 1998)
Carrier surface roughening	Carrier nanopores reduce adhesion force by reducing effective contact area between carrier and drug particles, while carrier micropores facilitate deagglomeration of fine drug particles	(Kawashima et al., 1998, Littringer et al., 2012, Shalash et al., 2015)
Carrier surface smoothening	Smoother surface increases surface contact area and reduces crevices where fine drug particles are tightly held to carrier particles	(Kawashima et al., 1998, Young et al., 2010, Zeng et al., 1999)
Use of force control agents	Passivation of active sites on carrier particles/ reduction of cohesive forces through selection of FCAs e.g. MgSt, Leucine, Polymers e.g. PVP, Ethyl cellulose	(Begat et al., 2009, Kumon et al., 2006, Zhou et al., 2010b) (Traini et al., 2012)

1.8 Surface energetics and particle interactions

To determine the performance of DPI formulations, FPF is used as a measure of the aerodynamic dispersion of bulk powder into primary particles or drug agglomerates. For dispersion to occur, separating forces have to overcome interparticulate attraction within the bulk powder to produce primary particles of API in the respirable size range. Therefore, overcoming interparticulate interactions is critical to DPI performance (Pilcer et al., 2012). Despite an understanding of the interparticulate interactions involved in particle adhesion and cohesion and the study of particle properties and how they affect DPI performance, the effects of bulk powder properties on DPI performance are still not fully understood and the correlations between the two have not allowed consistent prediction of DPI formulation performance. This is due to the complexity created by the interactive influence of particle properties such as size, shape and surface morphology on DPI formulation performance making it difficult to predict DPI performance based on particle properties alone. Therefore, it is highly recommended to establish a relationship between the comprehensive powder properties of DPI formulations and pulmonary drug deposition for the purpose of DPI formulation performance prediction, to accelerate the process of research and development in early formulations screening, based on powder properties (Marriott and Frijlink, 2012).

Surface energy, an intrinsic particle property has the potential to establish such a relationship and to be used as a predictive tool for DPI formulation performance (Apte, 2012, Cline and Dalby, 2002). Surface energy refers to the free or excess energy at the surface of a solid particle compared to the bulk. Solid particles consist of molecules, which within the bulk are normally bound together on each side. However, at the solid-gas interface, due to intermolecular attraction towards the bulk of the particle, there is a net force on molecules away from the particle surface, leaving unbound atoms at the surface. The measurement of this excess energy at the solid surface, due to the unbound atoms is known as surface energy (Johnson et al., 1971). There are two components of surface energy, dispersive and polar surface energy. Dispersive surface energy is a result of fluctuations in charge distributions, which induces transient dipoles i.e. van der Waals interactions. Polar surface energy is due to

permanent dipoles from charged particles or polar groups on the particle surface. Since surface energy is a result of intermolecular attractions within the particle, there is a direct relationship between the strength of intermolecular attraction, surface area and surface energy. Therefore, the stronger the intermolecular attraction, the higher the surface energy, and as surface area increases, more molecules are forced to the particle surface hence, increasing surface energy (Das et al., 2011a). Interactive mixtures are formed using the thermodynamic instability created by unbound atoms at the solid particle surface, which allows for physical adsorption of molecules to particle surface. 'Solids with high surface energy have a high tendency to form strong bonds with other materials and vice versa. The stronger the bond between the drug and carrier particles in an interactive mixture, the less easy it is for the drug to detach. Correspondingly, the weaker the bond, the less stable the interactive mixture and the more easily particles can be detached from the carrier (Das et al., 2011b, Johnson et al., 1971). The relationship between surface energy, interparticle bond strength and formation of interactive mixtures may be leveraged as a predictive tool in designing the performance of DPI formulations. For this reason, the measurement of surface energy has become an important part of formulation development.

1.8.1 Surface energy determination

There are a number of ways to measure surface energy including interaction with water vapour (Buckton et al., 1988), by contact angle measurement (Traini et al., 2005, Clint, 2001), atomic force microscopy (AFM) (Davies et al., 2005, Zhang et al., 2006, Grimsey et al., 2002) and most recently, inverse gas chromatography (IGC) (Butler and Williams, 2000, Das and Stewart, 2012). The use of contact angle and AFM methods in surface energy determination are limited by challenges such as reactivity of particulate pharmaceutical materials to contact angle fluids and ambiguous indices for AFM (Williams, 2015). The IGC method is particularly advantageous primarily because it allows materials to be characterized in their native state thereby retaining the integral particle surface properties more representative of those in

formulation. IGC requires minimal sample preparation, and samples can be recovered post analysis i.e. it is a non-destructive method.

1.8.2 Use of IGC in measuring surface energetics

The basic concept of IGC is that of gas chromatography (GC). In contrast to conventional GC, IGC measures the unknown surface of a sample powder that is packed in a column into which a series of known alkane probe vapours is consecutively injected. There are two types of IGC, IGC at infinite dilution (IGC-ID) occurs at low and fixed probe concentrations, usually less than 0.01 P/P_0. Due to the low concentration of probe molecules in this case, there is an increased tendency of preferential interaction with high energy sites. Therefore, the surface energy values obtained from IGC-ID is more representative of the highest energy sites (Butler and Williams, 2000, Das et al., 2010). Secondly is IGC at finite concentration (IGC-FD), in which case different probe concentrations are injected into the sample column to target a fractional surface coverage of the material, usually between 0% to 20% surface coverage. This allows more interaction of the probe molecules with different energy sites and gives a surface energy profile of the material, which is more representative of the total energy sites. The surface energy of the powder is calculated from the retention times of the probes. The acid-base properties of the particle surface are determined using monopolar basic and acidic probes (Bungert et al., 2021, Karde and Ghoroi, 2015). The principles of IGC are highlighted as follows:

1. IGC is the reverse of traditional gas chromatography, where the column is packed with the material of interest usually a powder, fibre or film.
2. A gas probe is injected at a constant concentration, carried by an inert gas at a fixed flow rate. Different gas probes can be used to assess varying physicochemical properties of the material of interest.
3. A detector, usually a flame ionisation detector (FID), measures the retention volume of the gas probe, which indicates the strength of interaction between the particle surface and the gas probes.

4. A series of n-alkane probes of varying carbon chain lengths are used to measure the dispersive component of the surface energy, while polar probes are used to measure the acid-base component of the surface energy.
5. IGC measured at infinite dilution uses a low concentration of probe molecules injected through the sample column at a specific surface coverage. Therefore, only high-energy sites interact with the available probe molecules. This method gives a single value of surface energy, which may not fully represent the entire particle surface.
6. IGC measured at finite concentration is a more recent advance in IGC methodology. In this case, the probe molecules are injected through the sample column at different surface coverages. This produces a surface energy distribution over the different surface coverage used. This approach is more representative of the entire particle surface and shows the degree of surface energy heterogeneity.
7. Using the iGC-SEA 2000 by Surface Measurement Systems Ltd, surface energy measurements can be done under controlled temperature and humidity, to eliminate any interference of both on obtained values or profile ((Khoo et al., 2012; SMS, 2013).

1.8.3 Use of surface energetics to optimise and control DPI performance

Many different methods have been investigated in the creation of engineered particles to control adhesion/cohesion forces both between micronized drug and carrier particles and also between the micro fine drug particles themselves. Methods such as particle surface smoothening, roughening, coating the carrier surface with force control agents have all been found to influence DPI formulation performance. There remains a gap between formulation design and converting theory to practice by using such materials to control the manufacturing process to deliver DPI formulations with the targeted aerodynamic performance. These particle-engineering methods will no doubt have effects on the surface energetics of the particles, since particle history and presence of surface contaminants are major factors that influence surface energy. The importance of particle surface energetics in determining particle adhesion and cohesion means that surface energy could potentially be used in the manufacturing process to predict and optimise DPI formulations through a quality by design approach. This would not only accelerate product development but also give regulators more confidence in the formulations being processed. Therefore, in addition to using other physicochemical properties to optimise DPI performance, particle surface energetics could be potentially used to both optimise and predict DPI formulation performance.

The challenge with solid surface energetics is the heterogeneous nature of the powder surface. Unlike the liquid state where free movement of molecules homogenise surface energy, surface energy is unevenly distributed and heterogeneous, with some regions possessing higher surface energy than others do. It is more realistic to characterise a surface with a range of surface energy values over a specified surface area, but a median value is often specified to represent the overall surface. In reality, adhesion characteristics differ within the same batch of powder (Heng et al., 2006)

The complexity associated with different surface energy values and their effects have been reported in several studies. Two different studies by Das et al. (2011b), Kumon et al. (2006) showed that surface energy values obtained at infinite dilution mainly reflect that of high energy sites whilst supposed passivation of lactose particle surface with MgSt increased rather

than decrease the surface energy as would have been expected. API aerodynamic performance was reported to be better despite the increased surface energy

Another study by Cline and Dalby (2002) aimed to correlate surface energy values of carrier particles with the FPF of an interactive mixture whilst incorporating the specific surface area to understand the amount of surface available for interaction. This study shows a similar correlation between FPF and surface energy interaction to the studies mentioned above in which only surface energy was correlated with FPF. The unexpected increase in FPF as surface energy interaction increased is believed to be due to the fact that a minimum threshold of surface energy interaction between drug and carrier particles is required to facilitate better dispersion of cohesive drug particles and increase aerodynamic performance. Below this threshold, drug particles may remain aggregated and produce low FPF (Cline and Dalby, 2002). In addition to median surface energy values and energy distribution, a wider set of data can be obtained from the IGC measurement of surface energy. Work of cohesion and work of adhesion, which represent the thermodynamic interaction between similar and dissimilar surfaces respectively can be calculated. Using these values, a cohesion-adhesion balance, which is the ratio of work of adhesion to work of cohesion can be obtained. Interestingly, a review of studies in which the in-vitro inhalation performance of DPI formulations is correlated with the cohesive-adhesive balance identifies also shows a similar trend as those mentioned earlier. (Jones et al., 2008) investigated 16 drug-carrier formulations; optimal performance was reported in those with a slightly cohesive cohesion-adhesion balance. Another study by (Hooton et al., 2006) investigated the correlation between the cohesion-adhesion balance of salbutamol sulphate with different carriers and FPF, they reported similar findings; a corresponding increase in FPF with increase in cohesion-adhesion balance. These findings all agree that a level of drug-carrier adhesion has to exist for optimal DPI performance. However, there is need to control this API-carrier adhesion strength to enable optimal separation of API from carrier particles when required.

The investigation of surface energy and its derivatives provides useful information about DPI formulations, demonstrating that both cohesive forces between micronized API particles and

adhesive forces between API and carrier particles are critical to aerodynamic performance. While the use of surface energy, surface energy interactions and cohesion-adhesion balance (CAB) approach cannot precisely replicate the exact interactions between drug and carrier particles in a formulation; the ability to quantify surface interactions between drug and carrier may provide a useful structure to predict and optimise the possible behaviour and performance of carrier based DPI formulation. The quantitative representation of surface interactions eliminates the subjectiveness associated with qualitative examination, and mathematical and statistical models can be used to predict and optimise DPI formulation performance. Correlations obtained in this way may accommodate other particle properties such as size, shape, morphology, polymorphic form, presence of impurities etc., as these factors all contribute to the surface energetics of the particle. Despite the promising prospects of using surface energy for formulation development, it is unlikely that a one-size-fits-all approach will be found. This is because surface energy values are specific to materials; therefore, significant changes in formulation behaviour may be expected with different carriers and APIs as a function of their differing cohesive–adhesive properties. Considering that lactose is the most commonly used carrier, a larger proportion of research should be dedicated to lactose. Even for carrier free formulations in which all the particles are drug particles, the focus on how drug surface properties and cohesive behaviour can be optimised for DPI formulation performance is useful.

One interesting way of optimising surface interactions for DPI formulations is to leverage the acid-base component of particle surface energy, as it is useful in predicting drug-carrier interactions. The acid-base parameters of a drug of interest and potential carrier particles once determined can be compared to identify the drug-carrier combination that will produce the desired strength of interaction (SMS, 2013). This will be particularly useful in DPI formulations where a reversible drug- carrier interaction is desirable especially when explored using a quality by design approach.

1.9 Pharmaceutical Quality by design

Quality by design is the process of building quality into a product rather than examine the final product for deficiencies. In the Pharmaceutical industry, QbD is crucial to patient safety, and reproducible efficacy of drug products. These are achieved through manufacturing process characterisation, which ensures that consistent manufacturing processes are used to develop quality products that deliver the proposed action of the product consistently (ICH, 2009; Sangshetti et al., 2014). The concept of QbD involves having a desired quality for the intended product and defining the critical quality attributes (CQAs) of the product. A scientific understanding of the pharmaceutical processes and methods is then required, particularly identifying the critical process parameters (CPPs) and material attributes and how they influence the CQAs of the final product. This understanding allows the manufacturer to develop a process control strategy to achieve the desired product quality, in terms of efficacy and safety, rather than test the final product for quality. QbD benefits both consumers and manufacturers; for consumers, it consistently ensures their safety and the efficacy of drug or drug products, while for manufactures it controls production cost and eliminates the need for a trial and error approach to achieving quality in product development (ICH, 2009; Sangshetti et al., 2014).

The development of DPI formulations is still largely restricted to trial and error experimental approaches, due to the fact that interactive effects of particle properties that influence DPI formulation performance are complex and difficult to quantify. The capability of using measured particle properties in prediction of DPI formulations performance is slowly becoming a reality in combination with the development of new mixing technologies. Particularly, the novel isothermal dry particle coating, the device of interest in this research, which potentially allows a reproducible scientific approach for the preparation of interactive mixtures for carrier-based DPI formulations (Dahmash E.Z, 2016 PhD thesis). With the bulk of the formulation being the carrier, there is need to establish a relationship between a quantifiable carrier particle property and DPI formulation performance. This will enable the use of QbD approaches to build quality into DPI formulations in the early formulation stages, rather than

evaluating their quality through the resultant performance. The prevalent use of lactose as the carrier of choice in DPI formulations has resulted in extensive research on its modification to optimise DPI formulation performance. Effects of particle size, particle size fraction, shape, morphology and surface additives of lactose have been investigated with useful discoveries. Through more research of the dynamics of particle interaction, cohesive and adhesive forces and their roles in the deagglomeration of composite particles, it is possible to relate quantifiable particle properties such as surface energy and other surface energy derivatives to DPI formulation performance. Using these values, a more direct and less ambiguous relationship has been established with DPI formulation performance. This presents an advantage of predictability along with optimisation over the conventional empirical methods that have been used to date. There is still a knowledge gap in how best to apply carrier particle modification methods to deliver predictable formulation performance through QbD. Although some work has been done using this approach, discoveries based on a robust experimental design is still lacking. This needs to be investigated, particularly for different grades of alpha lactose monohydrate to generate a better understanding of this widely used carrier.

1.10 Research aims and objectives

Despite the development of new mixing technologies, which are suited for the formulation of powder based delivery systems, and the growing use of carrier – based DPIs, the relationship between lactose, the most commonly used carrier for DPIs, physicochemical properties and DPI formulation performance is still vague, and the optimisation of formulation is largely dependent on a trial and error approach. The difficulty in studying in isolation, the critical lactose physicochemical properties, which affect DPI performance, has stalled advancements in associating any one lactose property to resultant DPI performance. The success of the novel iDPC device to consistently produce composite materials and its success in overcoming prevalent challenges faced by other dry coating technologies such as particle attrition and heat generation, which further complicate the complex interactions between carrier physicochemical properties that limit DPI formulation performance prediction, make it a suitable candidate for DPI formulations.

The primary aim of this research is to use the mechanistic understanding of the iDPC to explore the formulation of optimal lactose – based dry powders for inhalation through a Quality by design approach. The objectives of this work are therefore:

- Development of a mechanistic understanding of the novel isothermal dry particle coating (iDPC) device with respect to the established mechanisms of dry particle coating
- Determination of lactose surface modification by processing in the iDPC device
- Development of optimal lactose – based DPI formulations employing the mechanistic understanding of the iDPC, carrier selection and a Quality by design approach
- Determination of the role of surface energetics in the performance of DPI formulations prepared in the iDPC device

2. Chapter Two

Proof of Concept – Mechanistic Understanding of Novel Aerosolized and Isothermal Dry Particle Coating Device (iDPC)

2.1 Introduction

Mixing is a unit operation in several manufacturing processes, and it is critical to many industries such as pharmaceutical, food, engineering and cosmetic. The aim of mixing is to achieve a homogenous mixture using minimal energy and within the shortest time (Daumann et al., 2009, Fan et al., 1970). A homogenous mixture is one with equal amounts of constituents throughout the whole mixture, the components of a homogenous mixture are uniform throughout the whole blend, and random samples, which are expected to be representative of the whole mixture, are analysed to determine blend homogeneity. The mixing process of powders used in DPIs and other pharmaceutical formulations is vital to the quality and performance of the product. The need for blend homogeneity in DPI formulation blends cannot be over-emphasised, as this directly affects drug content uniformity, the lack of which may result in over dosing of API, dangerous side effects and potential death or the under dosing of API of which may result in poor therapeutic effect and deterioration of patient disease and health. (Bridgwater, 2012, Fan et al., 1970).

Segregation and agglomeration are the two phenomena that impede good mixing. The properties of powders to be mixed determine which of these two phenomena will affect them. While free flowing powders have the tendency to segregate, cohesive particles are more likely to agglomerate. These properties are usually considered when choosing a suitable mixer for a powder based on the powder properties. Segregation is a common problem that occurs when particles that differ in size density or shape are mixed, difference in size being the most important factor that predisposes particles to segregation (Alonso and Alguacil, 1999). Generally, smaller particles tend to move down between the inter-particle spaces. However, when cohesive powders are involved, their higher inter-particle interaction reduces mobility hence; they tend to form agglomerates rather than segregate.

Studies carried out to control segregation led to the discovery of “ordered mixtures”. Ordered mixtures are particulate systems created by the adsorption of cohesive particles on the surface of larger particles through mixing (Saharan et al., 2008)

Hersey et al., (1975) established that when fine particles are mixed with coarse particles of at least a twofold difference in size, rather than segregate, the smaller particles attach to the surface of the larger ones, which are able to serve as carrier particles. They form particulate systems, called ordered mixtures (Hersey, 1975 cited in Pfeffer et al., 2001; Alonso and Alguacil, 1999). The negligible impact of gravity on the fine particles limits its mobility; the force of adhesion between the host and guest particles also exceeds the weight of the guest particle. These combine to ensure that the guest particles are not easily detached from the host particle surface (Pfeffer et al., 2001, Saharan et al., 2008). Figure 2.1 shows a graphical illustration of ordered mixture formation.

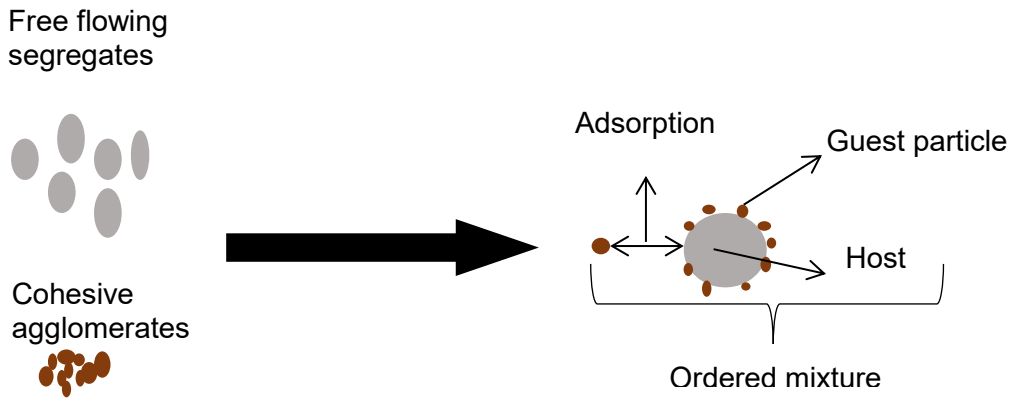

Figure 2.1 Graphical illustration of ordered mixing; smaller (guest) particles are attached to the surface of larger (host) particles to form composite particles; interaction is mainly by physical adsorption.

Ordered mixtures comprise primary composite units, which all have similar compositions. This allows for better homogeneity than a typical random mixture. The tendencies for segregation and/or agglomeration are also reduced in ordered mixtures. Ordered mixtures have also been used to improve dissolution of poorly soluble drugs by using soluble host materials (Saharan et al., 2008). The concept of ordered mixing leverages the high inter-particle forces that exist between cohesive particles as described earlier. However, the high sensitivity of these forces to small changes makes them insufficient to sustain the integrity of the ordered mixtures for practical use; as the attachment obtained is reversible. There is therefore the need to modify the process to achieve more stable composite particles (Pfeffer et al., 2001, Singh et al., 1997,

Dahmash and Mohammed, 2015). Dry particle coating was subsequently developed out of the ordered mixing concept, but with the cutting edge of stronger host-guest attachment produced by the mechanical forces generated by the coating device used (Honda et al., 1991; Pfeffer et al., 2001).

2.2 Dry Particle Coating

Dry particle coating is a particle engineering process used to modify the surface characteristics of particles. Submicron (guest) particles are coated onto the surface of micron sized (host) particles with the aid of strong mechanical forces generated by the coating device (Pfeffer et al., 2001). This results in the production of a compound or composite particle, with enhanced properties different from those of the individual particles (Gera et al., 2010; Pfeffer et al., 2001). The process of ordered mixing was qualitatively explained by Bannister and Harnby (1983) in three stages as follows

1. Deagglomeration of fine guest particles into individual particles
2. Attachment of the individual particles onto the host particle surface in close proximity to them
3. Redistribution/rearrangement of the fines between already coated and non-coated host particle surfaces upon further collisions to attain an even distribution of guest on host particles

Although, these steps are not necessarily expected to occur in this order, the deagglomeration step is critical for the two other steps to occur.

Alonso et al., 1989 later gave a similar quantitative explanation of the process in three stages as follows:

1. Adhesion of cohesive agglomerates to coarse particles in close proximity to them
2. Transfer of fines between agglomerate-coated coarse particles and uncoated ones
3. Redistribution and dispersion of fines between coarse particles occurring through particle collisions until even coating is achieved.

Clearly, the two explanations emphasise the need for deagglomeration of fines and their exchange between coarse particles, either as individual particles or as agglomerates until they are evenly distributed to achieve an even coat. Therefore, for a device to accomplish dry coating, it must be able to generate sufficient mechanical energy to break up these agglomerates. The presence of coarse particles with cohesive agglomerates also helps the deagglomeration process, as the former serve as a channel for breaking up the latter into individual particles (Alonso and Alguacil, 1999; Pfeffer et al., 2001). Figure 2.2 shows a graphical illustration of the dry coating stages.

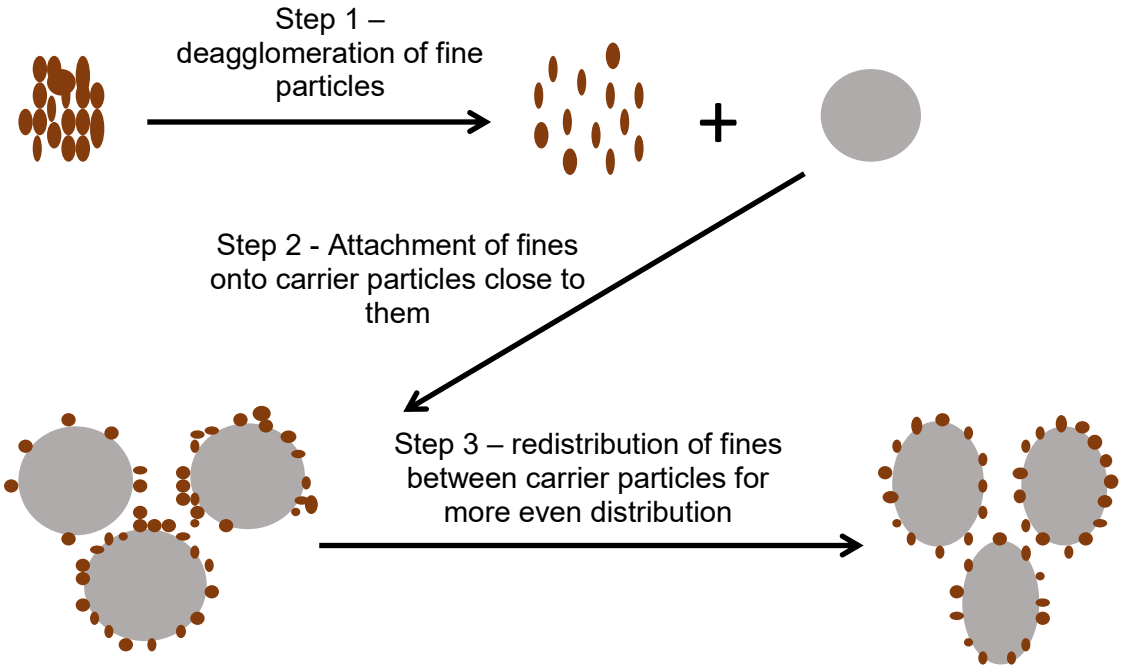

Figure 2.2 Mechanism of dry particle coating, showing the three stages involved. The steps do not exclusively occur in a particular order. However, deagglomeration is a key step, which ensures cohesive particles are broken down to primary particles

The process of dry coating is connected to mixing, as they both involve the adsorption of separate components to form a composite particle. There are three main mechanisms by which mixing occur: convective, diffusive and shear mixing, these are described in more detail

in chapter one. The mixer design determines which mechanism is predominant and it is essential for these to be considered to achieve a homogenous mixture (Fan *et al*., 1970).

2.3 Novel Isothermal Dry Particle Coating Device (iDPC)

The novel aerosolized and isothermal dry coating device that was used in this study will be henceforth referred to as the Isothermal Dry Particle Coating Device (iDPC). The iDPC was developed based on the principles of (1) High G-force (2) Diffusional and convectional currents and (3) Shear and compaction forces (Dahmash E.Z. PhD thesis, 2016). In the design of this device, the three mixing mechanisms described above have been deployed.

The laboratory scale device which is shown in figure 2.3 consists of the following units:

1. A rotating cylindrical vessel which houses the powders to be dry coated. This vessel is connected to a rotating motor that enables motion.
2. A hollow shaft which stays perpendicular to the radius of the rotating vessel; this shaft serves as both inlet and outlet for nitrogen gas. Nitrogen gas enters into the system under pressure through tiny apertures on the hollow shaft, while two air vents attached to the shaft collect nitrogen gas from the system to the outside. The apertures are directed towards the powder bed to aid deagglomeration.
3. Nitrogen gas is supplied from an external source through tubes connected to the hollow shaft.
4. The rotating vessel is covered on both sides with metal end pieces which prevent the loss of materials (Dahmash E.Z. PhD thesis, 2016).

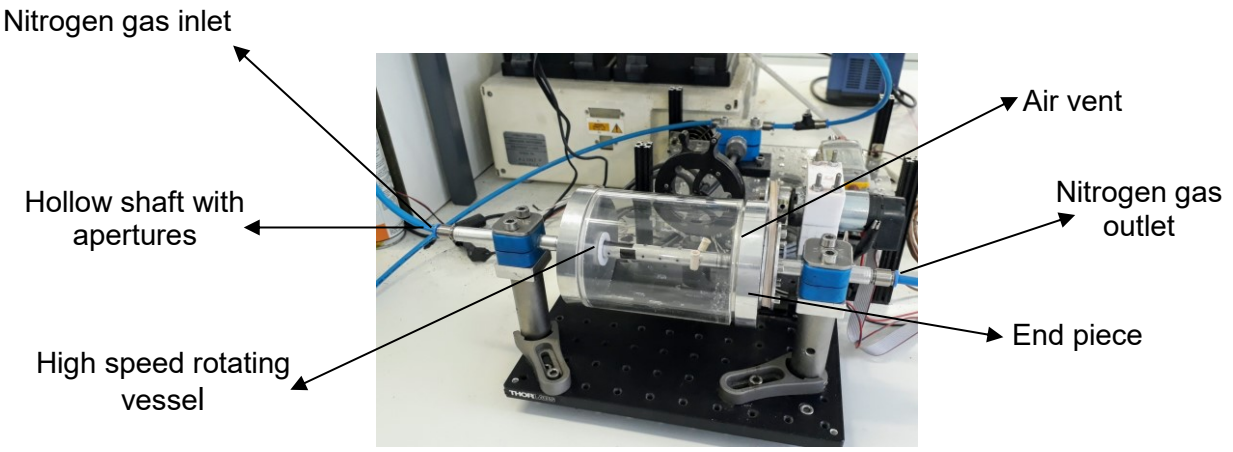

Figure 2.3 Novel laboratory scale iDPC for dry particle coating showing the different units

Since the dry coating process seeks to exploit the attraction force between host and guest particles which is greater than the weight of the guest particle; it is important for every dry coating device to be able to first deagglomerate the cohesive guest particles. This device was developed based on this principle; to enable deagglomeration and subsequent adhesion of the guest to host particles without altering the intrinsic properties of the individual components of the composite particles (Dahmash E.Z. PhD thesis, 2016)..

While the vessel is in motion, centrifugal force (G-force) is generated along the radius of the vessel which causes particle-particle as well as particle-wall interactions. Nitrogen gas is introduced into the system under pressure to supply additional mechanical energy by promoting collision of host-guest particles within the system. The mechanical energy generated by these two mechanisms combines to deagglomerate the cohesive guest particles and cause the adhesion of the guest onto the host particles. Beyond forming an air-blade for the system, the nitrogen gas also helps to keep the system at ambient temperature thus prevents the accumulation of heat within the system. The inert nature of the nitrogen gas also prevents any potential for reaction between host and guest particles (Dahmash E.Z. PhD thesis, 2016).. The laboratory scale iDPC has capacity for a maximum speed of 3500 rpm which is equivalent to 616G, and a maximum nitrogen flow rate of 40L/min.

2.4 Aim and Objectives

Aim

- To develop a mechanistic understanding of the dry coating process using the iDPC, through qualitative and quantitative measures

Objectives

- To dry coat inhalation grade lactose with particulate rhodamine B, a fluorescent dye
- To evaluate coating efficiency qualitatively and quantitatively
- To use the coating efficiency evaluation to identify the dry coating stages in the iDPC
- To establish a relationship between process parameters and coating efficiency

2.5 Materials and Methodology

2.5.1 Materials

Model powder blends were prepared using Rhodamine B a fluorescent dye and inhalation grade alpha lactose monohydrate, which is commonly used in DPI formulations. Rhodamine B was purchased from Sigma Aldrich®, while inhalation grade alpha lactose monohydrate (Inhalac® 251) was provided by Meggle.

2.5.2 Methodology

2.5.2.1 Particle Size Reduction

The required particle size for the guest material rhodamine B was achieved by milling; using a glass mortar and pestle and passing the milled powder through a 20 micron sieve. Using a Sympatec HELOS (Helium-Neon Laser Optical System)/ RODOS (sample dispersing system) particle size analyser with VIBRI/I feeder (Clausthal-Zellerfeld, Germany), the resultant particle size of the milled rhodamine B and Inhalac® 251 was determined. About 1g of the powder samples were fed into the vibratory feeder, which transfers the powder into the dispersing unit (RODOS). The powder samples were dispersed under compressed air at a pressure of 2 bar into the analyser (HELOS), where the particle size and particle size distribution of the dispersed powder is determined by laser diffraction (rhodamine B VMD – 6.27±0.45µm; Inhalac® 251 as supplied VMD – 52.91±0.42µm).

2.5.2.2 Preparation of Dry Coated Powder Blends

10g each of powder blends were prepared using 0.5% $^{w}/_{w}$ rhodamine B and 99.5% $^{w}/_{w}$ Inhalac® 251. Accurately weighed host and guest powders were gently hand mixed and transferred into the coating device for the dry coating process. The processing parameters, which are shown in table 2.1, were set as follows G-force 201G (2000rpm); nitrogen flow at 0L/min, 25L/min and 40L/min; and duration was varied between 4 minutes to 28 minutes. The processed powder blends were collected and stored in glass vials on shelf.

Table 2.1 Process parameters for dry coated powder blends of α-lactose monohydrate and rhodamine B

Centrifugal force	G-force 201G		
Nitrogen Flow rate (L/min)	**0**	**25**	**40**
Blending duration (minutes)	4	4	4
	8	8	8
	12	12	12
	16	16	16
	20	20	20
	24	24	24
	28	28	28

2.5.2.3 Confocal Laser Scanning Microscopy (CLSM)

Confocal laser scanning microscopy (CLSM) was used as the primary visualisation method in this study. Due to the fluorescent properties of the guest particles, we expected to see the guest particles clearly defined against the non-fluorescent host particles. All processed powder blends as described above were observed on a Leica Mirosystems Confocal Microscope TCS SP5 II, using a 10X dry objective lens. The dry coated powder samples were placed on a slide and viewed under the microscope as such, no further treatment was required. Images of the dry coated powder blends were obtained between 528-560nm.

2.5.2.4 Scanning Electron Microscopy (SEM)

SEM was used to corroborate the images obtained from the confocal laser microscopy. Powder samples were dispersed onto a double-sided adhesive carbon tape and placed on a sample holder. In order to maintain the original state of the surface coating as much as possible, no surface metallization, such as gold or platinum coating was done to these set of samples. The samples were imaged as such, using a field emission scanning electron microscope Zeiss Supra SS-VP (Zeiss, Oberkochen, Germany). Using an accelerating voltage of 1.0kV, which allows for imaging without gold coating, images were taken at 1000X, 4000X and 5000X magnification.

2.5.2.5 Particle Size Analysis

The particle size of the powder blends was measured using Sympatec™ HELOS/RODOS particle size analyser which works by laser diffraction principle. Powder samples were fed into a vibratory feeder which transfers the powder into the dispersing unit (RODOS). The powder samples were dispersed under compressed air at a pressure of 2 bar into the analyser (HELOS), where the particle size and particle size distribution of the dispersed powder is determined by laser diffraction. X_{10}, X_{50}, X_{90} and VMD values were recorded for each sample.

2.5.2.6 Image Analysis

The confocal laser microscope images were processed with a Java image processing and analysis programme; Image J version 1.50i. The images were analysed on the basis of: fluorescence intensity, degree of coverage and size of agglomerates. Intensity was measured by drawing a region of interest (ROI) around the particles; the average intensity of the image (calculated from intensities of different areas of the image) is given as a value. The degree of coverage was measured by converting the image to an 8 bit gray scale image; the watershed function on the program was used to separate clusters of particles by drawing a 1 pixel thick line at assumed boundaries. The numbers of particles were counted as an indication of the rhodamine B particles on the coated surface of the lactose particles (since the lactose particles blend with the field of view, and are only made distinct by rhodamine B coated onto their surfaces). Values given for number and average size of particles were used as an estimate of degree of coverage and size of agglomerates respectively.

2.5.2.7 Statistical analysis

Statistical analysis of particle size distribution analysis was done using GraphPad Prism 8 software, using a one-way ANOVA test.

2.6 Results and Discussion

2.6.1 Imaging and Qualitative Characterisation of dry coated powders

In this study, model dry coated particles were prepared using rhodamine B and α-lactose monohydrate, to ascertain the capability of the iDPC to produce composite particles of cohesive guest particles and coarse carrier particles. The data are presented in form of qualitative and quantitative image analysis as well as particle size analysis data.

Using the images obtained from the confocal laser scanning microscopy, the coating efficiency of the novel dry coating device was qualitatively assessed. The fluorescent nature of the rhodamine B enabled us to see it clearly deposited on the surface of the non-fluorescent lactose. Although the composite particles are formed as single particles, their colour difference enabled recognition of the primary particles which is critical in characterisation (Wei et al., 2002). Since handling and storage challenges the integrity of any mixing process more than during the actual mixing process, it is suggested that sampling be done after the mixing process and outside the mixing vessel (Alonso and Alguacil, 1999). All imaged powder samples in this experiment were taken after the composite powder blends had been transferred into glass vials for storage. All confocal imaging was also done on the same day the powder blends were produced. This was to prevent any error due to increased fluorescence which was noticed on storage of the powder blends. Micrographs were taken under the fluorescent field only, as well as bright and fluorescent fields combined. This was done to clearly identify the outline of the lactose particle surface upon which the particulate rhodamine had been deposited. It is clear from the images obtained that rhodamine was coated onto lactose surface. The fluorescence intensity, degree of coverage and presence and size of agglomerates were qualitatively assessed. Coating efficiency was evaluated based on these three factors and their progression with change in process parameters was assessed. Optimum conditions also exist for mixing processes. Demixing, which is described as the segregation of coarse from fine particles due to differences in particle size, shape and density, may begin to occur if optimum conditions are exceeded (Pilcer et al., 2012). More so, mixing and demixing both occur through the same mechanisms i.e. interparticle percolation

and particle migration (Alonso and Alguacil., 1999). The potential to reach the stage of segregation was identified in this study.

In order to mimic the features of a carrier-based DPI formulation, the rhodamine particles used in this study were micronized to obtain particles of VMD 6.27±0.45μm. Usually, as particle size is reduced, particle weight becomes less than the interparticulate force between them. This results in a high inter-particulate force/weight ratio i.e. bond number which causes cohesion. The high bond number and drag force (i.e. air resistance / force opposing particle motion), resist particle motion in bulk powder and cause such fine particles to form agglomerates. In addition, milling increases the thermodynamic activity of particle surface, which also contributes to cohesion. The resulting cohesiveness makes it difficult to handle and formulate fine particles (Castellanos, 2005, Yang et al., 2005).

To achieve a homogenous blend, these cohesive agglomerates of guest particles, rhodamine in this case, must be broken down and dispersed onto the lactose carrier surface. Figures 2.4, 2.5 and 2.6 show the confocal microscopy images of rhodamine B coated onto lactose surface at 10X magnification. The fluorescent rhodamine B are seen as the red colour coated round defined portions of the field of view, which outlines the non-fluorescent lactose. This images show that the iDPC is capable of coating fine cohesive powders (rhodamine) onto larger carrier surfaces (lactose). The quality of coating achieved however differs based on the process parameters used.

2.6.1.1 Effect of nitrogen blade on blend quality

Figure 2.4 A – C show the composite powder blend images at 4 minutes with no nitrogen flow i.e. 0L/min, and nitrogen flow at 25L/min and 40L/min respectively. These images show a progressive coverage of rhodamine on lactose particles as nitrogen is introduced. Although, some coverage is seen without nitrogen flow, more coverage can be seen at 40L/min compared to when no nitrogen flow is used. The same trend is observed for the composite powder blends processed at 8 minutes (figure 2.4 D-F); and 12 minutes (figure 2.4 G - I). Some of the visible agglomerates in the field of view are circled in green. Their size and

number can be seen to have reduced with the introduction of nitrogen flow at 25L/min and 40L/min, this is attributed to increased energy input in the blending process, which facilitates deagglomeration of the cohesive rhodamine powder and their dispersion onto the coarse lactose carrier. A previous study by Le et al. (2012) demonstrates a correlation between energy input during the mixing and blend homogeneity. The researchers used increasing percentage of mixing aid (silica-gel beads) in a TURBULA® mixer to blend cohesive fluticasone propionate with α-lactose monohydrate. They observed increasing blend homogeneity, demonstrated by progressively reducing RSD values, which was significant up to 30% silica-gel beads (de Boer et al., 2012, Wei et al., 2002).

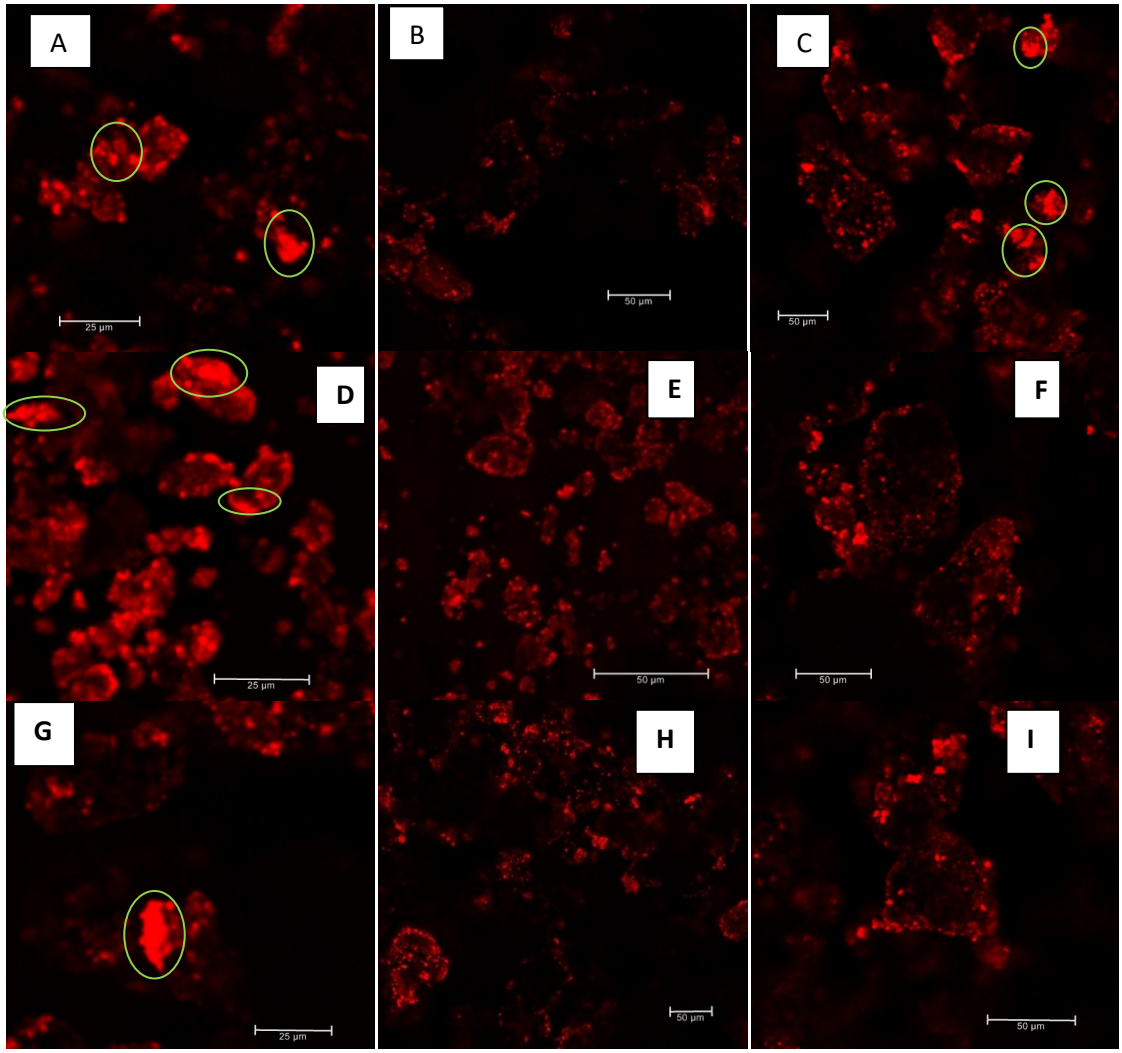

Figure 2.4 Confocal images of dry coated powder blends at 201G (rotation speed of 2000rpm) A-C at 4 minutes, 0L/min, 25L/min and 40L/min respectively; D-F at 8 minutes, 0L/min, 25L/min and 40L/min respectively and G-I at 12 minutes, 0L/min, 25L/min and 40L/min respectively

In this study, our observations reveal the synergistic effect of the nitrogen-blade in generating additional mechanical energy to break up cohesive agglomerates of rhodamine and promote the whole coating process. This demonstrates that the nitrogen-blade is critical to producing shear forces which are necessary to break up agglomerates. To support this claim, computational fluid dynamics (CFD) done to simulate the interactions between the solid and gaseous multiphase within the iDPC show that at nitrogen flow rates of 40L/min, vortexes are generated within the system, which causes both host and guest particles to be displaced towards the mixing vessel wall in the form of a powder mass. In addition, the pressure from the nitrogen blade promotes frequent collision of the particles, which aids mixing (Dahmash

E.Z. PhD thesis, 2016).. The mechanism highlighted by the CFD may be likened to what occurs in convective mixers, where the rotating impeller moves the powder against the mixing vessel (Fan et al., 1970; Bridgwater, 2012). When this occurs, slip zones will certainly be created between these powder blocks (Alonso and Alguacil, 1999) providing shear regions where agglomerates can be broken up (Bridgwater, 2012). In contrast to convective mixers, in which the impeller is a solid surface usually made of metal, the nitrogen blade simulates the impeller in the iDPC. On the other hand, the CFD studies also showed that at low nitrogen flow rate of 5L/min, vortexes were absent within the blender; although the whole mixing vessel still served as an “active particle interaction zone” (Dahmash E.Z. PhD thesis, 2016). The presence of an active particle interaction zone without the nitrogen blade suggests that mixing will still take place without the nitrogen blade, probably through the diffusive mechanism, generated by vessel rotation. Although, it will require longer processing duration than when the nitrogen blade is present to achieve deagglomeration and blend homogeneity. Consequently, nitrogen flow rate is expected to be directly proportional to earlier onset of deagglomeration and accelerated dispersion of cohesive rhodamine particles.

2.6.1.2 Effect of mixing duration on blend quality

Evidence from literature demonstrates the importance of including the scope of time into energy input, as it contributes to adhesion forces, which affect adhesion of guest to carrier particles during blending (Apte, 2012). Figure 2.4 A – F show the composite powder blends as duration increases from 4 minutes to 8 minutes. There is an increase in coverage of the lactose particles by the rhodamine B particles, the same observations are made up to 12 minutes, as shown in Figure 2.4 G – I . Agglomerates of rhodamine are present in the field of view from 4 minutes to 12 minutes (figure 2.4 A - I). The number and size of the agglomerates however reduce as duration increases. This is attributed to the initial deposition of fine particle agglomerates on host lactose surface, which are broken up by shear forces as processing time increases.

The process of ordered mixing was qualitatively explained by Bannister and Harnby (1983) in three stages as follows

1. Deagglomeration of fine guest particles into individual particles

2. Attachment of the individual particles onto the host particle surface in close proximity to them

3. Redistribution/rearrangement of the fines between already coated and noncoated host particle surfaces upon further collisions to attain an even distribution of guest on host particles. Although, these steps are not necessarily expected to occur in this order, the deagglomeration step is critical for the two other steps to occur.

Alonso et al., 1989 later gave a similar quantitative explanation of the process in three stages as follows:

1. Adhesion of cohesive agglomerates to coarse particles in close proximity to them

2. Transfer of fines between agglomerate-coated coarse particles and uncoated ones

3. Redistribution and dispersion of fines between coarse particles occurring through particle collisions until even coating is achieved.

Clearly, the two explanations emphasise the need for deagglomeration of fines and their exchange between coarse particles, either as individual particles or as agglomerates until they are evenly distributed to achieve an even coat. Therefore, for a device to accomplish dry coating, it must be able to generate sufficient mechanical energy to break up these agglomerates. The presence of coarse particles with cohesive agglomerates also helps the deagglomeration process, as the former serve as a channel for breaking up the latter into individual particles (Alonso and Alguacil, 1999; Pfeffer et al., 2001). Therefore, the size of the carrier particles and the duration of mixing are two factors that presumably contribute to the decrease in the number and size of the agglomerates observed as duration increases. However, the same carrier was used in the preparation of all the blends, which rules out carrier size as a variable. This makes duration the only remaining variable, when centrifugal force and nitrogen flow rate are kept constant. The observations agree with the quantitative explanation of the dry coating process given by Alonso *et al*., (1989). Similar results have also

been reported with other high shear dry coating devices (Sato et al., 2012, Sato et al., 2013). The deagglomeration step involved in fine powder processing prolongs the dry coating process, therefore at the shortest coating duration; no extensive coating is expected to have occurred. The observations also suggest that as processing duration increases, with or without the air-blade, the agglomerates are broken up by mechanical forces generated; either by centrifugal forces only or in combination with the air-blade. The CFD studies by Dahmash E.Z. PhD thesis (2016).corroborates this observation, since there is an active particle interaction zone without the nitrogen blade where mixing still occurs

The presence of a large rhodamine B agglomerate at 12 minutes (figure 2.4 G – I) suggests that although deagglomeration may have started, it does not appear to have occurred throughout the sample. This was confirmed by the presence of fewer and smaller agglomerates at 16 minutes (figure 2.5 A – C) after which no agglomerates were visible anymore.

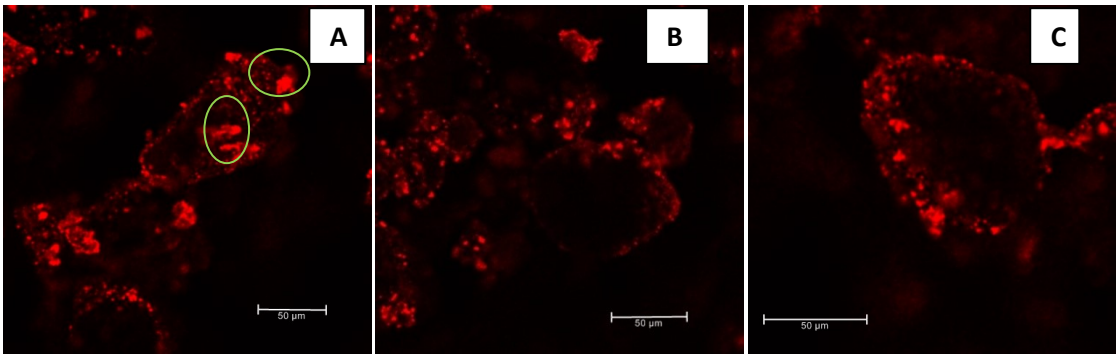

Figure 2.5 Confocal images of dry coated powder blends at 201G (rotation speed of 2000rpm) A-C at 16 minutes 0L/min, 25L/min and 40L/min respectively

Figure 2.5 A – C show the composite powder blend images at 16 minutes with no nitrogen flow i.e. 0L/min, and nitrogen flow at 25L/min and 40L/min respectively. Beyond this point, no agglomerates were visible in the field of view again. This suggests that the cohesive rhodamine B was completely deagglomerated between 16 minutes and the next time point which was 20 minutes (figure 2.6 A – C). The images obtained at 16 minutes (Figure 2.5 A-C) also show more coverage of the rhodamine B particles on the lactose surface compared to

shorter durations (figure 2.4 A-I). This suggests that dispersion and redistribution could also have started at this time point. As duration is further increased to 20 minutes and above, the effects of these two stages on coverage become more evident as seen in Figure 2.6 A-I.

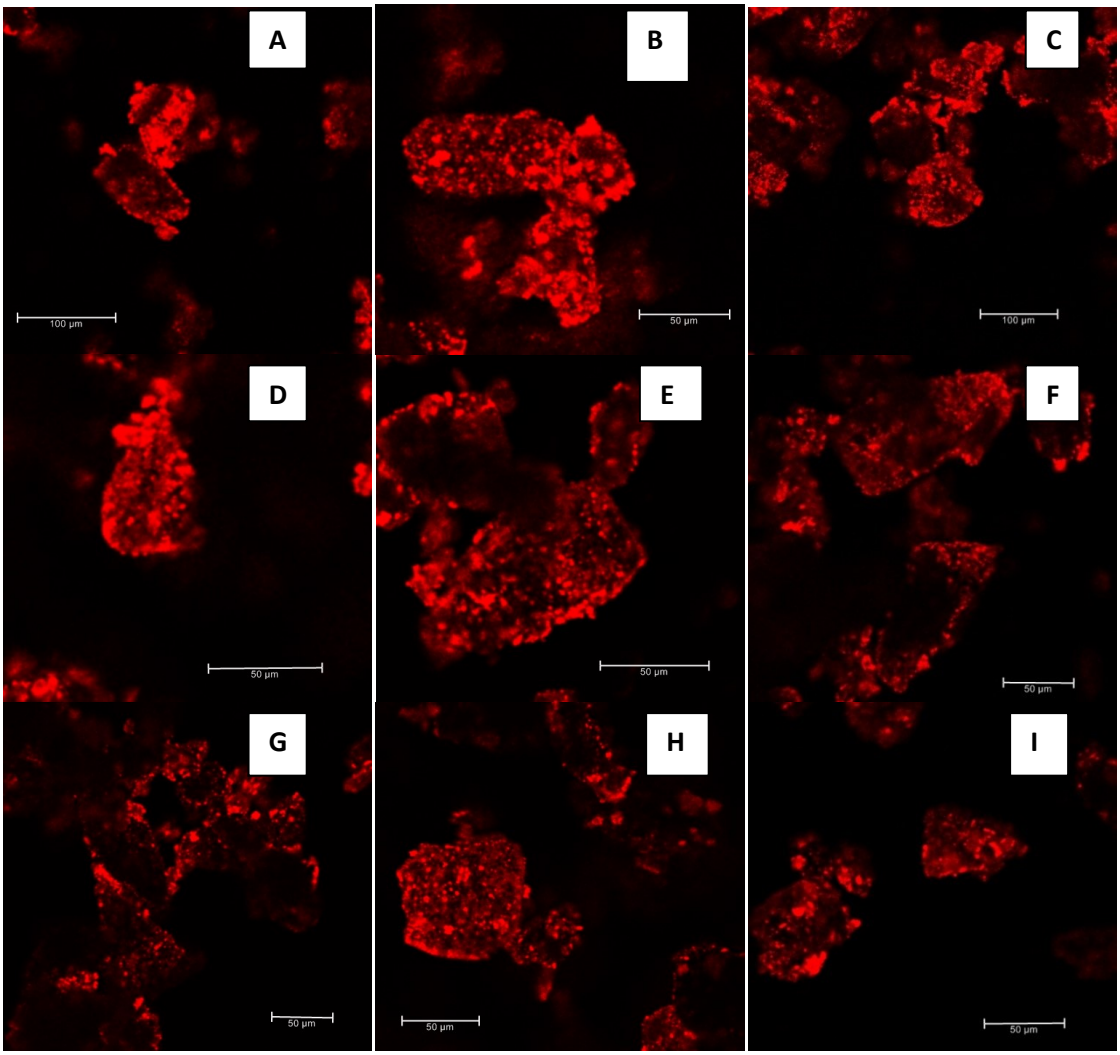

Figure 2.6 Confocal images of dry coated powder blends at 201G (rotation speed of 2000rpm) A-C at 20 minutes, 0L/min, 25L/min and 40L/min respectively, D-F at 24 minutes, 0L/min, 25L/min and 40L/min respectively and G-I at 28 minutes, 0L/min, 25L/min and 40L/min respectively

Figure 2.6 A-C show the composite powder blend images at 20 minutes with no nitrogen flow i.e. 0L/min, and nitrogen flow at 25L/min and 40L/min respectively. These images reveal full coverage of the lactose particles by the rhodamine B, no agglomerates are visible even without nitrogen flow (figure 2.4 A); similar trends are observed at 24 minutes and 28 minutes (figure 2.6 D-I). These suggest that the initial deposition of rhodamine B agglomerates on the surface of the lactose particles has been replaced by a more uniform film-like deposition of individual particles (Sato et al., 2012; Sato et al., 2013). This may be explained by the mechanical deagglomeration of the cohesive fines already deposited onto lactose surface either by high

shear force (Sato et al., 2012; Sato et al., 2013) or by high centrifugal force due to high rotational speed (Dave et al., 2003). This deaggloemeration is then followed by rearrangement or redistribution of the individual fines between coated and uncoated lactose particles (Alonso *et al*., 1989). This may be attributed to continuous particle – particle collision throughout the blending process. Since particle-particle or particle-wall interactions occur irrespective of the predominant mixing mechanism, redistribution or rearrangement of primary fine particles will be facilitated with or without nitrogen flow, provided that the centrifugal force is applied long enough. However, with the nitrogen flow present, there is faster deagglomeration, which aids the coating of the fine particles onto the carrier particles. Consequently, without the nitrogen blade, longer processing duration is required to replicate the results obtained when nitrogen blade is used. A high rotational speed up to 2000 rpm, which was used in this study, has also been reported to cause redistribution at shorter duration, although with a different device (Sato et al., 2012).

2.6.2 Scanning Electron Microscopy

SEM images of composite powder blend samples at the 16 minutes time point were taken (figure 2.7 A-I). Since this was the last time point where agglomerates were observed in the CLSM images; images were taken to evaluate the coverage of the particles across the different nitrogen flow rates. The images at this time point confirmed the initial deposition of rhodamine B agglomerates onto the lactose surface. In addition, the impact of nitrogen flow on deagglomeration and in facilitating dispersion and redistribution for even coating was confirmed.

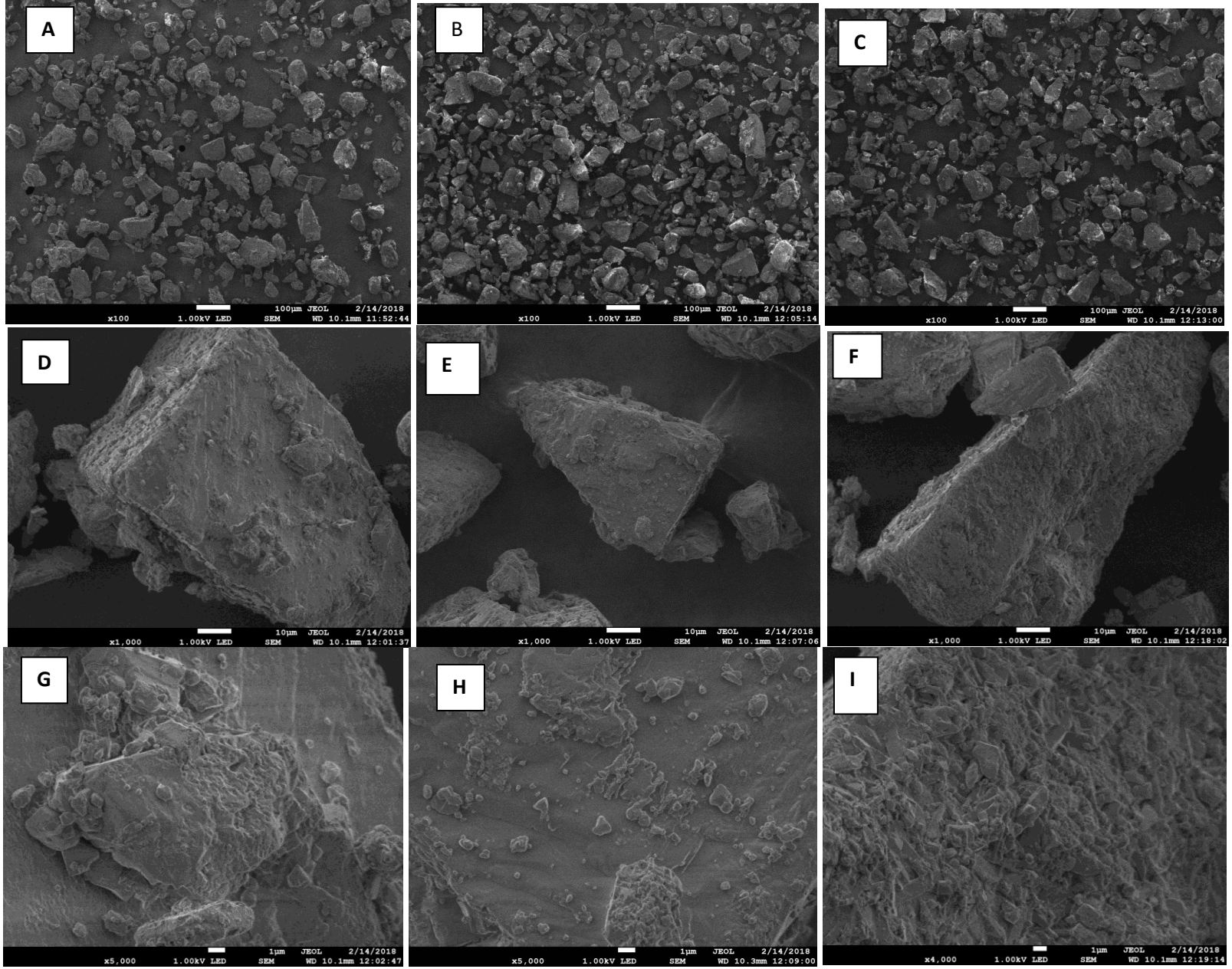

Figure 2.7 SEM images of composite powder blends at 16 minutes, 201G (rotation speed of 2000rpm) A,D,G at 0L/min, B,E,H at 25L/min and C,F,I at 40L/min respectively

The SEM images at X100 magnification (figure 2.7 A-C) show that with or without nitrogen flow, all the fine rhodamine B particles have been coated onto the surface of the lactose particles, as no fines are visible in the field of view. This agrees with results of earlier studies carried out by Koner et al. (2017) using the iDPC. However, images at X1000 and X5000 magnification reveal that the coating has occurred to different degrees with respect to nitrogen flow. Also, the images at X1000 and X5000 magnification reveal that at nitrogen flow rates of 25L/min and 40L/min (figure 2.7 D-I), there is a progressive coverage of the lactose particles as well as a progressive deagglomeration of the rhodamine B particles compared to when nitrogen flow is absent.

This ascertains the synergistic effect of the air-blade in deagglomeration of fines and the coating process. Large agglomerate size and sparse coverage of lactose particles are evident at 0L/min (figure 2.5 G). Agglomerate size has decreased at 25L/min with some more coverage (figure 2.7 H); while there is full coverage of the lactose particles at 40L/min (figure 2.7 I) with all coating appearing as individual particles rather than as agglomerates. This supports the CLSM observations and suggests that shear forces present, when the air-blade is operating, produce more even coating at a shorter processing time than when the air-blade is absent. It should be noted that because the inhalation grade lactose used contains a large proportion of fines, some of the fine particles coated onto the surface of the lactose particles are the fine portions of the inhalation grade lactose. The progression of the rhodamine B coating from agglomerates to individual fine particles also agrees with Alonso *et al*., (1989) quantitative explanation of the dry coating process which suggests initial attachment of guest particle agglomerates to host particle surface before redistribution occurs.

The CLSM and SEM images are in agreement that coating efficiency progresses as nitrogen flow increases. This is based on the deagglomeration of the fine rhodamine B particles and increased coverage of the lactose particles thought to be enhanced by shear forces generated by the air-blade. These evidences support the ability of this novel technology to carry out the dry coating process.

2.6.3 Quantitative Image Analysis

2.6.3.1 Fluorescence intensity

Image analysis was done using Image J version 1.50i software. The intensity of each 508X480 pixel image was given as a mean of the intensities of the different regions within the whole region of interest selected. Figure 2.8 shows a plot of intensity against processing time for the three nitrogen flow rates used. It is important to note that the intensity of the image background is also reflected in the values given. However, the plot shows a relationship between the process parameters and coating efficiency which is comparable to qualitative observations reported earlier in this chapter.

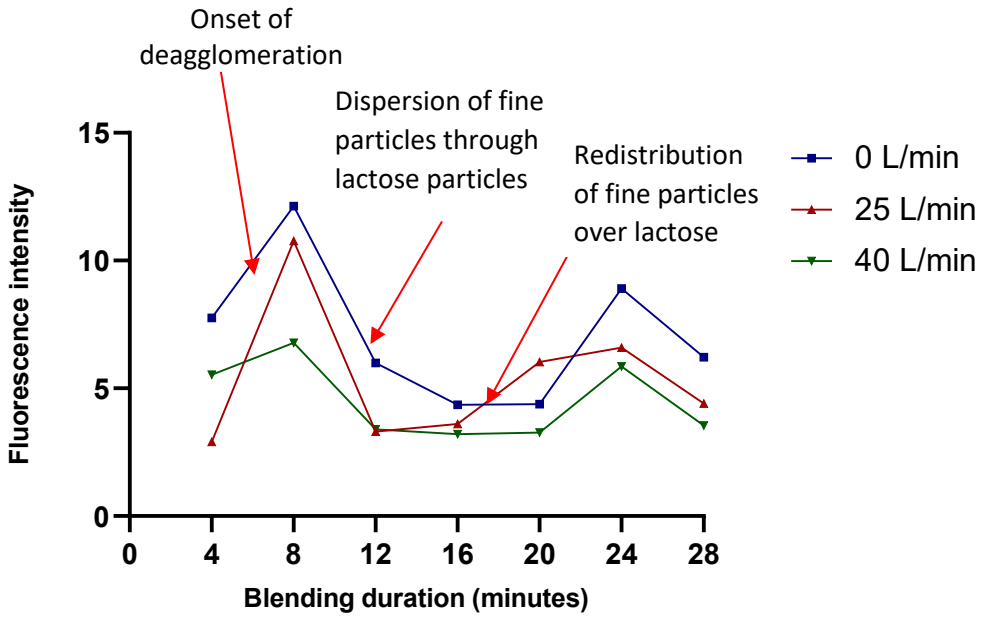

Figure 2.8 Graph of fluorescence intensity against processing duration showing the key stages in the dry coating process and the time points in which they were attained using the iDPC

Colour intensity can be used as an indication of presence of agglomerates as well as onset of deagglomeration. The observed colour or colour intensity of a dye depends on its current position within the absorption band of the dye. This position may be affected by the particle size of the dye (Barling et al., 2015). The initial increase in intensity from 4 minutes to 8 minutes, suggest that the fine powder agglomerates are only spread through the bulk lactose host particles but are yet to be deagglomerated. This agrees with the qualitative observations from the CLSM and SEM images, where there was an initial deposition of rhodamine B agglomerates

on lactose particle surface which was later deagglomerated and redistributed either by prolonged processing time or introduction of nitrogen flow.

As processing time is increased up to 12 minutes, the fluorescence intensity begins to decrease. This decrease in fluorescence intensity may be attributed to the onset of deagglomeration with the possibility that deagglomeration has not fully occurred. This is supported by the CLSM image (figure 2.4 G) of 12 minutes at 0L/min where one large agglomerate was visible. According to Barling et al (2015), a change in colour at constant intensity was expected and observed as the agglomerates began to break up; although, this is an iron oxide pigment property. Here, no colour change was observed, but intensity was constant between 12 minutes and 20 minutes especially at nitrogen flow rate of 40L/min. This suggests that the deagglomeration process had reached its peak after 12 minutes. This is supported by the CLSM images (figure 2.4 – figure 2.5) where no agglomerates were seen after 16 minutes (figure 2.5 A-C), suggesting that deagglomeration was completed between 16 and 20 minutes.

Between 20 minutes and 24 minutes, there is an increase in intensity. This increase in intensity is clearly different from the initial increase in intensity from 4 to 8 minutes which was attributed to presence of agglomerates. Rather, this increase in intensity suggests an increased surface area from the complete deagglomeration of the cohesive guest particles. The reduction in particle size of the rhodamine B as a result of deagglomeration changes its position with its absorption spectrum and reflects in fluorescence intensity (Barling *et al*., 2015). This agrees with the rearrangement or redistribution of the individual fines between coated and uncoated lactose particles once complete deagglomeration of the cohesive fines has occurred. Other researchers have explained this observation based on the synergistic effect of the high rotational speed of the device and long processing time (Dave *et al*., 2003; Sato *et al*., 2012).

Three main stages of the dry coating process have been identified as: deagglomeration of cohesive guest powder into individual particles; dispersion and adsorption of the individual particles to host particle surface and redistribution of the individual guest particles among host particle surface to achieve even coating (Pfeffer et al., 2001; Alonso and Alguacil, 1999). These results were used to identify the time points where these three stages occur in the iDPC.

Although, these steps have been said to occur simultaneously, the deagglomeration step is critical for the two other steps to occur (Pfeffer et al., 2001; Alonso and Alguacil, 1999).

Interestingly, after 24 minutes, there is a decrease in intensity which may be an indication that optimum processing time has been reached and demixing has started. This is a delicate time point which may be reinvestigated; as the mixing and demixing process have been suggested to occur simultaneously upon prolonged mixing especially when the participating particles differ in size (Alonso and Alguacil, 1999).

These results also suggest that it is the deagglomeration step that prolongs the dry coating process, and once deagglomeration is achieved, the process need not be prolonged much. Previous studies have also reported loss of functionalities such as flowability and wettability upon prolonged coating (Ramlakhan et al., 2000, Sato et al., 2013). This has been attributed to the deterioration of the coating layer as a result of further collisions beyond optimal duration. Desired features of the composite particles being produced should however be considered in creating a balance in processing time.

It is also important to note the intensity gradient especially between composite particles processed without nitrogen flow (0L/min) and at high nitrogen flow rate of 40L/min (figure 2.6). The lower intensity at high nitrogen flow rate of 40L/min suggests that the deagglomeration, dispersion, redistribution and overall even dry coating was achieved faster at nitrogen flow rate of 40L/min than when no nitrogen flow was used. This supports the input of the air-blade in producing dry coated particles.

Table 2.2 summarises the observations and inferences from the fluorescence intensity plot with regards to stages of the dry coating process.

Table 2.2 Summary of the fluorescence intensity plots showing the key stages in the dry coating process and the time points at which they were reached using the iDPC

Time point	Observation	Inference
4-8 minutes	Increased intensity	Agglomerates still present
8-12 minutes	Intensity decreases	Deagglomeration starts
12-20 minutes	Intensity remains constant	Peak deagglomeration and simultaneous dispersion phase
20-24 minutes	Intensity increases but not related to presence of agglomerates	Redistribution phase
24-28 minutes	Intensity decreases again which may be an indication that demixing has started	Demixing phase which occurs as a result of prolonged mixing

2.6.3.2 Degree of coverage and agglomerate size

The Image J software can also be used to analyse individual particles, by first converting the images to gray scale for analysis. Analysing these surface particles however requires that particles of the same colour are not in contact with each other, as this may be represented as a single particle. When a monolayer continuous coating is achieved however, the guest particles are in contact with each other on the host particle surface. This was minimized by using the watershed function in the program to add one pixel thick lines between some assumed boundaries. In spite of this, not all individual particles were recognised as such. Therefore, it is important to note that the degree of coverage plot (figure 2.10) and agglomerate size plot (figure 2.11) represent estimates and not absolute values. Figures 2.9 A and B show the 8 bit, gray scale, watershed images used for the individual particle analysis.

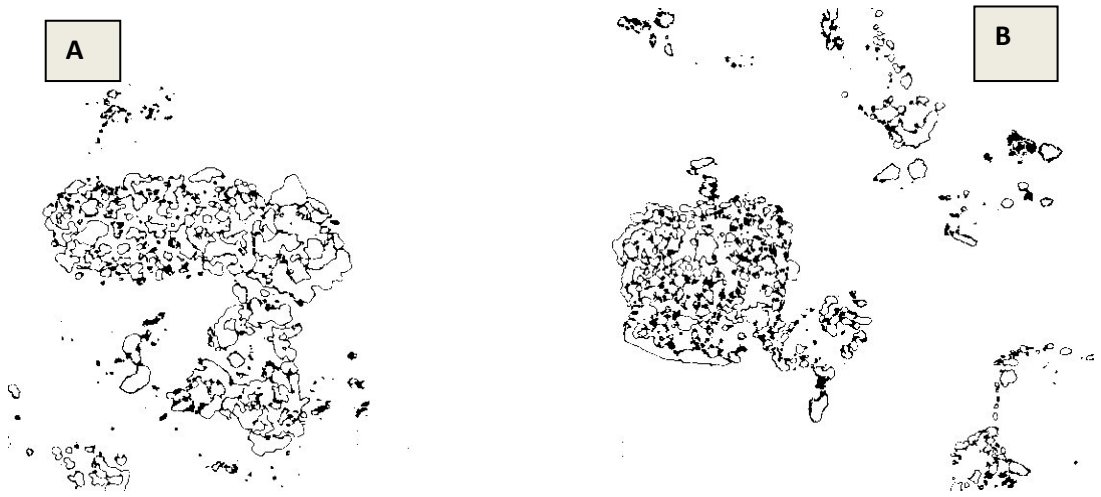

Figure 2.9 8- bit, gray scale, watershed images analysed using the Image J version 1.50i (Compare with figure 2.4 B and 2.4 H respectively)

After transforming the images to this format, the numbers of particles were counted as an indication of the rhodamine B particles coated onto the lactose particles surfaces. Values were given for number of particles and average size of particles; these were plotted against processing time as mean coverage plot (figure 2.10) and agglomerate size plot (figure 2.11) respectively.

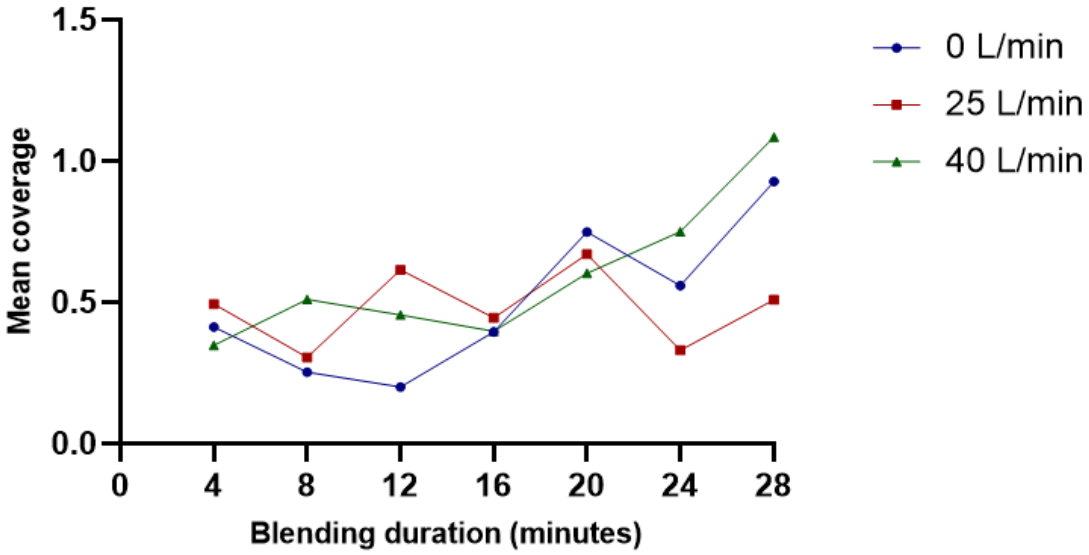

Figure 2.10 Graph of mean coverage of lactose particles by rhodamine B particles over time, showing an increased coverage as processing time increases especially between 0L/min and 40L/min

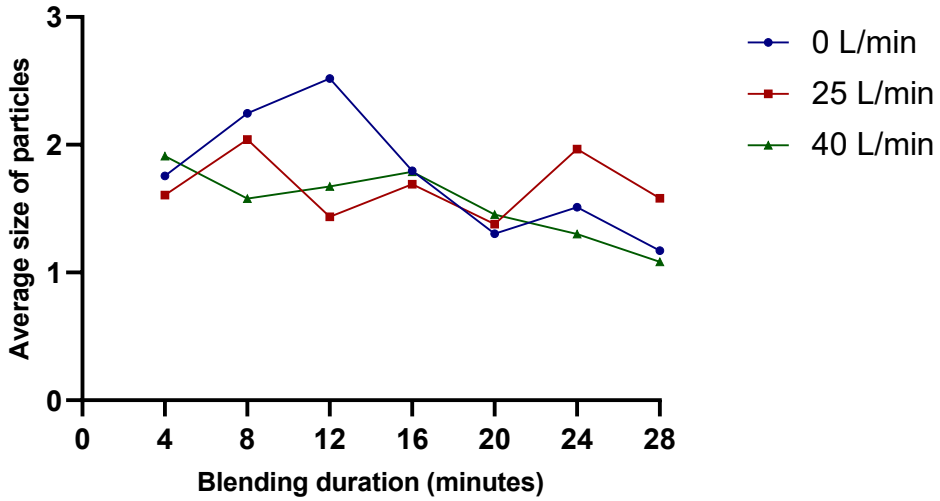

Figure 2.11 Graph of average size of rhodamine B particles on lactose surface, showing a progressive decrease in particle size over time. This indicates progressive deagglomeration of rhodamine B agglomerates.

The mean coverage plot (figure 2.10) and agglomerate size plot (figure 2.11) respectively show an erratic trend for the composite particles produced at 25L/min. This may be as a result of the inadequacy of the image processing software to completely recognise individual particles as such. The trends at 0L/min and 40L/min however support earlier qualitative observations. Coverage is seen to increase over time at 0L/min and 40L/min. Coverage at 40L/min is also seen to be higher than coverage at 0L/min. There is also a progressive decrease in the size of rhodamine B particles coated onto lactose surface with smaller sizes observed at 40L/min. These observations agree with earlier observations of increased deagglomeration and coating as processing is prolonged and faster deagglomeration and coating as nitrogen flow is introduced.

Table 2.3 summarises the degree of coverage plot and agglomerate size plot with respect to coating efficiency.

Table 2.3 Summary of the degree of coverage plot and agglomerate size plot, showing the differences in changes observed with time, between composite particles produced at 0L/min and 40L/min nitrogen flow

Observed changes	0L/min	40L/min
Reduction in agglomerate size	12 minutes	4 minutes
	Larger agglomerates	Smaller agglomerates
Coverage	Later onset	Earlier onset
	Less coverage	More coverage
Duration	Increased coverage with time	Increased coverage with time

2.6.4 Particle Size Analysis

One of the common limitations of existing dry coating devices is their potential to cause particle attrition; as a result of shearing and heat generation that occurs during the dry coating process (Gera et al., 2005). The mechanofusion device and cyclomix which are both high shear devices have been reported to cause particle attrition especially at extreme processing conditions (Ramlakhan et al., 2000, Sato et al., 2013, Yokoyama et al., 1987). Also, the MAIC which is a soft impact device has been reported to cause significant particle attrition (Ramlakhan et al., 2000). However, despite the use of shear forces to break up cohesive powder agglomerates, the iDPC has proven not to cause particle attrition (Dahmash E.Z. PhD thesis, 2016). This may be explained by the use of a nitrogen-blade rather than a solid surface to simulate a rotating impeller. The use of nitrogen gas also helps to keep the system isothermal and prevent heat accumulation. In other high impact dry coating devices, rotating blades are present which move particles against the vessel wall; heat is also generated which combines to cause particle attrition (Gera et al., 2005). Particle size analysis of composite particles produced using the iDPC confirms that no particle attrition occurs. Figures 2.12 – 2.14 show the particle size

distributions of all the dry coated powder blends in comparison to that of the control (unprocessed lactose).

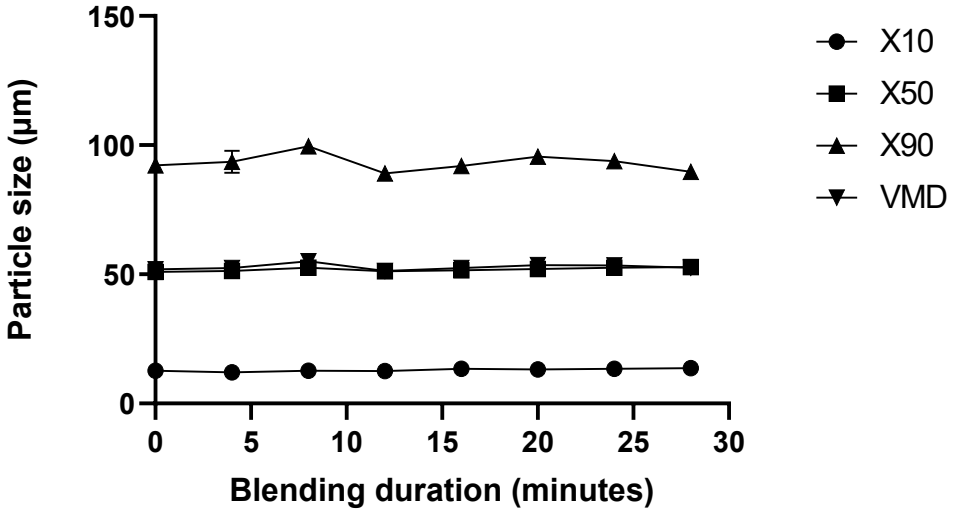

Figure 2.12 Effect of blending duration on particle size of lactose-rhodamine B powder blends without nitrogen flow (0 L/min) at 201G

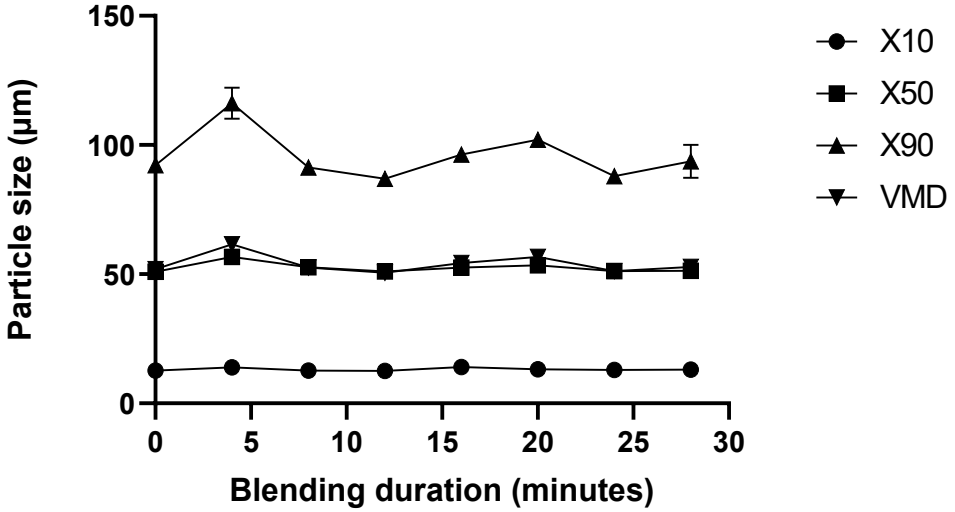

Figure 2.13 Effect of blending duration on particle size of lactose-rhodamine B powder blends at nitrogen flow of 25 L/min and 201G

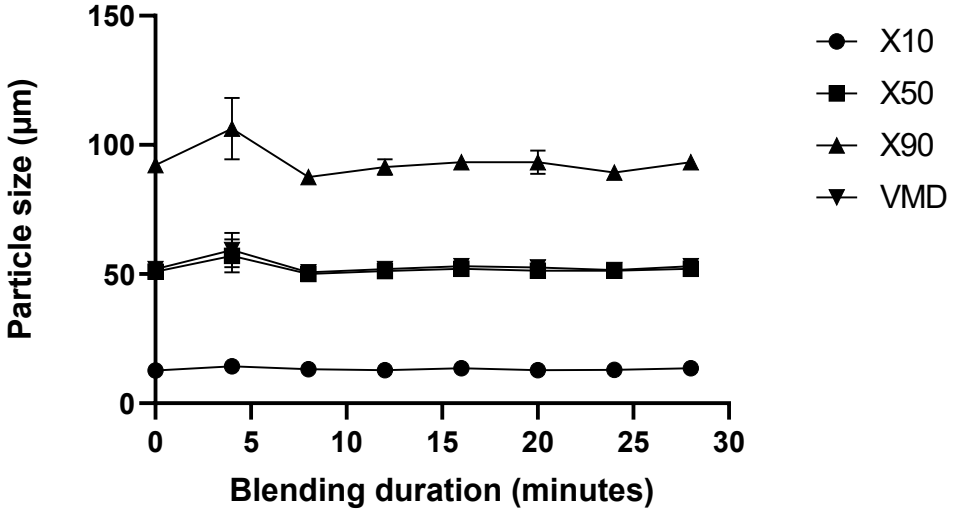

Figure 2.14 Effect of blending duration on particle size of lactose-rhodamine B powder blends at nitrogen flow of 40 L/min and 201G

The increase in X_{90} at 4 minutes, 25L/min and 40L/min and at 8 minutes, 0L/min (figures 2.12 and 2.13) may be attributed to the preferred affinity of fine particles to coarser particles. The larger mass of the lactose particles within the X_{90} distribution imparts higher kinetic energy on them; hence while in motion, they are likely to forcefully impact the finer rhodamine B particle agglomerates which have lower mass, causing the agglomerates to adsorb onto the coarse lactose surface (Pfeffer et al., 2001; Alonso and Alguacil., 1999). Further particle-particle and/or particle-wall interactions are required to break up these agglomerates into individual particles. However, if the coating process is not prolonged enough for these collisions to occur, the agglomerates remain on the coarse particle surface with the potential to increase their size during particle size measurement. These results also agree with earlier observations from the CLSM images where agglomerates of cohesive rhodamine B particles were initially deposited onto lactose surface and then subsequently deagglomerated and redistributed as processing time was increased.

Generally, the particle size analysis of the composite blends show no reduction in particle size is observed which confirms that no attrition occurred during processing. This is a very desirable property of a dry coating device, as potential functionality such as improved flow of composite particles may be lost once particle attrition occurs (Sato et al., 2013).

Overall, there are no appreciable differences in the particle size distribution, irrespective of the process parameters used. This confirms that the iDPC does not cause particle attrition, and as such the process maintains the intrinsic properties of the starting materials. The particle size distributions also show that regardless of the addition of fine rhodamine B particles with VMD less than 10μm, there is no resultant decrease in the X_{10} of the dry coated powder blends. Rather, there is an increase in the X_{10} values. This supports the ability of the iDPC to mop up the fine particles during the coating process (Koner et al., 2017).

2.7 Conclusion

The novel iDPC is capable of producing composite particles through the dry coating process. The air-blade produced when nitrogen flow is introduced into the system hastens the deagglomeration process, which is critical to the whole dry coating process. This may be achieved by shear forces generated by vortexes produced in the system, which simulates rotating impellers in other high shear mixers. This mechanism however does not lead to particle attrition as the nitrogen gas, which keeps the system at ambient temperature, also prevents heat generation.

The time frames when the different stages of dry particle coating i.e. deagglomeration, dispersion and redistribution occur in the novel iDPC have also been identified. The convective and shear mixing mechanism are suggested to be predominant in the novel iDPC when the air-blade is used while the diffusive mechanism is suggested to be predominant when the air-blade is not used.

With or without the air-blade, the novel iDPC is able to dry coat guest particles onto host particle surface; although longer processing times are required to achieve similar results when the air-blade is not used than when it is used.

3. Chapter Three

Lactose surface modification using the novel isothermal dry particle coating device and post-processing characterisation

3.1 Introduction

The formation of ordered mixtures and dry coated particles relies on interactive forces between host and guest particles. Van der Waals, electrostatic force, surface adsorption and mechanical interlocking are the main surface forces that bring about surface interactions. Generally, all these forces may be present, but the prevailing particle properties, environmental and storage conditions determine which predominates. Clearly, dry particle coating is a surface phenomenon and the knowledge of the physicochemical changes that occur to the particle surface during processing in relation to process parameters is crucial to determining the potential predominant interactive force (Young et al., 2010, Zeng et al., 2000)

This knowledge may be exploited in operating coating devices to achieve particular features. For example in the formulation of DPIs, it is important to create a balance between host and guest particle adhesion and subsequent separation for pulmonary drug delivery. Host particles with rough surfaces have greater tendencies to mechanically interlock fine active pharmaceutical ingredients (APIs). This may not be desirable in DPI formulations; as such interactions are significant and not as easily reversible as interactions caused by van der Waals force. A previous study confirmed the better dissociation of APIs from fine lactose surface than coarse lactose surface; the former produced a higher fine particle dose. Coarser particles are however useful in maintaining good flow for handling (Zeng et al., 1998).

Also, host particle surface energy is able to influence this adhesion-detachment balance. Attachment of APIs to low energy sites has been found to increase aerosolization. This was investigated by the addition of ternary surface lubricants, which have affinity for host particle high energy sites therefore allowing APIs to bind to lower energy sites (Staniforth et al., 1997). In addition, in the development of carrier-free DPIs, reduction in strong cohesion forces of fine powder has been used as an approach to increase aerosolization. Zhou et al. (2010a) were able to demonstrate the improved aerosolization of salbutamol sulphate, salmeterol xinafoate and triamcinolone acetonide by mechanofusion with magnesium stearate. They explained that by using a lubricant to interfere with the normal cohesion between these micronised particles, the agglomerate strength was reduced and aerosolization was facilitated.

Similarly, flowability of cohesive powders has been improved by reducing cohesion. Since strong inter-particle cohesion is the primary reason for poor flow; modification of cellulose and corn starch surface by coating with silica was used to improve flow in a study by Ramlakhan et al. (2000). This phenomenon was also explained by Mei et al. (1997), as a surface phenomenon; that in the presence of a fine coating, the cohesion force between two host particles is directly proportional to the guest:host size ratio and significantly reduces cohesion Therefore, measuring the guest-host surface interactions and their changes in relation to process parameters will be beneficial in optimising the dry coating process and its use in formulation development.

3.1.1 Surface characterisation techniques

There are several surface characterisation techniques that have been used to study composite particle surface. Some of these techniques and the particle/powder properties they are used to measure are shown in Table 3.1 (Dahmash and Mohammed, 2015).

Table 3.1 Surface characterisation techniques used to determine physicochemical properties of particles (Dahmash and Mohammed, 2015)

Characterisation Technique	Measured property
Angle of repose **Shear cell test**	Flowability and cohesivity
Carr's index **Hausner's ratio**	Bulk and tapped densities
Particle size analysis by laser diffraction	Particle size distribution
X-ray particle diffraction (XRD) **Differential scanning calorimetry (DSC)** **Thermogravimetric analysis (TGA)**	Thermal properties
Inverse gas chromatography (IGC) **Atomic force microscopy (AFM)** **Contact angle measurement**	Surface energy
Scanning electron microscopy (SEM)	Surface morphology
Fourier transform infrared microscopy (FTIR) **X-ray photoelectron spectroscopy**	Chemical interactions/changes
Aeration test	Fluidizability
Brunauer Emmett and Teller (BET) technique	Specific surface area
Near infrared spectroscopy	Dispersibility

In this study, particle size analysis by laser diffraction was used to analyse the particle size distribution; flowability was measured using the shear test cell; thermal properties was measured using XRD, DSC and XRD; surface morphology was evaluated by SEM.

3.2 Aim and objectives

Aim

- To study the relationship between iDPC process parameters and changes in particle surface properties

.

Objectives

- To process lactose particles under different process parameters (nitrogen flow, G-force, duration)
- To measure surface properties of processed lactose particles after processing
- To investigate if any changes have occurred in the processed lactose particles
- To investigate the correlation between any observed changes and process parameters

3.3 Materials and Methods

3.3.1 Materials

This study was done using only inhalation grade alpha lactose monohydrate, no guest particles were used. Inhalation grade alpha lactose monohydrate (Inhalac® 251) was supplied by Meggle. Experiments were carried out using Inhalac® 251 as received as well as sieved Inhalac® 251.

3.3.2 Methodology

3.3.2.1 Preparation of coarse lactose

Inhalation grade alpha lactose monohydrate (Inhalac® 251) was sieved for 15 minutes through a 38µm sieve using a sieve shaker (Zeng et al., 1998). This was done to remove the fine lactose particles below the X10 particle size distribution .The lactose particles collected on the 20µm sieve were collected and processed in the dry coating device.

3.3.2.2 Experimental design

The experiment was designed using the MODDE software version 10.1 (MKS Umetrics Sweden). In the design phase, three critical process parameters were defined on a quantitative multilevel scale using three levels: Airflow at 0L/min, 25L/min and 40L/min; speed at 100rpm, 1500rpm and 2000rpm and duration at 10 minutes, 20 minutes and 30 minutes. These parameters were based on results obtained from the proof of concept of the iDPC device The run order was randomised, in order to obtain results independent of external factors. Table 3.2 shows the summary of experiments carried out and process parameters used.

Table 3.2 The D-optimal design worksheet with factors, responses, total number of runs and run order

Exp No	Exp Name	Run order	Airflow	Speed	Duration
1	N1	8	0	1000	10
2	N2	13	0.4	1000	10
3	N3	15	0.2	1500	10
4	N4	12	0	2000	10
5	N5	9	0.4	2000	10
6	N6	2	0.2	1000	20
7	N7	3	0.4	2000	20
8	N8	7	0	1000	30
9	N9	10	0.4	1000	30
10	N10	14	0.4	1500	30
11	N11	1	0	2000	30
12	N12	6	0.2	2000	30
13	N13	11	0.2	1500	20
14	N14	5	0.2	1500	20
15	N15	4	0.2	1500	20
16	N16	16	0.4	2000	30
17	N17	17	0.2	2000	20

3.3.2.3 Processing of lactose powder in dry coating device

30g each of Inhalac® 251 was weighed and transferred into the mixing vessel of the iDPC device. The processing parameters were set as generated by MODDE as shown in Table 3.2. The processed lactose powders were stored in plastic vials on shelf. The same process was repeated for the sieved fraction of the Inhalac® 251.

3.3.2.4 Particle size analysis

The particle size of the processed lactose powder was measured using Sympatec™ HELOS/RODOS particle size analyser with VIBRI/I feeder (Clausthal-Zellerfeld, Germany). About 1g of the powder samples were fed into the vibratory feeder, which transfers the powder

into the dispersing unit (RODOS). The powder samples were dispersed under compressed air at a pressure of 2 bars into the analyser (HELOS), where the particle size and particle size distribution of the dispersed powder is determined by laser diffraction. X_{10}, X_{50}, X_{90} and mean volume diameter (VMD) values were recorded for each sample. The same process was repeated for the sieved lactose powder.

3.3.2.5 Powder flow test

Powder flow was measured using a Brookfield shear cell tester PFT3230 (Brookfield Massachusetts U.S.A). About 25g sample of powder was loaded into the trough and packed using a rotating levelling tool. The sample weight was entered into the software and the test was started. The shear test runs by first pre-consolidating the powder in the trough by applying a normal stress between 0.3 - 5 kPa, and then vertically shearing the powder to failure using the trough's vane lid. The powder's yield stress is plotted against the principal consolidation stress. The ratio of the maximum stress and the stress required for flow ($\sigma 1/\sigma c$) represents the flow factor coefficient (FFC) (Wang et al., 2016; Ghoroi et al., 2013).

3.3.2.6 Scanning Electron Microscopy (SEM)

SEM was used to qualitatively observe morphological changes between the Inhalac® 251 subjected to different processing conditions compared to the the Inhalac® 251 as received. Powder samples were dispersed onto a double-sided adhesive carbon tape and placed on a sample holder. The samples were gold coated to increase conductivity during imaging. Imaging was done using a field emission scanning electron microscope Zeiss Supra SS-VP (Zeiss, Oberkochen, Germany), at an accelerating voltage of 10.0kV. Images were taken at 150X and 800X magnification.

3.3.2.7 Brunauer–Emmett–Teller (BET) Specific surface area analysis

BET technique was used to analyse the specific surface area of the model blends using Nova system (Quantachrome Nova 4000e) with liquid nitrogen at −196 °C. Each sample was

degassed at 120 °C for 24 hours to remove any moisture and impurities and to open the pores and then weighed prior to full isotherm BET analysis.

3.3.2.8 Differential Scanning Calorimetry (DSC)

Thermal analysis was carried out using DSC. A Q 200 DSC system from TA instruments Waters (New castle, Delaware, USA) was used to determine the dehydration temperature and melting point of the processed lactose particles. This was done to investigate the effect of processing the lactose on its thermal properties. About 2mg of the samples were loaded into aluminium pans and heated to 50-250°C at 10 °C/min with a nitrogen purge at a flow rate of 50ml/min. An empty aluminium pan was used as reference for all measurements. The graphs obtained were analysed by TA manager software to determine the dehydration onset temperature and enthalpy and melting onset temperature and enthalpy.

3.3.2.9 X-Ray Particle diffraction

X-ray diffraction patterns were recorded on an X-ray diffractometer (D2 Phaser , Bruker AXS GmbH, Germany). The X-ray generator was operated at 30 kV and 10 mA employing Co tube at λ 1.79026 Å as a radiation source using LYNXEYE detector. The angular range (2θ) varied from 10 to 80° at 0.02° increments 2θ s^{-1} with an integration time of 1seconds per increment. Powder samples were loaded onto the sample holder and placed on the stage and locked into place. Diffractive patterns were generated as counts per step and thereafter analysed using Eva 18.0.0.0 software (Bruker, AXS).

3.3.2.10 Specific surface area and surface energy determination at finite dilution (FD-IGC)

Specific surface area and surface energy of the conditioned lactose carrier were determined using a IGC surface energy analyser (iGC-SEA 2000, Surface Measurement Systems Ltd, London, UK). Approximately 800mg of each sample was packed into pre-silanised glass columns (30 cm length and 4mm internal diameter) and plugged at both ends with silanised

glass wool (Sigma Aldrich, UK). The samples were packed properly in the columns using a jolting voltameter Surface Measurement Systems Ltd, London, UK), which mechanically taps the column to ensure the powder bed is tightly packed without voids. The samples were conditioned at 0% RH for 1 hour at 30^0C before each experiment to expel volatile contamination

3.3.2.10.1 Specific surface area determination by BET

Using the described set-up, the Brunauer-EmmetTeller (BET) specific surface area was determined using 15 octane injections to obtain an adsorption isotherm. The SSA was calculated between p/p^0 range of 0.005 – 0.350, where p and p^0 are the equilibrium and saturation pressure of adsorbates at the temperature of adsorption.

3.3.2.10.2 Surface energy and surface energy heterogeneity measurements

To obtain the dispersive surface energy measurements, a series of alkane probes (octane, nonane and decane) were injected, while the specific surface energy measurements was determined using a monopolar acidic probe and a monopolar basic probe (dichloromethane and ethyl acetate respectively). To obtain the surface energy heterogeneity, probes were injected at increasing concentration to achieve fractional surface coverage between 0% to 20%. The dead volume was determined by methane injection, which does not interact with the samples significantly under the chosen conditions. All experiments were carried out at 0% RH and 30^0C, nitrogen was used as the carrier gas at a flow rate of 10sccm, and retention time was detected by a flame ionisation detector. Data were analysed using the SEA Analysis Software (Surface Measurement Systems Ltd., London, UK). The dispersive surface energy was calculated using the Doris and Gray peak maximum method, while the specific surface energy was calculated from the basic and acidic surface components using the van Oss concept (Karde and Ghoroi, 2015; Bungert et al., 2021). The control and processed lactose carriers are identified in table 5.1.

3.3.2.11 Statistical Analysis

Statistical analysis was done using one-way ANOVA where applicable and a multivariate statistical analysis based on the experimental design was done using the MODDE software version 10.1 (MKS Umetrics Sweden).

3.4 Results and Discussion

This study was done to investigate the effects of processing in the iDPC, using a statistically designed study, on Inhalac® 251 as received (unsieved) and Inhalac® 251 where fines have been removed (sieved). The physicochemical properties of the two categories of the Inhalac® 251 were investigated post-processing and compared with the control (unprocessed) for each category. The results are presented in two sections, first, the effects of processing on the physicochemical characteristics investigated are presented, and then a multivariate approach, which analyses the relationship between the critical process parameters and critical quality attributes with respect to particle size (X10), powder flowability (FFC) and specific surface area (SSA) is also presented.

3.4.1 Particle size distribution

The particle size distributions of the processed unsieved Inhalac® 251 is shown in Table 3.3 and summarised graphically in Figure 3.1, with particle size distributions of the control sample i.e. unprocessed Inhalac® 251. The mean volume diameter (VMD) of the unsieved lactose ranged from 51.28±0.36 µm – 55.50±1.78 µm. Unprocessed lactose had a VMD of 51.97±0.24 µm.

Table 3.3 Particle size data of unsieved Inhalac® 251 (presented as mean, where n=3)

	X_{10} (µm)	X_{50} (µm)	X_{90} (µm)	VMD (µm)
Control	12.63	50.88	92.24	51.97
N1	14.22	51.29	89.81	51.93
N2	15.07	52.60	94.43	53.99
N3	15.29	52.53	94.15	53.92
N4	15.80	52.99	95.42	54.62
N5	13.70	51.57	98.84	54.62
N6	14.40	51.57	94.73	53.49
N7	14.37	53.04	98.99	55.44
N8	13.86	50.43	88.67	51.28
N9	14.79	53.07	99.06	55.50
N10	14.10	51.95	95.85	53.89
N11	15.01	52.49	95.37	54.17
N12	14.23	51.10	90.96	52.13
N13	15.18	52.43	94.45	53.94
N14	14.93	52.82	97.26	54.95
N15	14.99	52.45	94.04	53.78
N16	14.53	51.69	92.45	52.87
N17	15.00	52.60	95.33	54.30

Despite the similarities in VMD, there is a significant increase in X10 ($P < 0.0001$) of the processed Inhalac® 251 compared to the Inhalac® 251 as received as shown in Table 3.3. This difference in X10 is expected and is presumably due to the adsorption of the fine lactose particles onto the coarse lactose surface. In addition, there is a slight, but statistically significant difference in X50 ($P < 0.0001$), X90 ($P < 0.05$) and VMD ($P < 0.05$) of the Inhalac® 251 exposed to different processing parameters and the Inhalac® 251 as received. The similarity in these particle size values of the Inhalac® 251 as received and that exposed to different processing conditions confirms that the iDPC device does not cause particle attrition, as observed in chapter 1. The increase rather implies that fine lactose in the carrier system has been mopped up by coarse lactose.

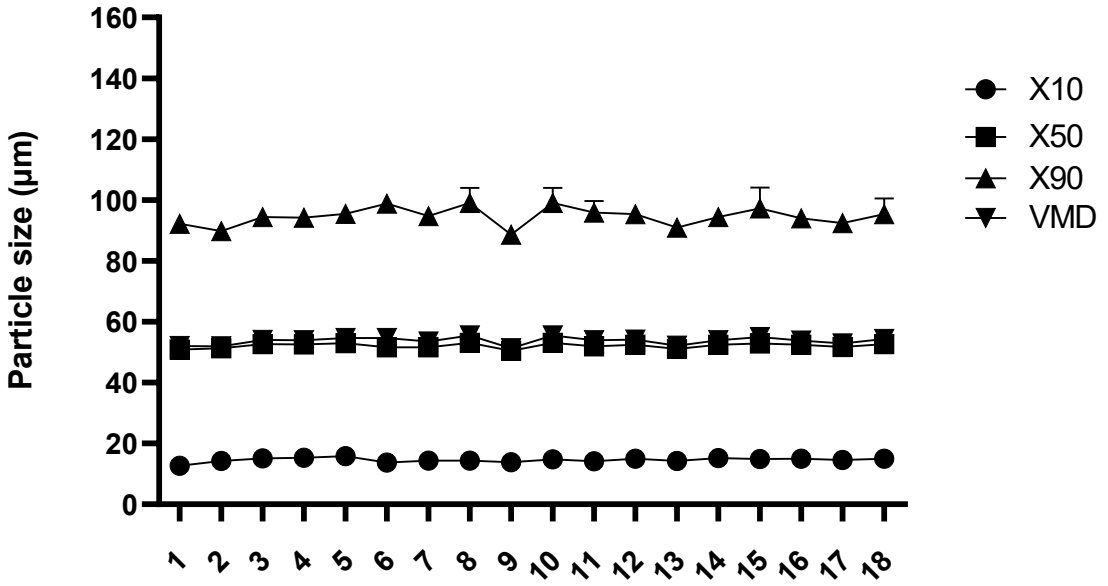

Figure 3.1 Change in particle size distribution with respect to process parameters (unsieved samples), showing a steadiness in all particle X10, X50, X90 and VMD comparable to the unprocessed sample regardless of processing condition

The inhalation grade lactose used (Inhalac® 251) is a fine sieved lactose grade, which contains a high proportion of fines about 11% of fine lactose < 15µm and has a broad particle size distribution. Based on the active sites theory, extrinsic lactose fines added to coarse lactose attach to active sites on coarse lactose (Jones and Price, 2006). Intrinsic lactose fines will also behave similarly especially when the carrier system is exposed to a dry coating process as seen in a study by Islam et al. (2004), where the removal of intrinsic lactose fines negatively impacted aerosolization performance. The high proportion of fines present in the IGL lactose grade used also makes this mechanism favourable. Therefore, when subjected to the dry coating process, the fine lactose content present will adhere to the surface of the coarse lactose in the system. Hence, the increase in X10. Scanning electron micrographs shown later on in this study confirm this observation.

The particle size distributions of the sieved processed Inhalac® 251 is shown in Table 3.4 and summarised graphically in Figure 3.2. The mean volume diameter (VMD) of the sieved lactose ranged from 55.48±1.27µm – 74.67±0.70 µm. Compared to the unsieved samples, the X_{10}

values ranging from 15.72±1.44 µm - 21.39±0.91 µm show that there has been a reduction in the proportion of fines as a result of sieving. In addition, there is an increase in X90 and VMD of the sieved lactose compared to the unsieved lactose, confirming that fine lactose has been removed from the lactose sample. Figure 3.2 shows a summary of the differences in X10, X50, X90 and VMD of the sieved batch of Inhalac® 251.

Table 3.4 Particle size data of sieved Inhalac® 251 (presented as mean, where n=3)

	X_{10} (µm)	X_{50} (µm)	X_{90} (µm)	VMD (µm)
Control	15.72	59.02	120.88	64.41
N1	19.17	57.51	95.50	58.24
N2	17.15	54.86	92.01	55.48
N3	21.21	67.33	138.91	74.67
N4	17.97	58.17	104.40	60.52
N5	18.07	60.27	114.69	64.22
N6	18.72	58.49	102.31	60.32
N7	18.75	60.88	118.90	65.69
N8	19.32	57.62	103.41	60.56
N9	19.61	58.72	99.36	59.71
N10	18.05	57.55	101.48	59.59
N11	21.39	58.46	99.26	59.98
N12	20.92	59.33	100.14	60.61
N13	17.92	57.04	98.33	58.26
N14	24.30	55.05	105.90	60.48
N15	20.92	57.06	91.81	57.06
N16	17.50	57.84	101.06	59.38
N17	16.40	58.25	98.08	58.83

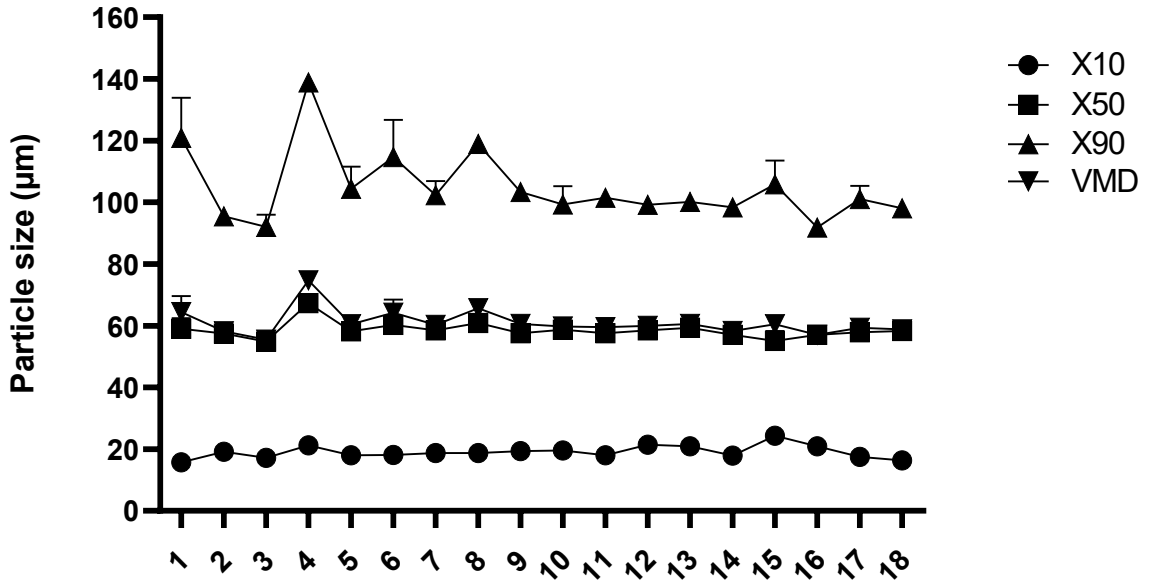

Figure 3.2 Change in particle size distribution with respect to process parameters (sieved samples), showing a steadiness in all particle X10, X50, X90 and VMD comparable to the unprocessed sample regardless of processing condition

Unprocessed sieved lactose has a VMD of 64.41±5.24 µm. As expected, there is a statistically significant increase ($P < 0.05$) in X10 of the processed Inhalac® 251 compared to the unprocessed Inhalac® 251, which is as a result of coating of any remaining fine lactose onto coarse lactose surface, as seen with the unsieved batch. The X50 significantly remains similar while there is no corresponding increase in X90, except for N3. Although at first glimpse, VMD and X90 of the processed samples appear smaller than that of the control sample, which may suggest particle attrition, however, the adsorption of any remaining fines onto the coarse lactose surface (as observed in the unsieved samples) may have increased the size of the coarse lactose beyond measuring range of the particle size analyser. Therefore, the distribution curve generated was limited to measurable particles and this was indicated during analysis. This may be responsible for the higher X_{90} and VMD in the control than the X_{90} and VMD of some processed samples, rather than being an indication of particle attrition. This is also be supported by the higher X_{10} values in all the processed samples than the control sample; which shows that the processed samples comprise larger particles.

Generally, the only significant difference observed from the exposure of unsieved and sieved Inhalac® 251 to different processing conditions in the iDPC device is increase in X10, which is attributed to the adsorption of fine lactose in both unsieved and sieved batches of Inhalac® 251 onto the coarser lactose particles in the carrier system. All other PSA indices confirms that particle attrition does not result from coating in the iDPC device.

3.4.2 Powder flowability

The flowability of the lactose samples was determined using a shear cell test. This test measures the unconfined failure strength i.e. how much stress is required for a powder to flow after being consolidated to a particular stress level. Flow factor coefficient (FFC) is used as flow index in this test. FFC values range from 4 to 10. FFC<4 represents poor flow while FFC>10 represents good flow. Figure 3.3 shows the flow function plot for unsieved lactose and control. The standard classification of powder flowability according to flow index is shown below. Classification of powder flow by flow factor coefficient (Wang et al., 2016; Ghoroi et al., 2013)

- ff<1 Non flowing
- 1<ff<2 Very cohesive
- 2<ff<4 Cohesive
- 4<ff<10 Easy flowing
- 10<ff Free flowing

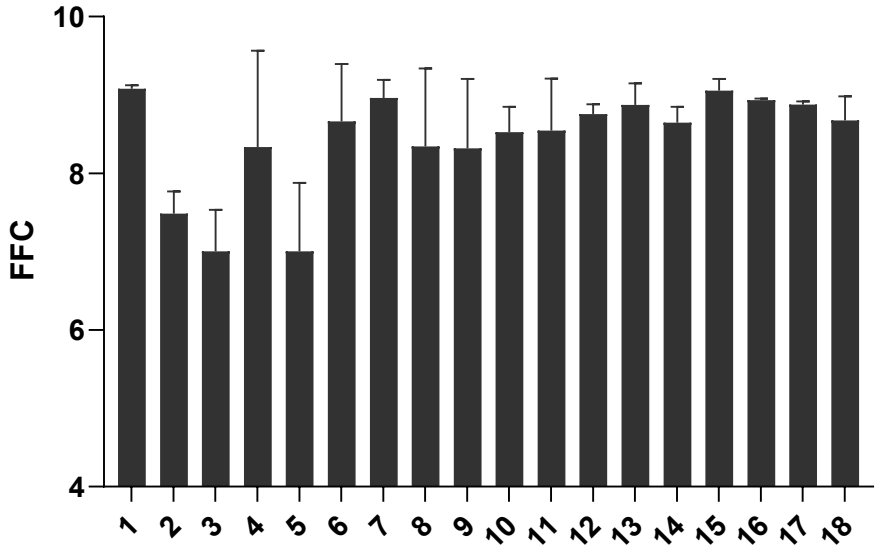

Figure 3.3 Flow function plot for unsieved lactose

The flow indices for unsieved lactose range from 7.00±0.53 to 9.05±0.15, showing that all samples are within the easy flowing category. N2 has the lowest flow index. However, there is no correlation between this low flow factor at N2 and X10, as N2 does not have the lowest X10. Interestingly, N16, which was processed at the highest speed (2000rpm), longest duration (30 minutes) and highest nitrogen flow rate (40 L/min) still maintained good flow. In previous studies by Sato et al., 2013, improved flow was observed up to 1 minute at a speed of 1500rpm after which possible attrition led to loss of improved flow. This also confirms the advantage of particle size retention in the iDPC. Figure 3.4 shows the relationship between FFC and X10, as expected, there is no correlation between FFC and X10 (R^2 = 0.1475), since all the samples have comparable FFC and X10.

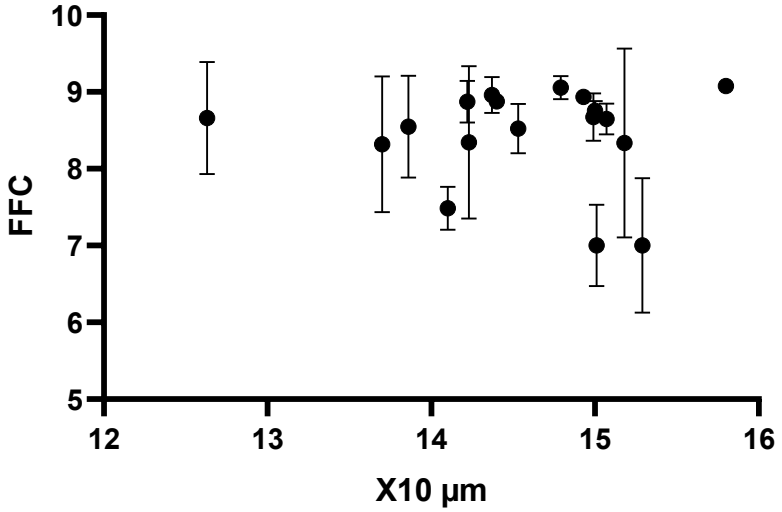

Figure 3.4 Relationship between flow factor and X10 for unsieved lactose samples

Figure 3.5 shows the flow function plot for sieved lactose. The flow indices for the sieved lactose range from 7.40±0.52 to 11.23±0.36. This shows that all samples are also at least easy flowing, but tend towards free flowing more than the unsieved lactose apparently due to the removal of fines. This is expected because cohesion of fines, which has been reduced in this case, has been attributed the reason for poor powder flow (Zeng et al., 2001).

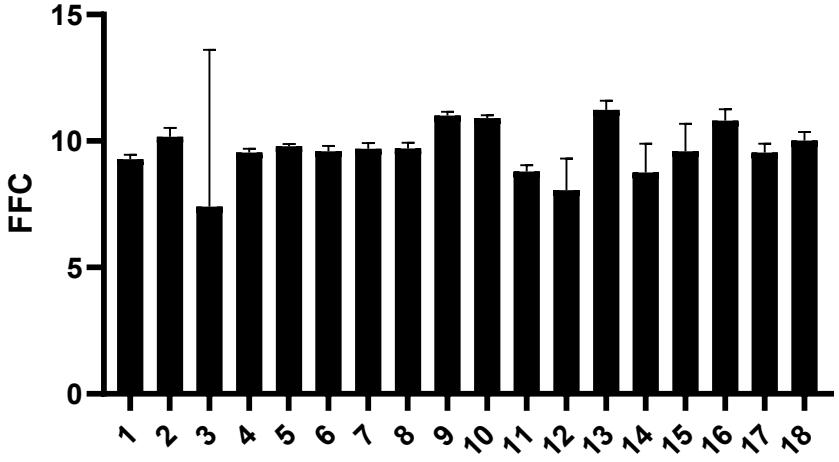

Figure 3.5 Flow function plot for sieved lactose

Similar to the unsieved samples, for unclear reasons, N2 also has the lowest FFC. This however does not correlate with X10. In addition, there is generally no correlation between X10 of all the samples and their FFC as shown in figure 3.6 (R^2 = 0.0565), since X10 increases slightly and remains similar for all processed samples, there is no appreciable change in FFC and all samples are easy flowing.

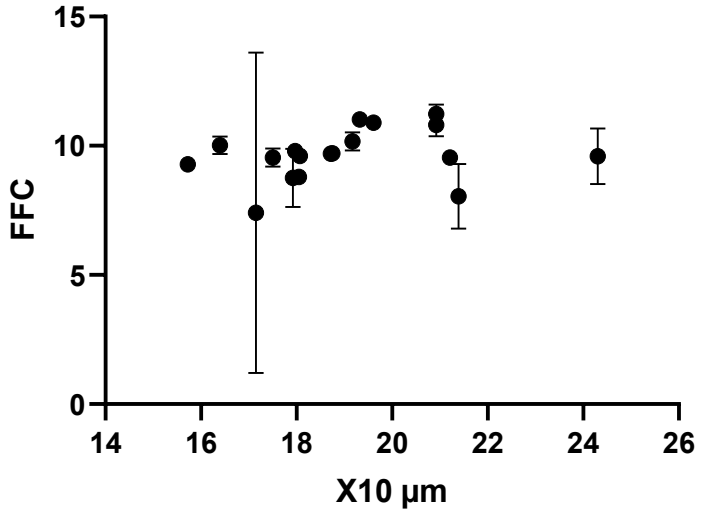

Figure 3.6 Relationship between flow factor and X10 for sieved lactose samples

3.4.3 Shape and surface morphology of lactose particles

Scanning electron micrographs of unsieved and sieved processed and control samples are shown in figure 3.7 A-F and 3.8 A-F. Micrographs of the following samples were taken N2, to investigate the effect of maximum airflow at low speed and short duration; N5, to investigate the effect of maximum airflow at high speed and short duration; N11 to investigate the effect of maximum speed (and G-force) at long duration without airflow; N13, to investigate the midpoints of all three factors and N16 to investigate the effect of the highest level of all three factors.

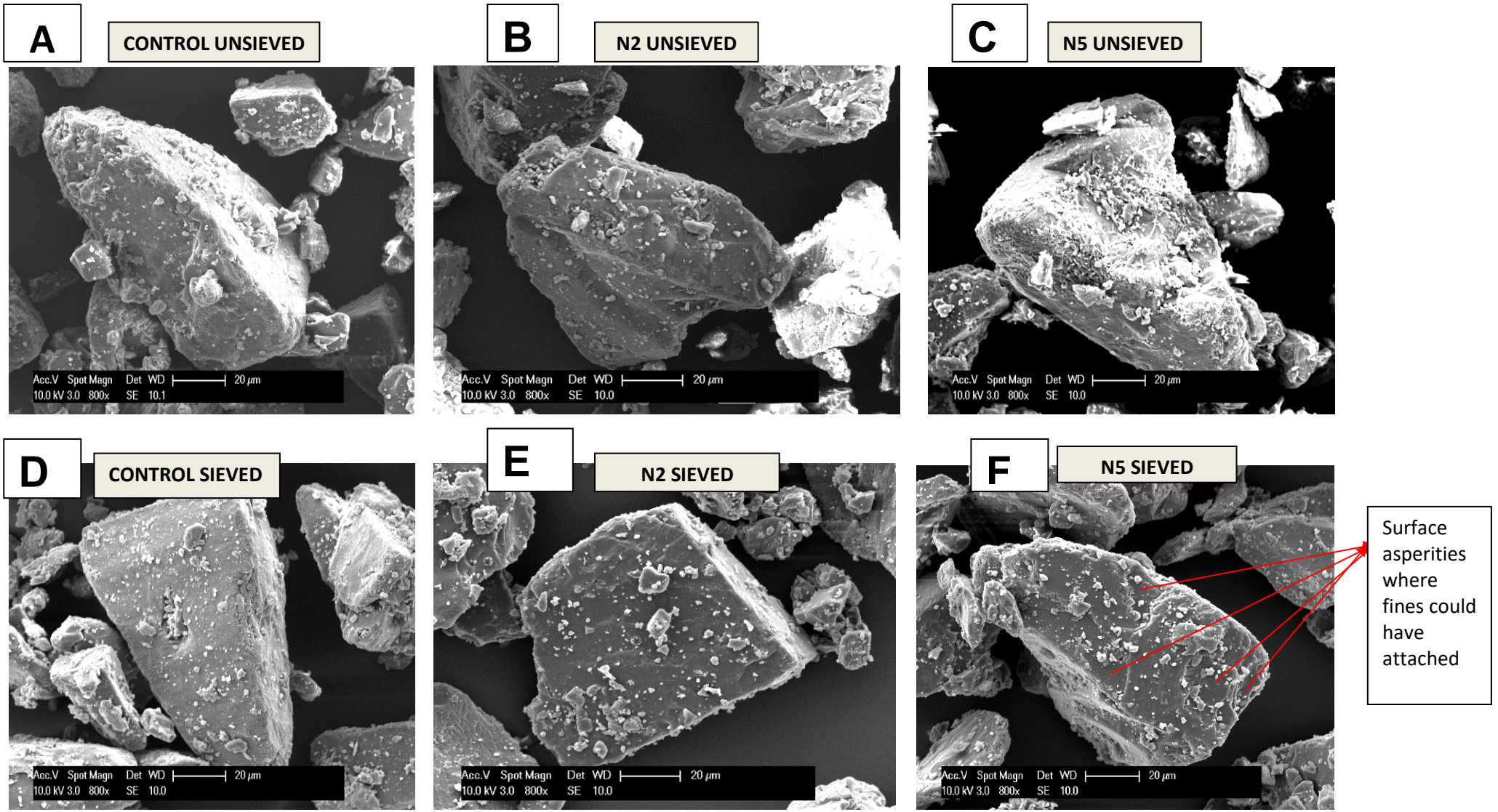

Figure 3.7 Scanning electron micrographs of control lactose (unprocessed), unsieved and sieved lactose processed under different conditions(N2 and N5) 800X magnification

From figures 3.7 A and B, (control and N2) few fine lactose particles can be seen on the coarse particle surface with fewer fines on the sieved (figures 3.7 D and E) compared to the unsieved (figures 3.7 A and B). This reveals that there is no appreciable difference between the control sample and N2. This could be as a result of the low speed which translates to low G-force used in processing as well as the short duration of processing; even though maximum airflow was used. This suggests that peak performance of the air-blade is obtained in synergy with G-force and not when used alone.

The relatively smooth surfaces of the lactose particles in figures 3.7 B and E comparable to the control (figure 3.7 A and D) could also mean that the force applied and the duration of processing were not sufficient to produce deformation. Plastic or elastic deformation is known to increase particle contact area and consequently particle interaction. When fine particles impact the surface of host particles, because they are concentrated on a small portion of the coarse particle surface, the force applied at this point causes deformation to the coarse particle surface. As a result of this deformation, more surface contact area is created for the fine particles and adhesion increases either by van der Waals force or mechanical interlocking (Zeng et al., 2001). The potential for this to occur is however proportional to the force introduced to the particles by the coating device in this case, and the duration of exposure to this force. The hardness of the particle also determines the extent of deformation (Zeng et al., 2001), but since the same particles are in use here, comparisons can be made on the basis of force and duration alone.

From figure 3.7 C, several fines can be seen attached to the coarse lactose surface. This sample (N5) was processed at 2000rpm (201G) which was the highest force used in this study. Although processing duration was at the lowest, 10 minutes, the impact of the G-force in synergy with airflow at 40L/min is evident. In its sieved counterpart (figure 3.7 F), fewer fines are seen attached onto the coarse particle surface, but several asperities which may be intrinsic or may be a result of deformation where fines could have attached are evident. Although, there may be insufficient fines present in this sample (N5 figure 3.7F) to cause deformation, but the possibility of the pressure exerted by the air-blade to generate enough load for deformation is another logical perspective.

Figure 3.8 A-F show the rest of the scanning electron micrographs for sieved and unsieved samples.

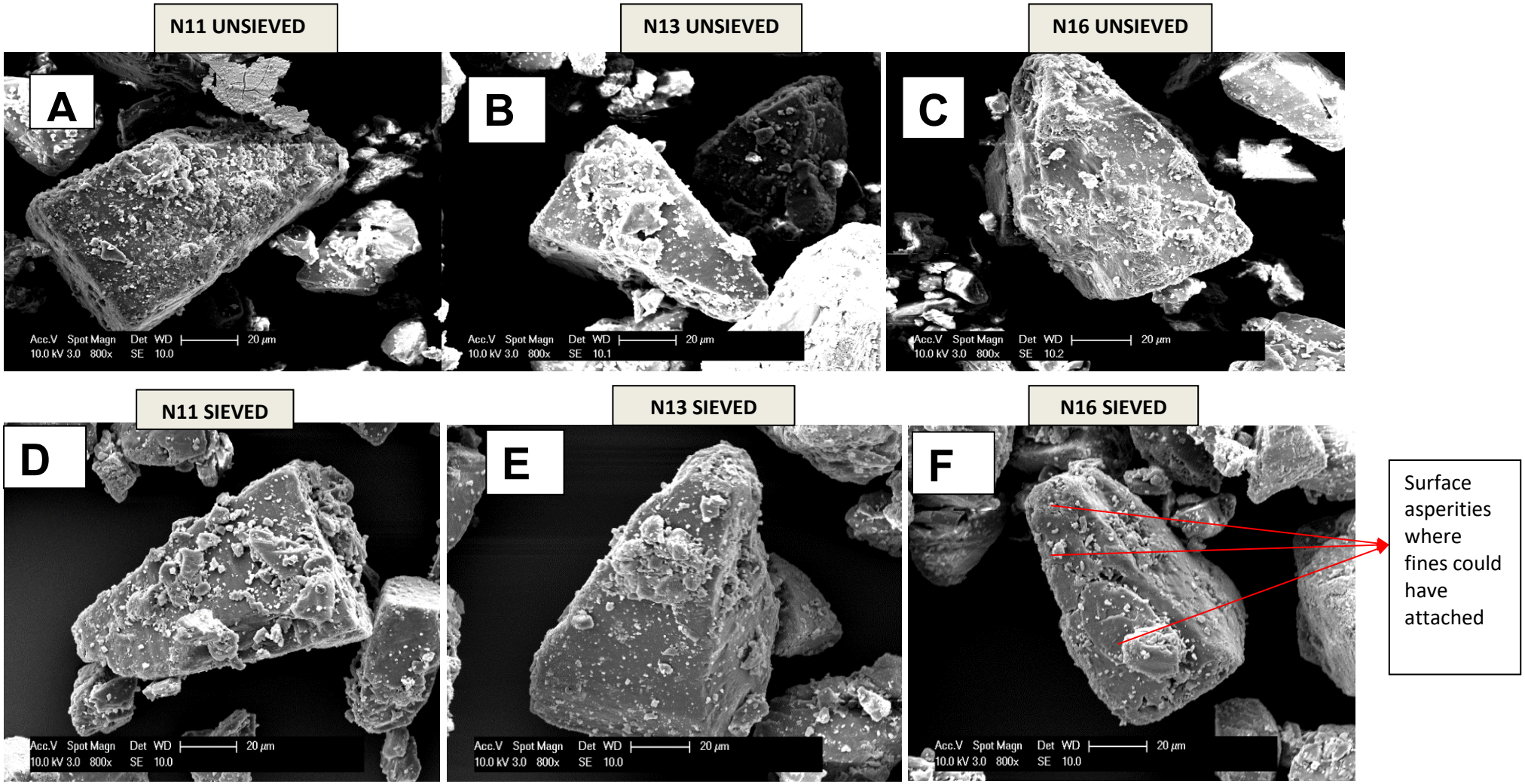

Figure 3.8 Scanning electron micrographs of unsieved and sieved lactose processed under different conditions (N11, N13 and N16) 800X magnification

Form figure 3.8 A (N11), several fines can be seen attached to the coarse lactose surface, comparable to figure 3.7 C (N5). This reveals that similar surface adhesion results may be obtained without airflow at longer duration than with airflow. Figure 3.8 C and F show the N16 sample with fewer fines attached to the coarse lactose surface, compared to figure 3.7 C (N5). This could be an indication that coating layer of fine lactose on coarse lactose degenerates on prolonged processing, as suggested by Ramlakhan et al. (2000).

Generally, more fines are seen attached to coarse lactose fines in the unsieved samples than the sieved samples. This confirms the reduction of fines by the sieving process. In the sieved samples, the absence of “very fine” lactose makes way for attachment of “larger fines” to attach to coarse lactose surface.

It may be worthwhile to investigate the effects of processing carrier lactose particles before introducing the guest particle to be coated onto its surface. Studies by Zeng et al., (1998) show that the addition of fines to DPI formulations allow for better dissociation of APIs due to easier detachment of the APIs from fine lactose surface than from coarse lactose where asperities may have caused mechanical interlocking to occur. Therefore, initial processing of the lactose particles alone may eliminate competitive adhesion between API and host particle fines, and ensure that the host particle fines attach to the high energy sites on the coarse host particles. Subsequent introduction of the APIs will potentially facilitate attachment of API fines onto the host particle fines which will then allow for easier detachment. This approach will be useful in design of dry powder inhalers where it is crucial to create a balance between ability of coating to withstand agitation and release of API when DPI device is actuated.

3.4.4 Thermal properties of lactose

The thermal properties of the IGL used are presented in this section and are typical of α-lactose monohydrate. DSC was done to investigate the thermal properties of the Inhalac® 251 and to identify any polymorphs; specifically to determine if the dry coating process causes any

change in solid form of the IGL. The thermodynamic instability of amorphous lactose makes it unwanted in pharmaceutical formulations. Under storage conditions, such amorphous content crystallise and this may alter the chemical composition of APIs. The thermal properties are represented by characteristic peaks i.e. melting point Tm and glass transition temperatures Tg (for amorphous materials and polymers). Figure 3.9 A-C show the DSC profiles of sieved and unsieved lactose, which are representative of all the DSC profiles, obtained.

The DSC thermograms of α-lactose monohydrate has a dehydration peak, which indicates the loss of its water of crystallisation and a second melting peak. As expected, the two batches of IGL investigated, unsieved and sieved samples, show an endothermic dehydration peak at onset temperature around 140^0C, and a melting peak at onset temperature around 210^0C, which are typical of α-lactose monohydrate (Gombas et al., 2002). A summary of onset temperatures and heat of enthalpies (ΔH) are presented in table 3.5 and 3.6 for the unsieved and sieved batches respectively.

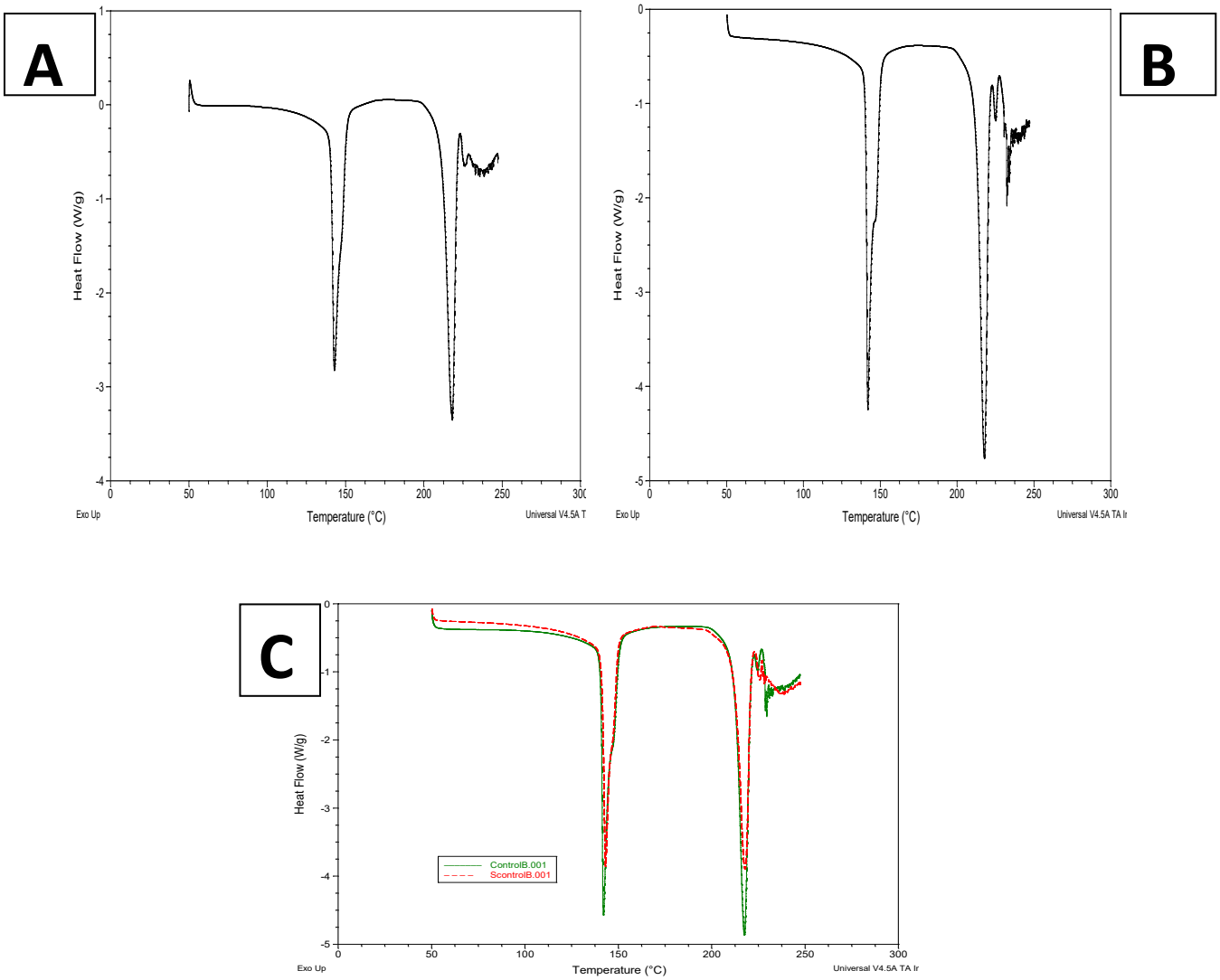

Figure 3.9 DSC profiles of unsieved and sieved lactose samples (A) N1- unsieved (B) N17-sieved (C) Sieved and unsieved control overlaid for comparison

Table 3.5 Summary of thermal properties of unsieved Inhalac® 251 determined by DSC showing onset temperatures and enthalpies of dehydration and melting

	Dehydration		**Melting**	
	Onset temperature	Enthalpy (J/g)	Onset temperature	Enthalpy (J/g)
Control	140.93	131.03	212.41	138.43
SN1	140.49	123.87	211.95	137.23
SN2	140.71	136.70	212.40	154.57
SN3	140.66	144.20	212.41	158.83
SN4	140.67	148.03	213.94	165.57
SN5	140.85	134.00	212.25	148.27
SN6	140.72	149.20	212.08	164.30
SN7	140.86	136.53	212.14	154.07
SN8	140.64	138.50	212.25	150.50
SN9	140.96	132.84	212.31	148.00
SN10	141.03	142.43	212.26	157.43
SN11	140.85	124.20	212.28	137.40
SN12	141.12	114.37	211.95	127.70
SN13	140.85	137.30	212.29	150.50
SN14	140.72	143.27	212.46	157.97
SN15	140.67	162.23	212.40	177.13
SN16	140.98	130.53	212.31	144.60
SN17	140.82	132.07	212.41	146.10

Table 3.6 Summary of thermal properties of sieved lactose Inhalac® 251 determined by DSC showing onset temperatures and enthalpies of dehydration and melting

	Dehydration peak		Melting peak	
	Onset temperature	Enthalpy (J/g)	Onset temperature	Enthalpy (J/g)
Control	140.40	141.77	212.30	151.10
SN1	140.54	143.73	212.02	156.13
SN2	140.54	145.13	212.34	158.23
SN3	140.80	149.33	210.94	155.67
SN4	140.59	150.27	212.11	162.57
SN5	140.47	146.03	212.29	158.53
SN6	140.88	132.70	211.40	138.87
SN7	140.76	136.17	211.90	148.40
SN8	140.71	130.43	212.24	140.80
SN9	140.61	135.63	212.28	149.67
SN10	140.61	132.23	212.13	144.37
SN11	140.18	139.80	212.14	151.77
SN12	140.24	134.97	212.41	146.33
SN13	140.71	121.80	212.16	133.60
SN14	140.25	143.97	212.42	158.30
SN15	140.47	124.73	212.13	138.80
SN16	140.51	143.13	212.29	156.07
SN17	140.61	141.03	212.29	155.13

From these results, the IGL used does not contain β-anhydrous lactose and has no amorphous content, which show an endothermic event between 230^0C -240^0C and an exothermic event between 170^0C -180^0C respectively (Listiohadi et al., 2009; Gombas et al., 2002) . This reveals that coating the IGL in the iDPC did not lead to any change in the solid form of the IGL in both sieved and unsieved samples. The DSC data is also supported by the XRD patterns obtained, which are more sensitive in detecting and quantifying polymorphs.

In the XRD patterns obtained, all the peaks obtained for both unsieved and sieved batches of the IGL used have peaks characteristic of α-lactose monohydrate, as shown in figure 3.10 and 3.11. All the samples were crystalline and the presence of anhydrous β-lactose was not

detected. Although, the intensity of the peak obtained varied across the samples, this was attributed to preferred orientation of the IGL crystal lattice.

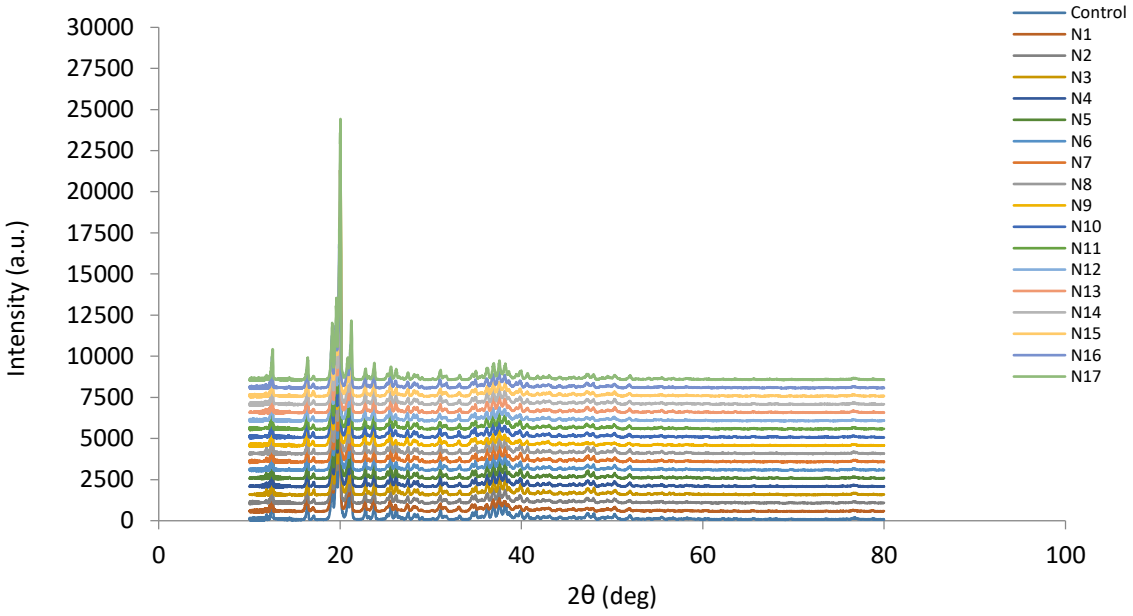

Figure 3.10 Powder X-ray diffraction patterns for unsieved Inhalac® 251, showing characteristic peak for α-lactose monohydrate

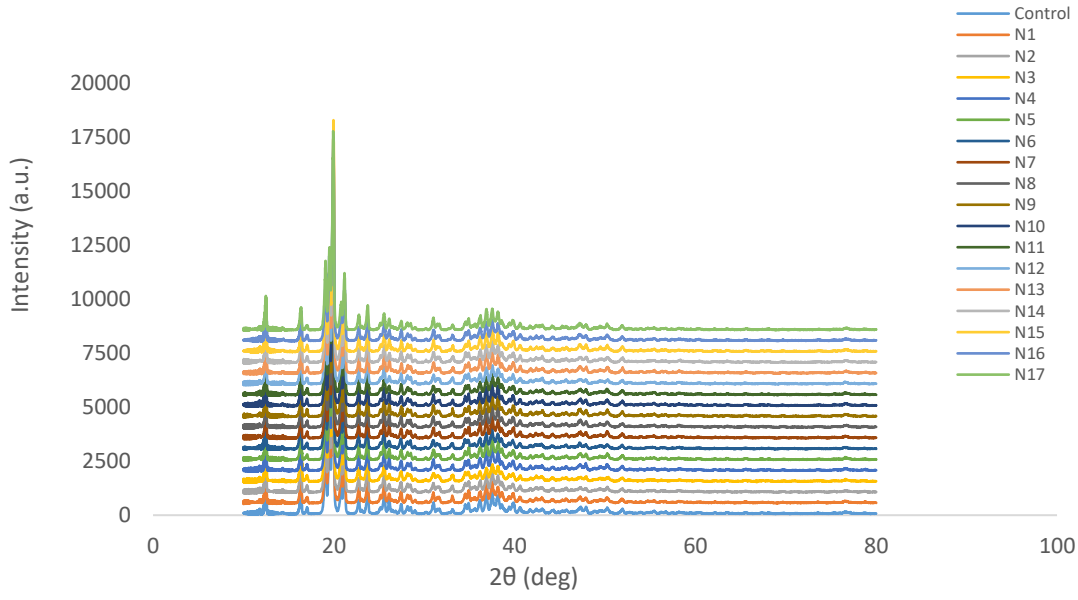

Figure 3.11 Powder X-ray diffraction patterns for sieved Inhalac® 251, showing characteristic peak for α-lactose monohydrate

The use of shear forces is one of the major mechanism in equipment used for particle size reduction, and prolonged transfer of mechanical energy from such equipment to particles interferes with crystal order and causes a disorder of the crystal structure or amorphisation (Loh et al., 2015, Naik and Chaudhuri, 2015). However, with the iDPC, regardless of processing speed, duration and nitrogen flow used, the thermal properties of the processed IGL remain consistent with the original characteristics of the lactose grade used, being a sieved lactose grade, which contains mono crystals. Hence, these results further confirm that the iDPC does not cause particle attrition, and in fact does not alter the crystalline form of particles during processing, in which case the crystals remain intact through processing and there is no formation of amorphous regions due to particle attrition. This is attributed to the use of the nitrogen blade to simulate shear forces necessary for particle-particle interaction, which facilitates the coating process.

3.4.5 Specific surface area

To understand the change in surface of the IGL after processing in the iDPC, specific surface area was determined by BET method. Dry coating of fines onto coarse particles may reduce surface area by reducing surface irregularities on coarse particles (Zhou et al., 2011). The specific surface areas of the unsieved samples are shown in Table 3.7, and they reveal significant changes in surface area to different degrees. Interestingly, there appears to be a connection between one or more of nitrogen flow rate, blending duration and speed with the specific surface area.

Table 3.7 Specific surface areas of unsieved Inhalac® 251 determined by the BET method

Sample Name	Specific Surface Area (m2/g)	Correlation Coefficient
Control		
N1	0.814	0.99092
N2		
N3	2.091	0.91444
N4	0.576	0.99690
N5	0.507	0.99002
N6	0.611	0.98899
N7	1.695	0.96131
N8	0.880	0.95793
N9	0.755	0.99246
N10	2.616	0.88100
N11	0.500	0.99615
N12	2.085	0.98245
N13	5.660	0.95368
N14	1.828	0.97681
N15	4.525	0.95501
N16	1.523	0.92588
N17	0.578	0.97729

**Data for Control and sample N2 are unavailable*

The lowest SSA values were obtained either when the nitrogen flow was absent i.e. at 0 L/min or at short processing duration i.e. 10 minutes (N11 – 0.5m^2/g; N5 – 0.507m^2/g and N4 – 0.576m^2/g). While the samples with higher SSA were processed with nitrogen flow rate of either 40L/min or 25L/min and at duration of 20 or 30 minutes (N13 – 5.660m^2/g; N15 – 4.525m^2/g; N10 – 2.616m^2/g). Data from this study have shown that there is no reduction in particle size during processing, hence, any increase in SSA is not due to increase in fine lactose content. Thus, the increase in SSA for the latter group of samples may be attributed to a multilayer coating of fine lactose present onto the coarse lactose, potentially creating more surface asperities. This may also be supported by the high proportion of fines present in the IGL grade used, and the process parameters that produced high SSA, which represent high

input energy (nitrogen airflow at 25L/min or 40L/min and blending duration of 20 or 30 minutes). Results from chapter one reveal that there was a positive correlation between nitrogen airflow rate and coating efficiency of rhodamine B onto lactose surface. The presence of the nitrogen blade facilitates dry coating, causing it to occur quicker than when the nitrogen blade is absent. This tendency for accelerated coating in the presence of the nitrogen blade may also be responsible for multilayer coating of lactose fines onto coarse lactose, which will consequently increase SSA. On the other hand, the samples with lower SSA, the absence of the nitrogen blade and short blending duration are not beneficial for accelerated coating of the fine lactose up to a multi-layer level, obtainable when the nitrogen blade is present.

3.4.6 Surface energetics

3.4.6.1 BET Specific Surface Area

This set of BET SSA analysis was required for surface energy determination, and was carried out using iGC Surface Energy Analyser. The BET Specific Surface Areas (BET-SSA) of both samples were determined with the physical adsorption of octane molecules by IGC-SEA. The results are presented in Table 3.8.

Table 3.8 Specific surface area determined from Octane sorption isotherm used by Peak Max retention times

Sample	Sorption Constant	Monolayer Capacity [mMol/g]	BET Specific Surface Area [m^2/g]	R^2
Control	3.3383	0.0008	0.3185	0.999
Sample N5	3.4234	0.0008	0.2935	0.999

The BET SSA results show a decrease in SSA of processed lactose compared to the lactose as received. This may be attributed to the mopping up of fine lactose by coarse lactose, thereby reducing surface irregularities on coarse particles with a corresponding decrease in

available surface area for adsorption. In addition, the mopping up of fines also causes an increase in particle size, which was evident in the PSA results, in which X10 increased for all processed samples compared to the unprocessed control sample.

3.4.6.2 Surface energy measurements

The surface energy profiles are shown in Figure 3.12 – 3.13, they show that both samples are energetically heterogeneous i.e. the surface energy changes as a function of surface coverage. In addition, it can be clearly observed that the dispersive component contributes a major part of the surface energy. The two samples have almost the same dispersive, specific and total surface energy, but there is a difference in their surface energy distribution.

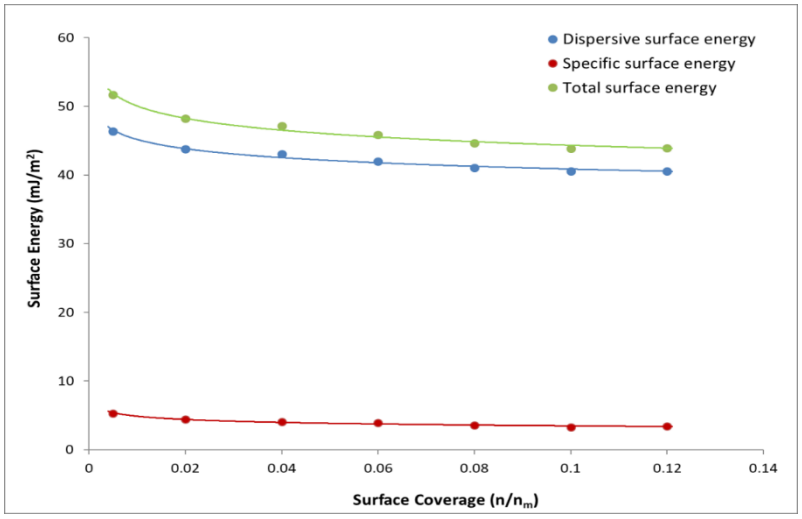

Figure 3.12 Surface energy profiles, as a function of surface coverage of the Control sample

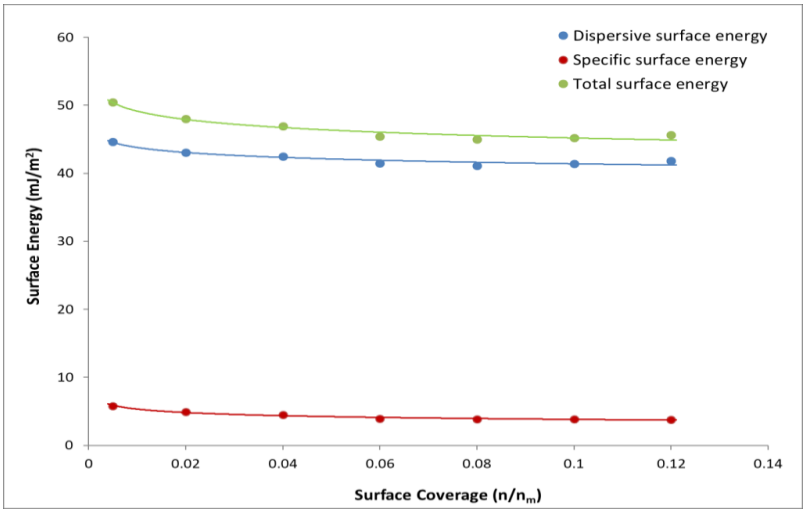

Figure 3.13 Surface energy profiles, as a function of surface coverage of the processed sample N5

3.4.6.2.1 Dispersive and Specific (Acid-base) Surface Energies

Dispersive (γ_S^D), acid-base (γ_S^{AB}) and total surface energy (γ_S^T) profiles obtained directly from the iGC-SEA for the two samples are shown in Figure 3.12 and 3.13 for each sample. The profiles show that all samples are energetically heterogeneous i.e. the surface energy changes as a function of surface coverage. The dispersive surface energy for the control sample was 41.27 mJ/m^2 while the specific surface energy was 3.67 mJ/m^2. The corresponding values for the sample processed at N5 were 42.13 mJ/m^2 and 4.16 mJ/m^2 respectively, while the total surface energy was 44.94 mJ/m^2 and 46.31 mJ/m^2 for control and N5 respectively. These results reveal that the dispersive component contributes a major part of the surface energy. The combined plot of dispersive, specific (acid-base) and the total surface energy of the samples are presented in Figures 3.14 – 3.16. The specific surface energy of the processed sample N5 is slightly higher than that of the unprocessed control sample, this suggests a change in specific surface energy sites. When combined with the polarity plot of the samples, as shown in figure 3.17, the increase in specific surface energy may be attributed to a change in the position of lactose water of crystallisation, which consequently increases the interaction of polar probes with particle surface causing an increase in specific surface energy and polarity of the processed sample.

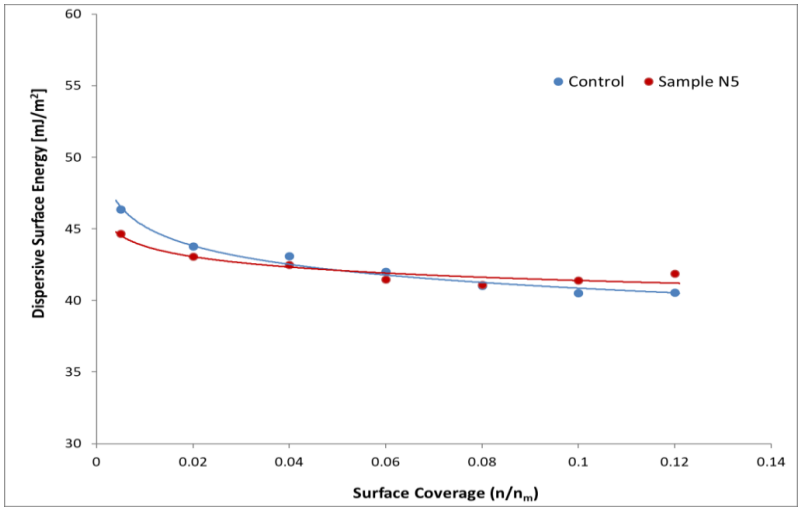

Figure 3.14 Comparison of the dispersive surface energy profile, as a function of surface coverage of the processed (N5) and control samples. Both samples appear to have comparable dispersive surface energy component.

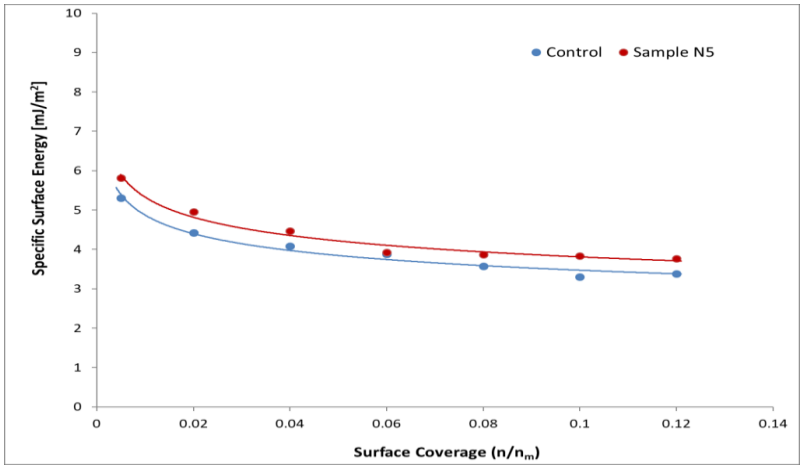

Figure 3.15 Comparison of the specific surface energy profile, as a function of surface coverage of the processed (N5) and control samples. The specific or polar surface energy of the processed sample N5 is slightly higher than that of the control sample; this implies that the processed N5 sample has a more hydrophilic surface. This difference in polarity may be attributed to the processing conditions that N5 was exposed to, considering that is the only differentiating factor in the two samples.

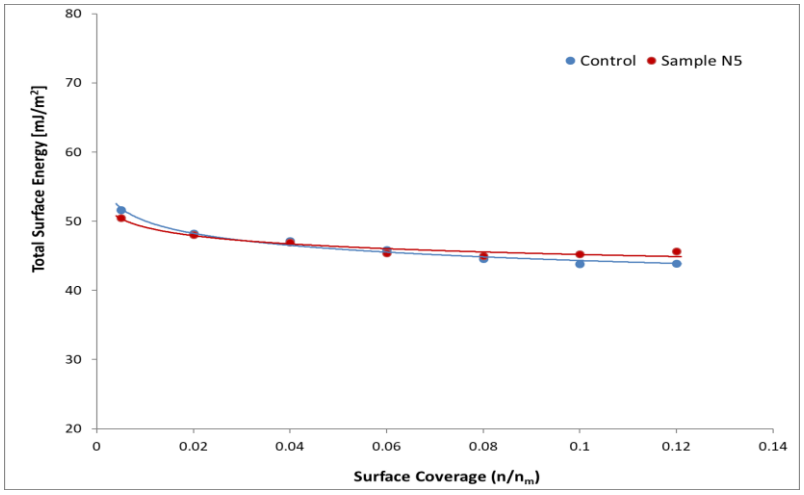

Figure 3.16 Comparison of the total surface energy profile, as a function of surface coverage of the processed (N5) and control samples. The two samples are energetically heterogeneous and the total surface energies for both samples are comparable.

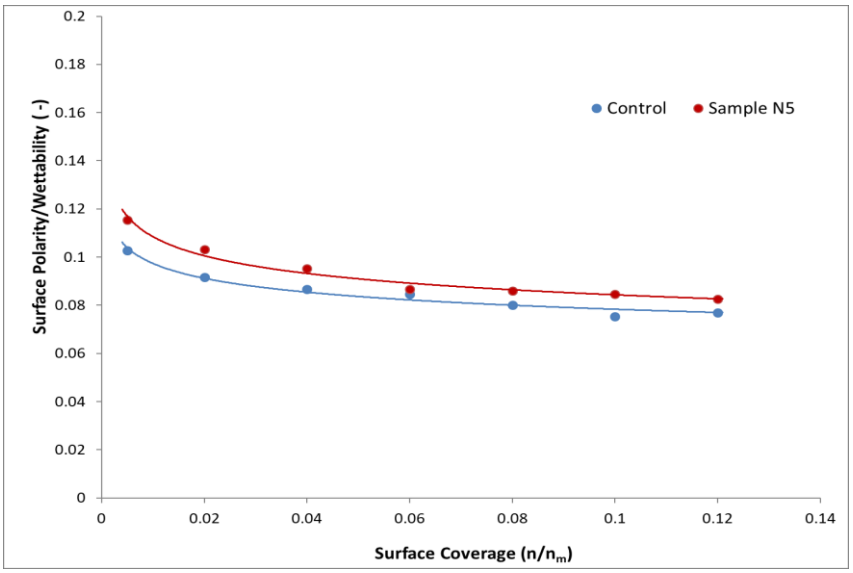

Figure 3.17 Polarity of the processed (N5) and control samples. The processed N5 sample has a higher polarity than the control sample, corroborating the specific or polar surface energy components seen in figure 3.15

3.4.6.2.2 Surface energy distribution

In order to represent the heterogeneity of the samples in a more illustrative manner, the surface energy distributions are obtained by a point-by-point integration of the surface energy profiles, resulting in plots of dispersive surface energy (γ_s^d), *specific surface energy* (γ_s^{ab}) *and total surface energy* (γ_s^t) surface energy versus area increment, as shown in Figure 3.18 – 3.19. The dispersive surface energy of the control sample ranges from a minimum of 40.02

mJ/m^2 to a maximum of 46.72 mJ/m^2 over a surface coverage of 0 to 12% while that of N5 ranged from 41.40 mJ/m^2 to 45.27 mJ/m^2 over the same surface coverage. The specific and total surface energy values ranges from 3.26 mJ/m^2 to 5.44 mJ/m^2 and 43.28 mJ/m^2 to 52.16 mJ/m^2, and from 3.71 mJ/m^2 to 6.12 mJ/m^2 and 45.14 mJ/m^2 to 51.39 mJ/m^2 for the control and N5 samples respectively.

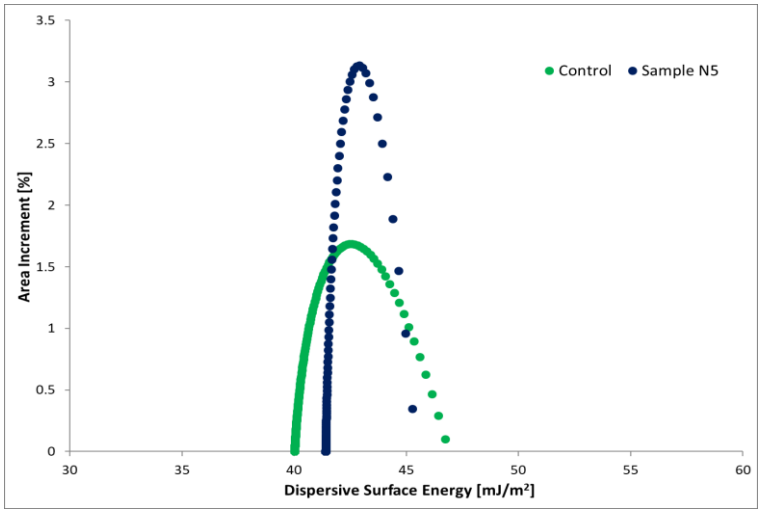

Figure 3.18 Comparison of dispersive surface energy distributions for the processed (N5) and control samples, showing a wider distribution for the control sample than the processed N5 sample

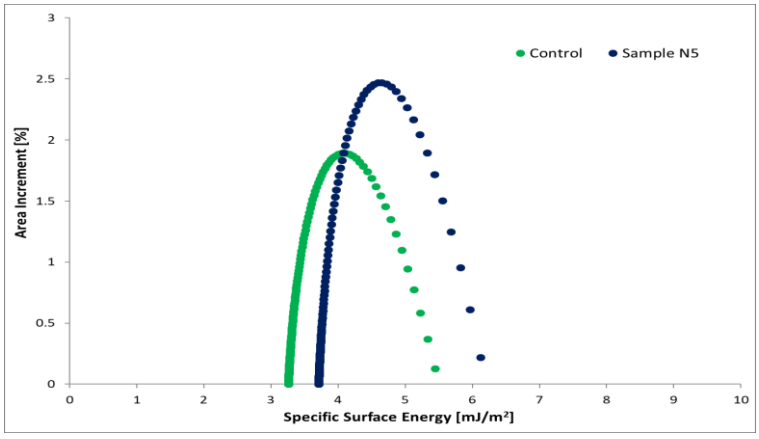

Figure 3.19 Comparison of acid-base surface energy distributions for the processed (N5) and control samples, showing a wider distribution for the control sample than the processed N5 sample

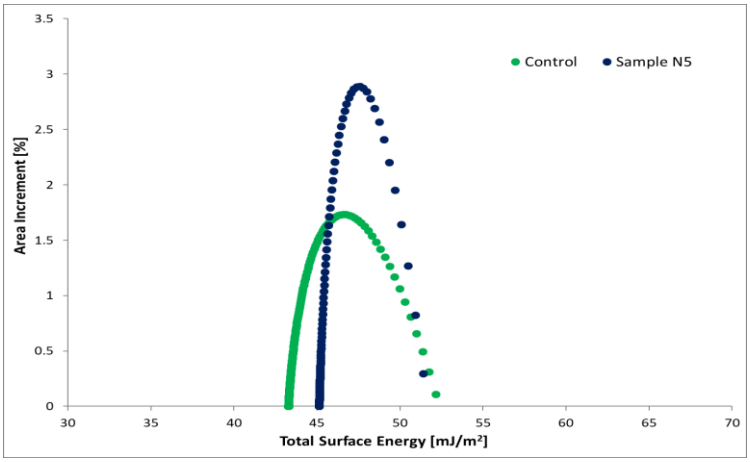

Figure 3.20 Comparison of total surface energy distributions for the processed (N5) and control samples, showing a wider distribution for the control sample than the processed N5 sample

The wider distributions observed for the control sample in figure 3.18 – figure 3.20 reveal that the surface energy of N5 is more homogenous than the control sample, while the control sample is relatively more heterogeneous possessing surface sites with the most different levels of energy. This distribution profile corresponds with the results obtained from the BET SSA, where there was a decrease in SSA of N5 compared to the control, attributed to the mopping up of fine lactose by coarse lactose. This mopping up effect, which entails the coating of fine lactose onto presumably high-energy sites on coarse lactose, may also passivate the high-energy sites producing a more homogenous surface. Similar findings have been reported, where the silanisation of D-mannitol was found to increase the surface energy homogeneity. Khoo et al., (2012) reported that the substitution of hydroxyl groups on D-mannitol as received with dimethylsilane groups produced a more energetically homogenous surface as determined by IGC. In addition, the higher polarity of the processed N5 sample is attributed to possible reorientation of the molecules of lactose water of crystallisation, increasing interaction between polar probes and particle surface, and resulting in increased polar surface energy. This is considered in detail in chapter five of this thesis, where multiple surface energy measurements are available.

3.5 Conclusion

The results in this study show that as with other studies with the iDPC, no particle attrition occurs during processing. It also shows that fine lactose adhere to coarse lactose surface during processing; and may compete with API for active sites on coarse lactose. Sieved lactose samples apparently had fewer fines than the unsieved samples. This reflected in better flow in the sieved samples and less attachment of fines to the coarse particle surface as seen in the scanning electron micrographs. The results reveal that the iDPC does not cause significant change to carrier particle size, thermal properties and powder flowability, but may cause some changes to the lactose surface properties such as surface rugosity, specific surface area and surface energy distribution. The changes observed are related to the adsorption of fine lactose to coarse lactose surface during processing in the iDPC. In addition, the extent of changes observed correlates with variations in processing parameters, which reflects input energy of the coating process.

4. Chapter Four

Investigation of the effect of fine lactose content and lactose surface pre-conditioning on DPI performance of fluticasone propionate and process optimisation by experimental design

4.1 Introduction

The incorporation of fine lactose particles in a carrier-based DPI formulation has been investigated. Supported by two major theories, the inclusion of lactose fines has been found to enhance formulation performance (Zeng et al., 1998; Zeng et al., 1999; Le et al., 2012; Kinnunen et al., 2014). The first is the “active site” theory, which explains that fine lactose particles attach to potential drug binding sites, leaving the drug particles to attach to less active sites on carrier surface from which they are more easily detached on inhalation. Surface active sites on lactose particles have been described based on surface morphology, surface energy and chemical properties. Surface crevices which are larger than drug particles and reduce the tendency for drug detachment are presumed to be active sites; so are sites with raised surface energy, related to polar or dispersive forces, increased surface interaction forces e.g. van der Waals or capillary forces; and sites which are charged or chemically contaminated (Zhou and Morton, 2012). There is however, no evidence of preferential binding of lactose fines over drug particles or vice-versa at such “active sites”; thus, a lactose fines before drug particles blending order was important for improved DPI formulation performance based on this theory (Zeng et al., 1998).

The second is the “agglomerate theory”, which was put forward based on contrasting evidence where blending order did not influence the formulation performance (Lucas et al., 1998). This theory speculates that rather than block active sites on coarse lactose, fine lactose particles form agglomerates with the fine drug particles. Upon inhalation, the fine API particles are more easily detached from the fine lactose surface due to smoother carrier surface, or the carrier-drug agglomerates may be small enough to be delivered as part of the respirable dose. There is also the possibility of easier detachment of the drug-carrier agglomerates, since its greater mass allows for greater effect of fluid forces for drug detachment by the nitrogen flow stream (Lucas et al., 1998; Jones and Price, 2006; Jones et al., 2008). Despite the benefits of incorporating fine lactose into a carrier system for enhanced DPI performance, optimal amounts have to be used to avoid drawbacks such as poor flow and blend inhomogeneity associated with increasing amount of fine lactose carrier (Guenette et al., 2009).

Following the mechanistic understanding of fine particle distribution and deagglomeration studies presented in chapter two, and the understanding of the surface characteristics of the lactose carrier Inhalac 251® as described in chapter three, the next step was to understand the impact of addition of fine lactose and lactose pre-processing on process characterisation. This chapter is divided into two parts; the first part involves preliminary experimentation to determine effects of different fine lactose concentration in comparison to the effect of carrier pre-conditioning in the iDPC on formulation performance. DPI formulation performance was evaluated based on formulation flowability, API content analysis and aerosolization performance, using fluticasone propionate as a model drug candidate. While the addition of fine lactose to improve DPI formulation performance is common practice, the use of pre-conditioned lactose helps to investigate the potential for a fines free DPI formulation with optimal aerosolization performance and added advantage of improved flow. In the second part of this chapter, all the elements of a robust QbD approach, as specified in the ICH guidelines Q8 (ICH, 2009) are then put together to develop a model DPI formulation, with the generation of a design space.

- **Aim**
    - To study the impact of fine lactose addition and lactose pre-conditioning on process characterisation, and compare the effects of both techniques on DPI formulation performance and to use a QbD approach to develop a model DPI formulation
- **Objectives**
    - To introduce different amounts of fine lactose to sieved lactose and blend with FP in the iDPC
    - To pre-process sieved lactose and blend with FP in the iDPC
    - To evaluate the performance of the model DPI blends based on FPF, CU and powder flow
    - To compare the performance of the two sets of model DPI blends

- To determine the optimal process parameters for DPI blend formulation in the iDPC, using experimental design and generate a design space

4.2 Materials and methods

4.2.1 Materials

Fluticasone propionate (VMD – 3.06 µm) was purchased from Pharmaserve (Runcorn, UK). Meggle (Wasserbyurg Am Inn, Germany) supplied inhalation grade alpha-lactose monohydrate Inhalac 251® and Inhalac 500®. Size 3 hard gelatin capsules were purchased from Qualicaps (Madrid, Spain), Aerolizer ™. HPLC grade methanol was purchased from Fischer Scientific (Loughborough, UK)

4.2.2 Methods

4.2.2.1 Preparation of coarse lactose

Inhalation grade alpha lactose monohydrate Inhalac® 251 (VMD 53.96 ± 0.46) was passed through a 38µm sieve for 60 minutes using a sieve shaker. Fine particles that passed through the sieve were collected at 20 minutes intervals (Zeng et al., 1998). This was done to remove the fine lactose particles below the X_{10} particle size distribution. The fraction retained on the 38µm sieve was collected, stored and used in this study.

4.2.2.2 Determination of theoretical surface coverage of coarse lactose

Theoretical surface coverage of the coarse lactose i.e. sieved Inhalac® 251 by fine lactose Inhalac® 500 was determined using the true density method. True volume was measured using a helium multipycnometer Quantachrome Instruments (Syosset, USA), based on Archimedes principle and Boyle's law of gas expansion. Helium gas was used as the displacement fluid, due to its ability to penetrate pores sizes up to 1 Angstrom. The gas was passed through the instrument between 30-60 minutes before sample analysis, and approximately 1g of powder was placed in the sample cell of the instrument. True volume (V_t) was obtained as the volume of the sample cell through which the helium gas could not penetrate, using equation 4.1.

Equation 4-1

$$\boldsymbol{V_t = V_c - V_R \left(\frac{P_1}{P_2} - 1\right)}$$

Where V_t = True volume of solid

V_c = Volume of sample cell

V_R = Reference volume

P_1 = Atmospheric pressure

P_2 = Change in pressure during determination

The true density was then calculated as a ratio of mass to volume using equation 4.2.

Equation 4-2

$$\boldsymbol{True\ density = \frac{M}{V_t}}$$

Using the true density values obtained, theoretical surface coverage was calculated using equations 4.3 and 4.4, which assume that the carrier is spherical.

Equation 4-3

$$\boldsymbol{Gwt\% = \frac{Nd^3P_d}{(D^3P_D) + (Nd^3\ P_d)} \times 100}$$

Equation 4-4

$$\boldsymbol{N = \frac{4\ (D + d)^2}{d^2}}$$

Where d = Diameter of guest particle (fine carrier)

D = Diameter of carrier particle (coarse carrier)

P_d = Density of guest particle

P_D= Density of carrier particle

4.2.2.3 Preparation of pre-blended carrier

100g of pre-blended carriers were prepared by mixing sieved Inhalac® 251 with Inhalac®500 in a cube mixer at 46rpm for 60 minutes (Kinnunen et al., 2014 used Tubular mixer). Fine lactose was added at concentrations of 4.7% $^{w}/_{w}$, 9.4% $^{w}/_{w}$, 14.1% $^{w}/_{w}$ and 18.8%$^{w}/_{w}$, which represent 25%, 50%, 75% and 100% surface coverage of the coarse lactose, as obtained from the theoretical surface coverage calculations. These pre-blended carriers were stored for at least 7 days before being used to prepare DPI formulations to eliminate static effect.

4.2.2.4 Preparation of pre-conditioned carrier

15g of sieved Inhalac® 251 was processed in the iDPC device using different processing parameters. These parameters were chosen from a previous experimental design (chapter three), in which Inhalac® 251 was processed using the iDPC to investigate changes that occur to lactose physicochemical properties during processing. The process parameters used for the carriers and model DPI blends are shown in Table 4.1.

Table 4.1 Process parameters used for the pre-conditioned carriers and model DPI blends

	Nitrogen flow	Speed	Duration
N2	0.4	1000	10
N5	0.4	2000	10
N7	0.4	2000	20
N11	0	2000	30
All model DPI Blends	0.4	2000	30

4.2.2.5 Preparation of model DPI blends

10g batches of model DPI blends containing 0.71% $^{w}/_{w}$ FP were formulated with the pre-blended carriers containing different concentrations of fine lactose and pre-conditioned carriers using the iDPC. 70mg of fluticasone propionate was weighed and hand mixed, using a spatula with a small amount of the required carrier after which the rest of the carrier was added. This was then poured into the mixing chamber of the iDPC device, and processed at 201G (2000rpm), 40L/min for 30 minutes for all the formulations. A control formulation using coarse lactose (sieved Inhalac® 251) as the carrier was also prepared to compare the effect of fine lactose and effect of lactose pre-conditioning. All formulations were stored at 25^{0}C and 60% relative humidity.

4.2.2.6 Particle size analysis by laser diffraction

The particle size of the lactose raw materials, pre-blended carriers, pre-conditioned carriers, API and model DPI formulations were measured using Sympatec™ HELOS/RODOS particle size analyser which works by laser diffraction principle. Approximately 1g of powder samples were fed into a vibratory feeder which transfers the powder into the dispersing unit (RODOS). The powder samples were dispersed under compressed air at a pressure of 2 bar into the analyser (HELOS), where the particle size and particle size distribution of the dispersed powder is determined by laser diffraction. X_{10}, X_{50}, X_{90} and the mean volume diameter (VMD) values were recorded for each sample.

4.2.2.7 Powder flow (Angle of Repose)

5g of the model powder blends was poured through a 50mm glass funnel (Pyrex), held with a retort stand, on a flat surface to form a cone of the powder. The height and diameter of the cone formed by the powder were then measured, and the angle of repose calculated using equation 4.5 (Kaialy et al., 2011). This was done in triplicate, and the mean angle of repose was determined.

Equation 4-5

$$\boldsymbol{Tan\ \alpha = \frac{2h}{D}}$$

Where h= height of powder cone

D= diameter of powder cone base

4.2.2.8 Scanning Electron microscopy

Powder samples were dispersed onto a double-sided adhesive carbon tape and placed on a sample holder. The samples were gold coated to increase conductivity during imaging. Imaging was done using a field emission scanning electron microscope Zeiss Supra SS-VP (Zeiss, Oberkochen, Germany), at an accelerating voltage of 10.0kV. Images were taken at 150X and 500X magnification.

4.2.2.9 Content uniformity by HPLC

In order to determine the homogeneity of the model powder blends, drug content assay was carried out. Samples containing an equivalent of 100 µg FP were dissolved in 10 ml of methanol, sonicated for 10 minutes and filtered through a 0.5 mm filter membrane, and then analysed using a validated high performance liquid chromatography (HPLC) method described as follows. An Agilent-1260 infinity attached to a standard auto sampler 600bar and a variable wavelength detector which uses the Open Lab instrument driver for Agilent LC software for signal detection was used with a C18 Agilent Eclipse plus 3.5µm 4.6X100mm column for compound separation. 0.1% TFA in water: acetonitrile 40:60 was used as the mobile phase at a flow rate of 1.5ml/min for 6 minutes and detection wavelength of 230nm. Peaks were observed between 4.5 -4.7 minutes consistently for all concentrations, with reproducible peak areas across concentrations. This method was used to obtain a calibration curve, and then subsequently to carry out the content uniformity tests.

4.2.2.10 In-vitro aerosolization and deposition

In-vitro aerosolization from a capsule DPI and deposition of the model DPI blends was evaluated using a Copley® Next Generation Impactor™ (NGI – Copley Instruments UK). NGI cups were coated with 1% $^{w}/_{w}$ glycerol in acetone and the pre-separator was filled with 15 ml of methanol, to eliminate loss of particles. Six size 3 hard gelatine capsules were filled with 14±0.2mg of the model DPI blends, which contains an equivalent of 100 µg FP. Using an Aerolizer™, the formulation was aerosolized into an NGI at 60 l/min for 10 seconds. After aerosolization and deposition, the particles collected on each section of the NGI were washed into known volumes of methanol, and analysed for drug content using the same HPLC method described above for drug content uniformity.

The abbreviations used for the different lactose carriers are identified as follows:

Lactose as received – L

Sieved lactose – SL

Fine lactose – FL

Sieved lactose pre-blended in the cube mixer with different concentrations of fine lactose - BSL

Sieved lactose pre-conditioned in the iDPC using different process parameters – PSL

4.3 Results and Discussion

4.3.1 Particle size distribution of the starting materials, carriers and model DPI blends.

Several studies have reported the beneficial effect of adding fine lactose to coarse lactose carrier system on DPI performance (Zeng et al., 1998; Zeng et al., 1999; Le et al., 2012; Kinnunen et al., 2014). In order to correlate the amount and size distribution of fines present to their effects on DPI formulation performance precisely, the lactose used in this study (Inhalac® 251) was pre-treated by passing through a 38µm sieve to remove intrinsic fine particles. The specified particle size distributions of Inhalac® 251 and Inhalac® 500 by laser diffraction as indicated by the manufacturer are shown in table 4.2.

Table 4.2 Particle size distributions of L (Inhalac® 251) and FL (inhalac 500®) as indicated by manufacturer

X_{10} µm	X_{50} µm	X_{90} µm	Span[(X_{90} – X_{10})/ X_{50}]	% fines < 15 µm
Specified/typical	Specified/typical	Specified/typical		
7 – 22 / 13	40 – 70 / 49	80 – 120 / 91	1.6	11
NA	5 µm / 3.1 µm	10 µm / 7.9 µm	2.4	99

The particle size distribution of the lactose as supplied (L) and the fine lactose (FL) obtained in this study by laser diffraction are shown in Table 4.3. The results show a similarity in the manufacturer's values and the obtained values as expected. Also shown in table 3 is the particle size distributions for FP, the model API, which has a similar X_{10}, X_{50}, X_{90} and VMD to FL. A similarity in geometric size of fine carrier and API has been suggested to facilitate DPI performance (Peng et al., 2016).

Table 4.3 Particle size distributions of L (Inhalac® 251) and FL (inhalac® 500) as determined in this study by laser diffraction. Data is presented as Mean ± Standard deviation S.D. where n = 3

	X_{10} (µm)	X_{50} (µm)	X_{90} (µm)	VMD (µm)
Fluticasone propionate (FP)	1.08 ± 0.20	2.59 ± 0.39	5.17 ± 0.74	3.08 ± 0.48
FL (Inhalac® 500)	0.84 ± 0.06	2.82 ± 0.29	6.71 ± 0.37	3.37 ± 0.24
L (Inhalac® 251)	13.24 ± 0.54	52.11 ± 0.30	96.84 ± 0.69	53.96 ± 0.46

The particle size distribution of the lactose as supplied (L), sieved lactose (SL) and pre-blended lactose (BSL) are shown in table 4.4 for comparison. X_{10} increased more than two fold post sieving from 13.24 ± 0.54 µm in L to 29.53 ± 0.58 µm in SL, showing that intrinsic fines were removed adequately from L. During the sieving process, approximately 20g of lactose passed through the 38µm sieve per every 100g of lactose powder, representing 20% fines, therefore this increase in X_{10} was expected.

Table 4.4 Particle size distributions of L (Inhalac® 251), SL (Sieved Inhalac® 251) and BSL (SL pre-blended with different concentrations of FL). Data is presented as Mean ± Standard deviation S.D. where n = 3

	X_{10} (µm)	X_{50} (µm)	X_{90} (µm)	VMD (µm)
L (Inhalac® 251)	13.24 ± 0.54	52.11 ± 0.30	96.84 ± 0.69	53.96 ± 0.46
SL (Sieved Inhalac® 251)	29.53 ± 0.58	62.75 ± 0.37	101.90 ± 1.86	64.18 ± 0.73
SL +4.7% FL	4.35 ± 0.04	58.07 ± 0.38	96.81 ± 1.54	56.44 ± 0.70
SL +9.4% FL	2.18 ± 0.06	53.57 ± 0.39	96.34 ± 2.18	50.97 ± 0.91
SL +14.1% FL	1.64 ± 0.12	47.77 ± 0.41	89.27 ±1 .61	44.14 ± 0.56
SL +18.8% FL	1.35 ± 0.03	41.02 ± 0.32	87.02 ± 0.56	39.56 ± 0.23

Upon addition of FL lactose to SL, there was a significant drop in the X_{10} and VMD of the pre-blended carriers as fine lactose content increased. Also, the lowest fine lactose concentration 4.7%$^{w}/_{w}$ substantially reduced the X_{10} from 29.53µm to 4.35µm. This substantial decrease in X_{10} is due to the low mean particle size (< 5 µm) of FL. With further addition of FL, there was

no corresponding decrease in X_{10} to the same extent as seen with the 4.7%$^{w}/_{w}$ FL concentration. The VMD of FL was 3.37μm (Table 4.3), therefore, regardless of further increase in FL concentration, the X_{10} of resulting pre-blended carriers was not expected to be far from this value. The changes observed in the particle size distributions are also evident in the SEM micrographs of the carriers shown in figure 4.1.

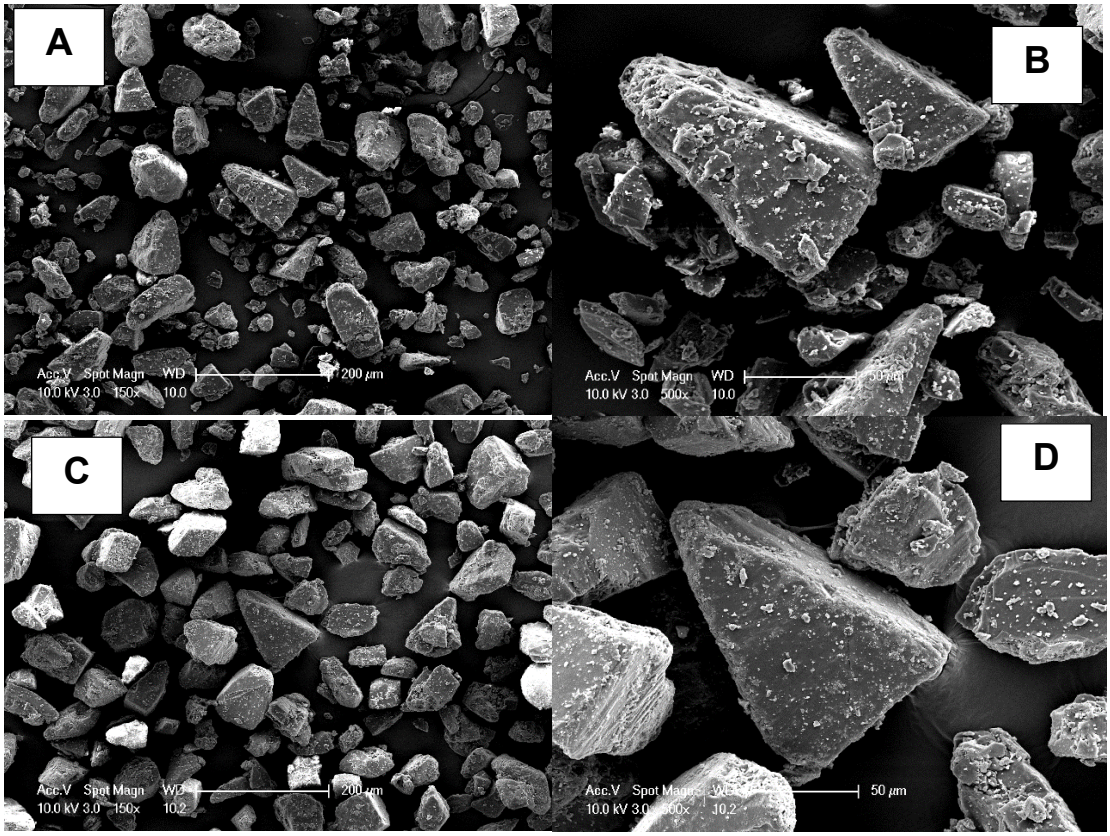

Figure 4.1 Scanning electron micrographs (SEM) of (A and B) Lactose as received, (C and D) at differrent magnifications (A and C X150) (B and D X500)

The SEM images shown in figure 4.1 provide qualitative correspondence to the particle size results. In figure 4.1 (A and B), the image of the Inhalac® 251 as supplied shows fine lactose in the field of view, which are the intrinsic fines. This was expected because the inhalation grade lactose used contains a high proportion of fines about 11% of fine lactose < 15µm and has a broad particle size distribution. However, after sieving as shown in figure 4.1(C and D), there are no longer fines in the field of view, although, some fines still appear to be attached to the coarse lactose surface. The increasing content of fine lactose is also evident in the SEM images shown in figure 4.2 as the concentration of fine lactose added to the sieved lactose increases. Upon addition of 4.7% of fine lactose (figure 4.2 A and B), some fine lactose can be seen in the field of view, although, most of the fine lactose are attached to the coarse lactose surface. There is a marked increase in the amount of fine lactose agglomerates at 14.1% fines compared to 9.4% fines. This may be attributed to the attainment of a monolayer coverage of the coarse lactose by fine lactose at 9.4% concentration. Whereas the theoretical

surface coverage calculation suggests that 18.8% of fine lactose is required for a complete monolayer surface coverage, the calculation assumes that the particles are spherical, which is not the case. The impact of the change in fine lactose content of the pre-blended carriers is expected to reflect in the flow properties of the model DPI blends made with these carriers.

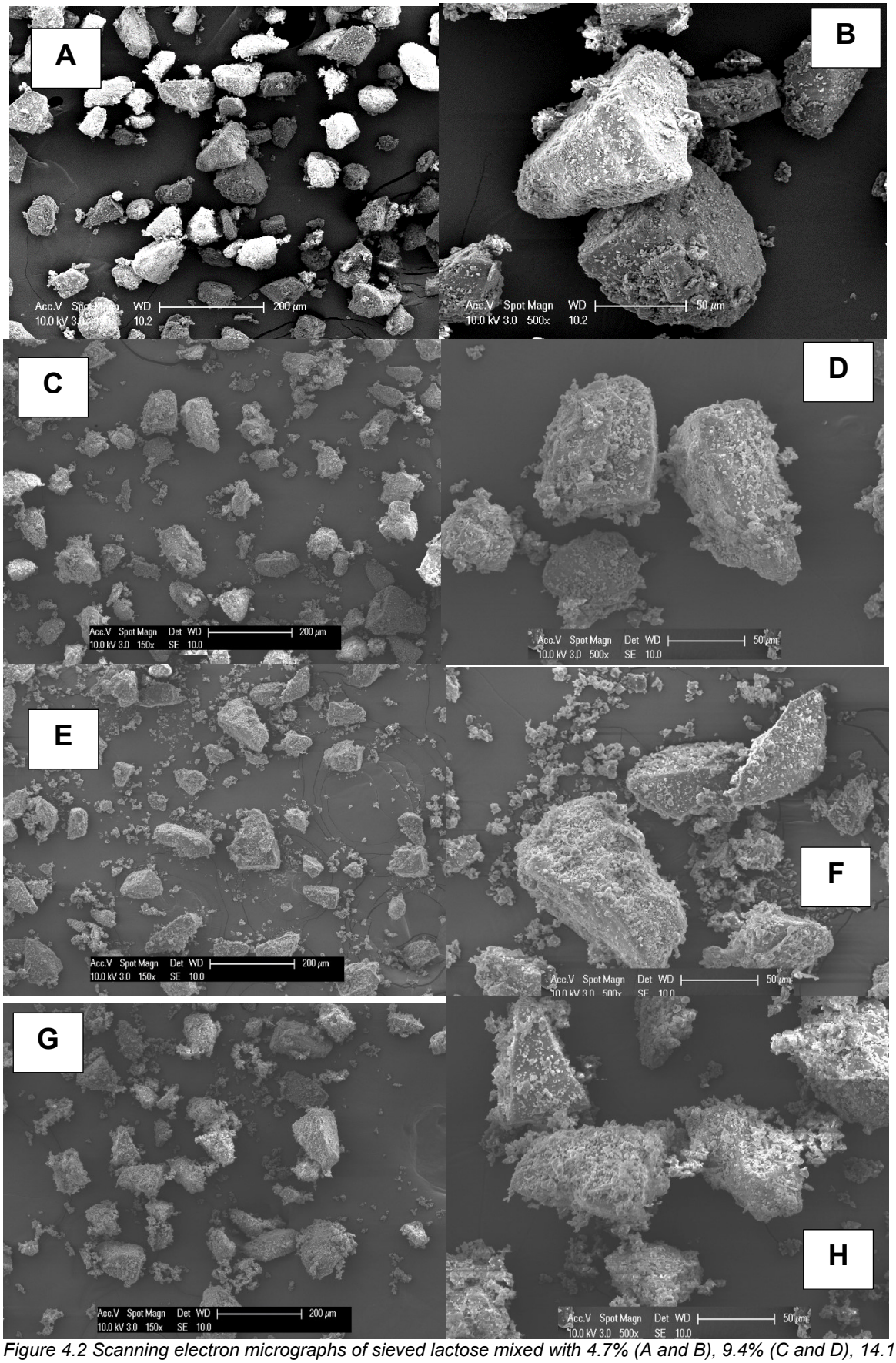

Figure 4.2 Scanning electron micrographs of sieved lactose mixed with 4.7% (A and B), 9.4% (C and D), 14.1% (E and F) and 18.8% (G and H) fine lactose at different magnifications (A, C,E and G X150) (B, D, F and H X500)

The particle size distribution of sieved lactose (SL) and sieved lactose pre-processed in the iDPC under different conditions (PSL) are shown in table 4.5 for comparison. There is a slight increase in X_{10} of the processed carriers compared to SL, which is attributed to the coating of any remaining fines after sieving to the coarse lactose surface during processing. This was expected, as the dry coating process using the iDPC has been shown in previous studies to be able to "mop up" fine particles by deposition onto coarse particle surface (Koner et al., 2017).

Table 4.5 Particle size distributions of the sieved lactose (SL) and sieved lactose pre-conditioned in the iDPC under different conditions (PSL). Data is presented as Mean ± Standard deviation S.D. where n = 3

	X_{10} ± S.D. (µm)	**X_{50} ± S.D. (µm)**	**X_{90} ± S.D. (µm)**	**VMD (µm)**
SL	29.53 ± 0.58	62.75 ± 0.37	101.90 ± 1.86	64.18 ± 0.73
SL Processed as N2	32.16 ± 1.61	64.22 ± 0.62	106.08 ± 4.94	66.64 ± 0.74
SL Processed as N5	30.85 ± 1.50	61.96 ± 1.03	97.46 ± 3.09	62.70 ± 1.87
SL Processed as N7	31.39 ± 0.27	63.11 ± 0.44	101.38 ± 1.61	64.63 ± 0.70
SL Processed as N11	31.50 ± 0.31	63.12 ± 0.21	101.01 ± 1.31	64.56 ± 0.48

In addition, the particle size distribution of all the PSL carriers is consistent post-processing. This implies that the processing conditions did not have an impact on the carrier particle size. The consistency in particle size post-processing also corresponds with results from previous chapters that the iDPC does not cause particle attrition, which is a major concern with the use of other dry particle coating devices (Gera et al., 2010; Dahmash and Mohammed, 2015). The SEM images of the PSL carriers shown in figure 4.3 also confirm these results. All pre-conditioned carriers appear to have a similar appearance, there is no fine lactose in the field of view and any remaining fines are attached to coarse lactose surface. The impact of this steady particle size distribution is expected to reflect in the flow properties of the model DPI blends made with these carriers.

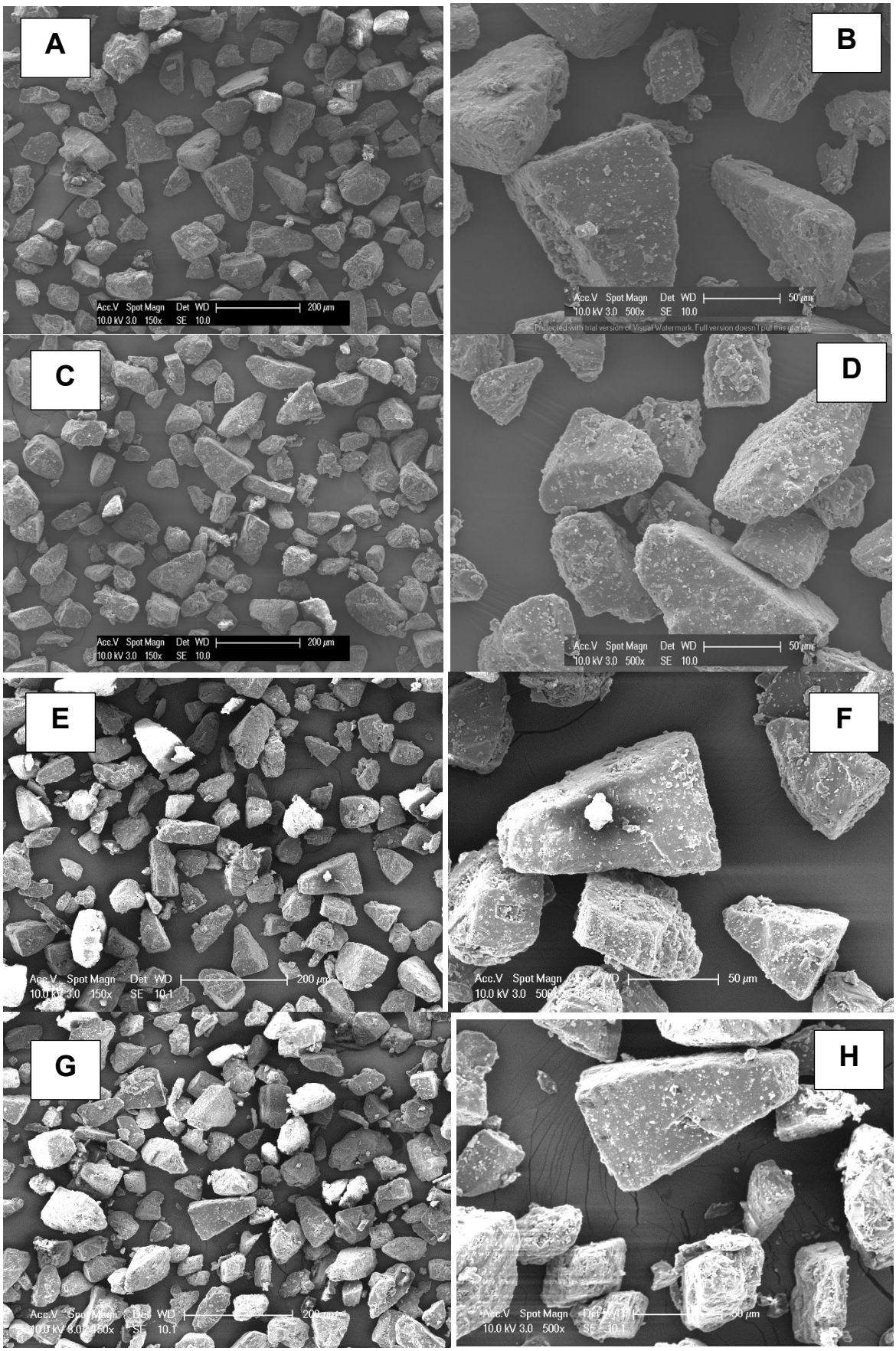

Figure 4.3 Scanning electron micrographs of sieved lactose processed at N2 (A and B), N5 (C and D), N7 (E and F) and N11 (G and H) at different magnifications (A, C, E and G X150) (B, D, F and H X500)

4.3.2 Powder flow properties of the DPI blends

The powder flow properties of a DPI formulation is critical in determining the ease of handling and dosing into a reservoir or unit or multi dose device, which in turn affects dose uniformity (Zeng et al., 2001). The powder flow properties of the model DPI blends were measured by angle of repose, the USP Angle of Repose classification for powder flow is shown in table 4.6.

Table 4.6 USP Angle of Repose classification for powder flow

Flow property	Angle of repose (^{0})
Excellent	25 – 30
Good	31 – 35
Fair	36 - 40
Passable	41 - 45
Poor	46 - 55
Very poor	56 - 65
Very very poor	>66

4.3.2.1 DPI blends prepared using carriers pre-blended with fines

Figure 4.4 shows the relationship between increasing fine lactose concentration and powder flow for DPI blends prepared. Increasing fine lactose concentration resulted in a corresponding increase in angle of repose (AoR), which infers a decline in powder flow. As expected, the impact of the change in fine lactose content reflects in the flow properties of the model DPI blends.

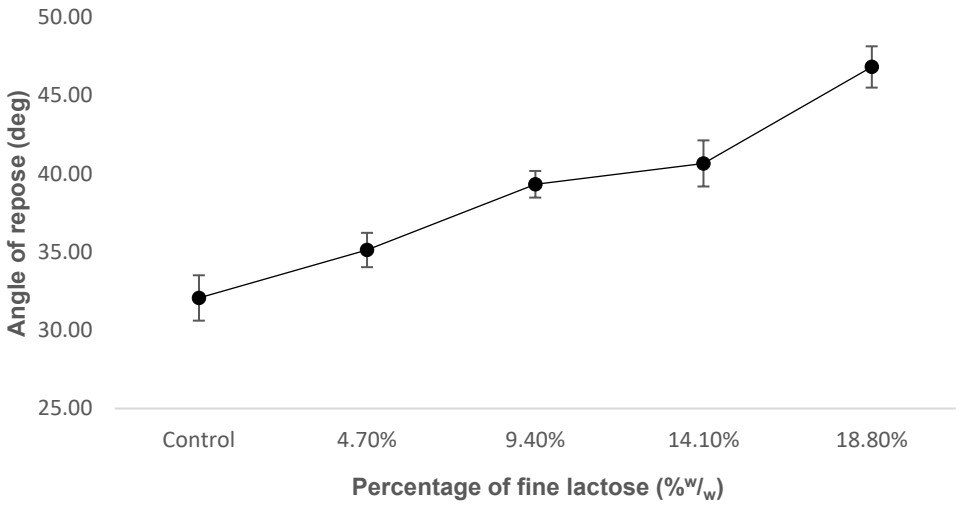

Figure 4.4 Relationship between fine lactose concentration and powder flow as assessed by AoR, showing a progressive decline in powder flow as fine carrier content of the DPI blends increases

As concentration of FL increases, there is a corresponding increase in AoR, which is related to the cumulative percentage of fine particles as shown in table 4.7. As concentration of FL increases, there is a linear increase in the cumulative percentage of fine particles below 5µm, at 6.25%, 12.33%, 16.24% and 20.44% for 4.7% $^{w}/_{w}$, 9.4% $^{w}/_{w}$, 14.1% $^{w}/_{w}$ and 18.8% $^{w}/_{w}$ of FL concentration respectively compared to 3.03% in the control sample. This adequately reflects the impact of increasing FL concentration in the model DPI blends. The relationship between powder flow and interparticulate cohesion, which is more pronounced with fine particles, was evident in the AoR for each sample with respect to the amount of fines present.

Table 4.7 Particle size distributions of the model DPI blend prepared with BSL carriers, the data is presented as Mean ± Standard deviation S.D. where n = 3

Sample ID	X10 (µm)	X50 (µm)	X90 (µm)	< 5 µm (%)
Control	30.27 ± 1.01	65.10 ± 1.17	114.61 ± 4.76	3.02 ± 0.22
4.7% Inh 500 - FP	7.73 ± 0.54	60.45 ± 0.29	100.31 ± 1.03	6.25 ± 0.31
9.4% Inh 500 -FP	3.52 ± 0.71	56.24 ± 2.10	96.25 ± 2.57	12.33 ± 2.16
14.1% Inh 500 -FP	2.84 ± 0.23	54.29 ± 1.06	96.02 ± 0.31	16.24 ± 1.50
18.8% Inh 500 - FP	2.39 ± 0.08	43.17 ± 3.44	91.34 ± 1.65	20.44 ± 1.09

Furthermore, according to the USP AoR classification for powder flow (Table 4.6), the DPI blend prepared using 4.7% $^{w}/_{w}$ FL and the control sample prepared using SL both have good flow (35.13 ± 1.10^{0} and 32.07 ± 1.45^{0} respectively). This was an interesting observation, considering the huge drop in X_{10} observed in the particle size distribution on addition of 4.7% FL. Although, the drop in X_{10} was expected to reflect significantly in the flow properties of the DPI blend, it is important to note that the DPI blends were processed in the iDPC, while the pre-blended carriers were mixed in a cube mixer. One of the applications of the dry coating technology is to improve powder flow. Mei et al. (1997) quantitatively examined the mechanism of improved powder flow by dry coating. They came up with an explanation using the extended Johnson Kendall-Roberts (JKR) theory, which shows that in the presence of a fine coating, the cohesion force between two host particles is directly proportional to the guest: host size ratio and significantly reduces cohesion. Therefore, the presence of a fine coating is able to reduce the van der Waals attraction between host particles. The fine particles (carrier and API) in this case may not have improved the powder flow compared to the control sample, but were able to keep the flow properties of the DPI blend within the “good flow” range despite the considerable fine particle content produced by adding 4.7% $^{w}/_{w}$ fine lactose to the carrier system. There is also a slight increase in X_{10} for all DPI blends (Table 4.7) compared to their corresponding carriers (Table 4.4), which shows that carrier and API fine particles have been coated onto coarse carrier surface during the dry coating process, and carrier fines have formed larger agglomerates with API fines as seen in SEM images (figure 4.5). The impact of fine carrier addition on powder flow is evident in subsequent FL concentration, as the powder flow of the remaining DPI blends changes from good (control and 4.7% FL) to fair (9.4% FL) to passable (14.1% FL) and to poor flow (18.8% FL). The SEM images of the model DPI blends shown in figure 4.5 agree with the results obtained. Figure 4.5A shows the DPI blends prepared with carrier containing 4.7% fine lactose. In addition to the carrier and API fines attached to the coarse carrier surface, there are agglomerates of carrier and API fines that are apart from the coarse carriers. This trend continues to increase as the amount of fine lactose in the carrier system increases as seen in figure 4.5 (B) 9.4%, (C) 14.1% and (D) 18.8%, in

which the agglomerates of carrier and API increases continuously. Beyond the impact of these agglomerates of carrier and API on flow properties, it is expected that they will also influence the aerosolization performance of the DPI blends with respect to API detachment mechanism and the resultant NGI deposition profile.

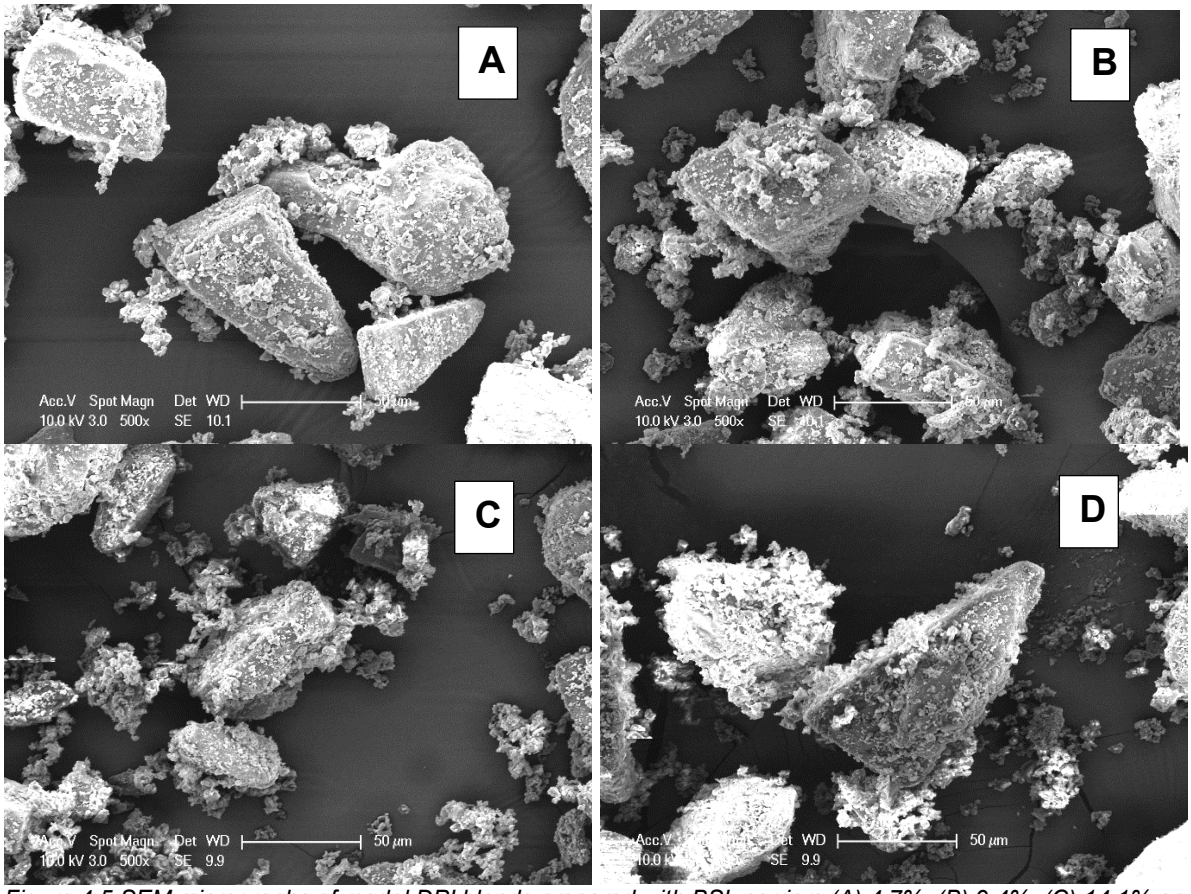

Figure 4.5 SEM micrographs of model DPI blends prepared with BSL carriers (A) 4.7%, (B) 9.4%, (C) 14.1% and (D) 18.8% fine lactose concentration. There is an increase in the agglomerates of carrier and API fines as fine lactose concentration increases

4.3.2.2 DPI blends prepared using pre-processed carriers

The relationship between carrier process parameters and powder flow properties of DPI blends prepared using the pre-processed carriers are shown in Figure 4.6. The removal of fine particles from the carrier system contributed to better flow in this set of DPI blends, due to reduced cohesion. Although all samples have slightly higher AoR than the control sample, they all remain within the good flow region according to the USP Angle of Repose classification.

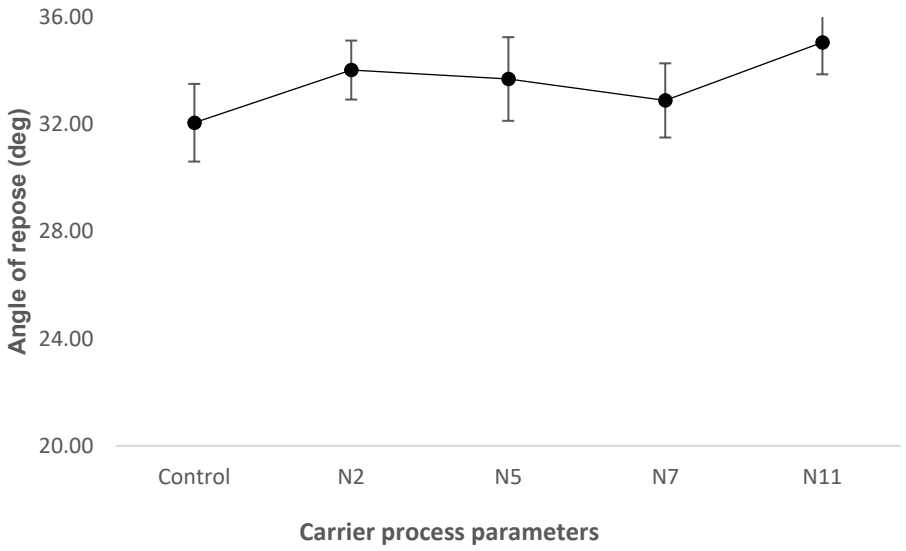

Figure 4.6 Relationship between carrier process parameters and powder flow of DPI blends as assessed by AoR, showing all samples with flow properties within the good flow region

Similar to the particle size distribution result of the carriers, the DPI blends also show a consistency in powder flow regardless of the processing parameters in the iDPC (Note that carriers were previously processed in the iDPC device between 10 minutes to 30 minutes as shown in Table 4.1, before being blended with the API for another 30 minutes). The percentage of fine particles below 5 µm is between 2% - 2.5% as shown in table 4.8 compared to 6% - 20% as seen in the model formulations prepared with the BSL carriers.

Table 4.8 Particle size distributions of the model DPI blends prepared with PSL carriers, the data is presented as mean ± Standard deviation S.D. where n = 3

Sample ID	X_{10} ± S.D. (µm)	X_{50} ± S.D. (µm)	X_{90} ± S.D. (µm)	< 5 µm (%)
Control	30.27 ± 1.01	65.10 ± 1.17	114.61 ± 4.76	3.02 ± 0.22
FP - N2	29.72 ± 1.98	64.93 ± 1.28	112.17 ± 10.2	2.05 ± 0.44
FP - N5	33.11 ± 1.49	65.26 ± 2.07	104.01 ± 4.53	2.29 ± 0.52
FP - N7	32.82 ± 1.22	64.50 ± 0.48	102.60 ± 0.30	2.45 ± 0.21
FP - N11	31.36 ± 0.51	63.76 ± 1.04	101.11 ± 0.83	2.26 ± 0.13

In addition to having more favourable powder flow properties compared to the DPI blends prepared with BSL, these results show that regardless of processing parameters which may vary depending on material of interest (carrier and API), the iDPC produces consistency in powder flow properties. This is primarily dependent on the bulk properties of the materials used and not influenced by process parameters in in the iDPC. The SEM images in figure 4.7 of the model DPI blends also confirm the results obtained.

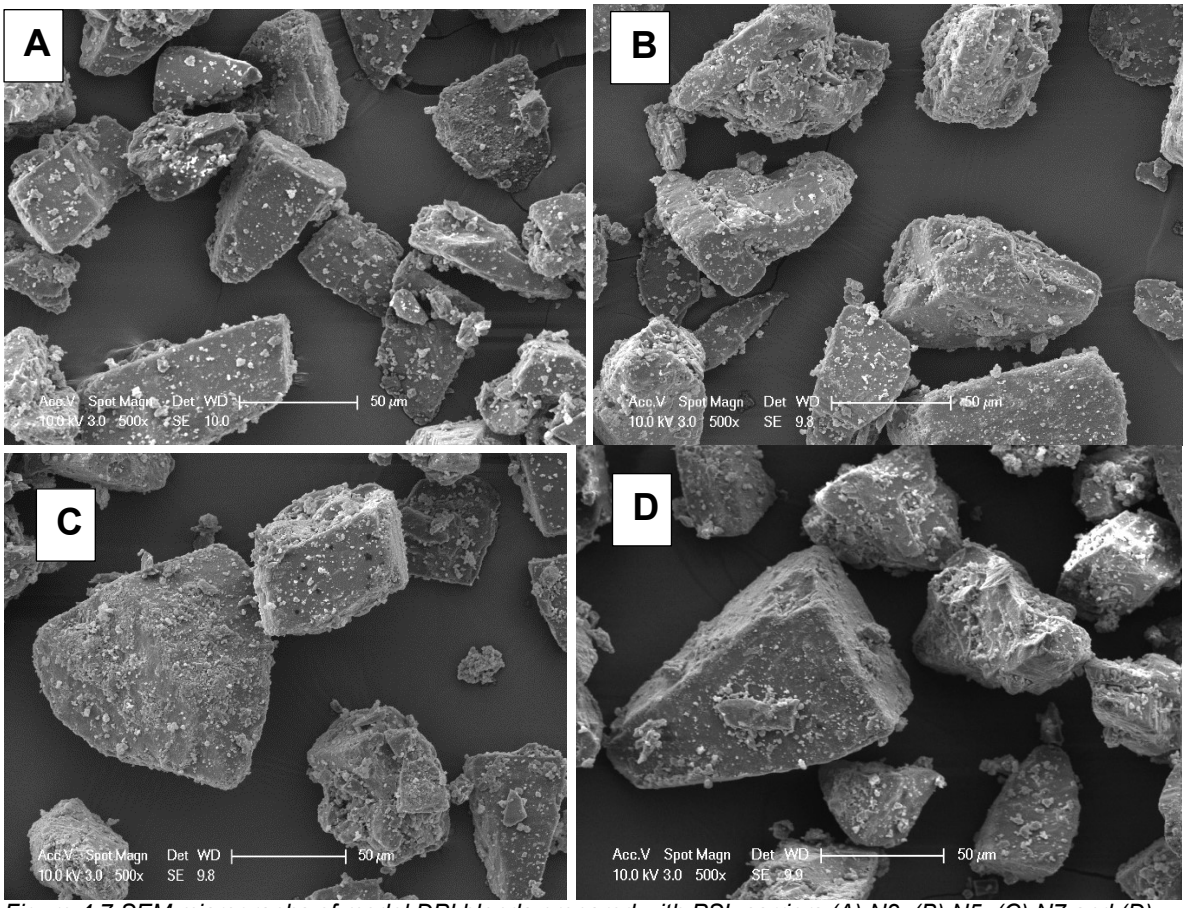

Figure 4.7 SEM micrographs of model DPI blends prepared with PSL carriers (A) N2, (B) N5, (C) N7 and (D) N11. All formulations appear similar, with the API attached to coarse lactose surface more like primary particles

As shown in figure 4.8, all the formulations appear similar, and the API are attached to coarse lactose surface as deagglomerated primary particles contrary to observations with the BSL carriers. Also, there are no agglomerates of carrier and API as observed with the BSL carriers. It is expected that this pattern of API attachment will similarly influence detachment mechanism and NGI deposition profile.

4.3.3 Content Uniformity of DPI blends

One of the purposes of dry particle coating is to achieve a homogenous blend, which has a uniform API content throughout the whole blend reflected in random samples that are representative of the whole mixture. The API used in this study, fluticasone propionate (FP) has a mean particle size less than 5µm; hence, it is cohesive in nature and has the tendency to form agglomerates. The formation of agglomerates in a powder blend is one of the causes

of blend inhomogeneity, the other being segregation, which is associated with particles of larger size (Pfeffer et al., 2001). The content uniformity assay analyses the efficiency of the dry coating process to produce homogenous blends. Since all the DPI blends were processed under the same iDPC conditions, any differences observed in blend homogeneity is down to variations in the carrier used i.e. varying content of FL in the carriers containing different proportions of FL and the different process parameters used for the pre-conditioned carriers..

4.3.3.1 DPI blends prepared using carriers pre-blended with fines

Figure 4.8 shows the percentage recovery and RSDs of the model DPI blends prepared using BSL. Although, the percentage recovery is less than 90 for all formulations, the control formulation has the highest recovery. This is an indication of the absence of fines in this formulation, as coarse carrier particles have been suggested to facilitate the breakdown of agglomerates and dispersion of fine API (Alonso and Alguacil, 1999; Pfeffer et al., 2001). However, the loss of API across all formulations may be attributed to the process parameters, which is yet to be optimized, specifically exposure of the blends to high centrifugal force, maximum nitrogen flow in the iDPC prototype used (40 L/min) for an extended blending duration of 30 minutes. Zheng (2009) reported the undesirable effect of prolonged mixing time on the content uniformity of the mixture. The mixing process is optimal when there is sufficient force necessary to de-agglomerate the cohesive powder as an initial step followed by dispersion and then homogenous redistribution of the deagglomerated powder throughout the mixture. When mixing duration is prolonged beyond optimal limits, there is a potential for API loss and blend heterogeneity due to prolonged particle-particle and particle-wall interactions, generating electrostatic forces within the device and creating the possibility of API particle loss through triboelectrification (Zheng, 2009).

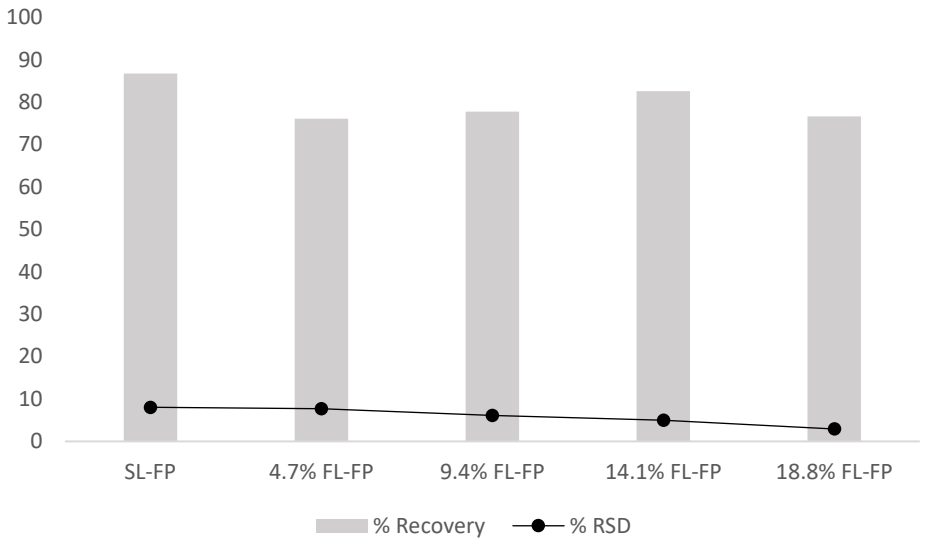

Figure 4.8 Percentage recovery and RSDs of FP from the DPI blends prepared with sieved lactose pre-blended in the cube mixer with different concentrations of fine lactose as analysed by HPLC

Furthermore, there is a difference in the RSDs of all the DPI blends. While the blends containing 14.1% and 18.8% FL have RSD < 5%, the blends prepared with 4.7% and 9.4% and the control sample, which does not contain FL have RSD > 5%. As FL increases, RSD decreases, indicating an increase in blend homogeneity. This may be attributed to the active sites theory in which case, the active sites on the SL is increasingly saturated by increasing FL concentration. The API then adheres to either less active sites on the SL or onto FL surface. This pattern of API deposition on carrier surface may facilitate a more homogenous blend during the redistribution stage, as the API is not trapped on active sites from where it is more difficult to detach and be more evenly distributed. On the other hand, in the blends containing none or lower FL concentration, there is an increased chance of the API being adsorbed onto active sites on the SL. This creates the potential for more difficult detachment during the redistribution stage of dry coating and leads to a less homogenous blend.

4.3.3.2 DPI blends prepared using pre-processed carriers

Figure 4.9 shows the percentage recovery and RSDs of the model DPI blends prepared using PSL. All the DPI blends in this category, regardless of processing conditions of the carrier

have RSDs < 5%, which represents a homogenous blend. This trend may be due to a surface conditioning to the lactose particles during pre-processing. In chapter three where the changes to lactose surface properties post processing in the iDPC were examined, it was observed that processing in the iDPC has the potential to homogenise the surface energy of the lactose particles. This may allow for a more uniform redistribution of deagglomerated fine API, thereby producing a more homogenous blend. In addition, the large carrier size also facilitates deagglomeration and distribution of cohesive API. Also, out of four blends, three have API recovery of at least 90%, the exception being the blend prepared with the carrier processed at 2000rpm for 30 minutes without nitrogen flow; the same blend has the highest RSD of 4.8%. It is not completely clear why this sample has the lowest API recovery and highest RSD, but it may very likely be due to the processing conditions of the carrier used for this blend. The carrier processing in the iDPC without nitrogen flow presumably did not create similar surface conditioning on the lactose as when the nitrogen flow was used. Recall from chapter two, it was observed that processing in the iDPC without the nitrogen flow did not produce the same quality of coating (with respect to deagglomeration and redistribution of cohesive rhodamine B particles) as when the nitrogen flow was present. Overall, the blends produced with the PSL demonstrate better blend homogeneity than those produced with BSL. The significant loss of API in both categories reflected by low API recovery may be attributed to extended blending duration, which subjects the API particles to triboelectrification. The high surface charge possessed by micronised particles makes it typical for them to adhere to container walls (Chow et al., 2007).

The impact of the tribolectrification concept becomes more paramount when APIs are mixed with excipients in formulation, as this increases the tendency of electrostatic charges being generated on the surfaces of the particles (Ghori et al., 2015).

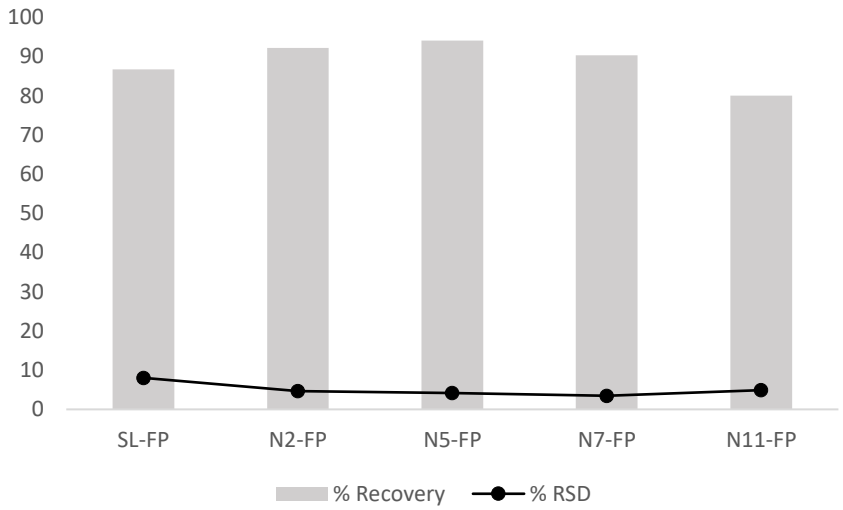

Figure 4.9 Percentage recovery and RSDs of FP from the DPI blends prepared with sieved lactose pre-processed in the iDPC under different conditions as analysed by HPLC

4.3.4 In-vitro aerosolization and deposition

4.3.4.1 DPI blends prepared using carriers pre-blended with fines

To investigate the influence of FL content on in-vitro lung deposition, aerodynamic properties of the DPI blends were tested using the NGI. The NGI profile of the DPI blends showing drug deposition in the different stages of the NGI is shown in figure 4.10. Drug deposition in the artificial throat and preseparator is notably high for the control sample followed by the blend containing 4.7% FL, with a corresponding lower deposition in the different stages of the NGI. The high deposition in the artificial throat in the control formulation may be attributed to API being deposited along with lactose, because the fine API particles in the control formulation may be adhered to carrier active sites from where detachment is less likely. Secondly, the coarse carrier size in the control formulation promotes detachment of API from carrier by momentum transfer during impaction with inhaler wall over the nitrogen flow stream. Therefore, only one mechanism of drug detachment is prevalent in the control formulation. This results in the lowest FPF obtained at 24.34% (Table 4.9) due to inadequate API detachment from carrier.

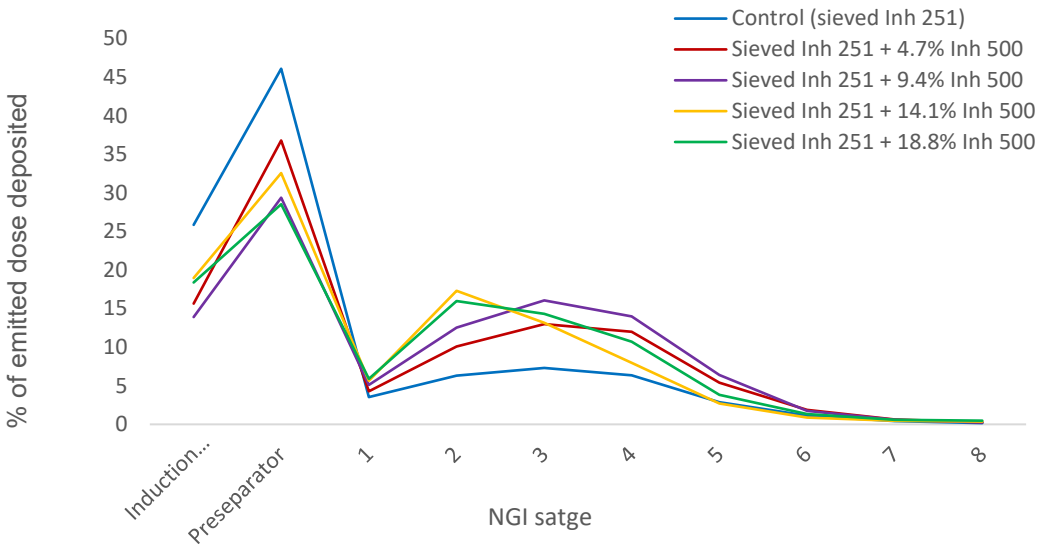

Figure 4.10 NGI profile of model DPI blends prepared with BSL carriers

With the addition of FL, there is a decrease in API deposition in the artificial throat and preseparator, and a corresponding increase in FPF (Table 4.9). This indicates that more primary particles are generated to reach the different stages of the NGI. In the presence of fine lactose, the two detachment mechanisms may act in synergy to disperse more API. The API attached to the carrier fines are detached by the nitrogen flow stream upon actuation of the DPI device, while the API attached to the coarse carrier are detached by momentum transfer when collision with other particles or inhaler device wall occurs.

In stages 1 and 2 of the NGI, there is an increase in API deposition as FL content increases, with the highest API deposition seen with blends containing 14.1% and 18.8% of FL and lowest API deposition with the control blend. This trend is consistent with the agglomerates theory, which explains how fine carriers facilitate aerodynamic performance of DPI formulations. The formation of agglomerates between the API and carrier fine particles will generate a larger particulate system than primary API particles, which are more likely to be deposited in the upper stages of the NGI as FL content increases. SEM micrographs of the formulations shown in figure 4.6 C and D respectively substantiates this observation, in which there are more agglomerates of carrier and API present compared to the formulations containing 4.7% and

9.4% fine lactose figure 4.6 A and B respectively. Another reason that supports the formation of carrier – drug agglomerates in this category may be the blending order and energy input used. The fine lactose was mixed with coarse lactose using the cube mixer at 46 rpm for 1 hour, while the API was blended with all BSL in the iDPC at 2000 rpm for 30 minutes. Earlier research has shown that when the blending energy input used for API and fine – coarse carrier system exceeds that used for blending fine and coarse carrier, the API is able to break the fine – coarse carrier adhesion, and form agglomerates with the fine carrier component (Apte, 2012).

Table 4.9 Aerosolization performance of model DPI blends prepared with BSL carriers, expressed as fine particle fraction (FPF) and mass median aerodynamic diameter (MMAD)

Sample ID	%FPF (Emitted)	%FPF (Theoretical)	MMAD
Control	24.34	16.94	3.42
4.7% Inh 500 - FP	42.98	25.49	3.19
9.4% Inh 500 -FP	51.34	31.25	3.28
14.1% Inh 500 -FP	42.45	21.92	4.28
18.8% Inh 500 - FP	46.73	25.44	3.85

As the NGI stages progress to stages 3 – 7, API deposition increases for DPI blends with lower FL content (4.7% and 9.4%), while that of blends with higher FL content (14.1% and 18.8%) reduces. The blend containing 9.4% FL shows the highest API deposition through stages 3 to 6 of the NGI. This indicates that with lower FL content, detachment of API from carrier yields primary particles with increased tendency to reach lower regions of the lungs, while higher contents of FL yield drug-carrier agglomerates, which target the upper lung region as represented by the NGI stages. Table 4 shows the overall FPF of all the DPI blends and respective MMAD. The blend containing 9.4% FL has the highest FPF, indicating optimal DPI performance. This is may be attributed to the monolayer coverage presumably achieved at this concentration of fines, as shown in SEM images in figure 4.2 (C and D), in which case

there is minimal carrier fines agglomerate present in the carrier system, rather, the fine lactose is mostly attached to the coarse lactose surface. This limits the formation of API – carrier agglomerates and facilitates the active sites theory, which produces higher FPF through the release of more primary API particles than API – carrier agglomerates. On the other hand, the blend containing 4.7% FL has the lowest MMAD indicating optimal dispersion of the DPI formulation into primary particles. This is plausible, as the low amount of fine lactose present facilitates API detachment by momentum transfer, which produces primary API particles that reach latter stages of the NGI. Despite a significant increase in aerodynamic performance of the model DPI formulations, there is need to optimise the blend uniformity and API recovery of the blends.

4.3.4.2 DPI blends prepared using pre-processed carriers

The highest increase in FPF in this category of DPI blends was a 10% increase from 24.34% in the control sample to 34.25% in the sample prepared with N5, as shown in table 4.10, which is lower than that obtained with the DPI blends prepared with BSL. This shows that the BSL carriers were more effective in increasing aerodynamic performance of FP. However, looking at the NGI deposition profile of the blends and control sample, they appear to follow a similar pattern up to stage 6 of the NGI as shown in figure 4.11.

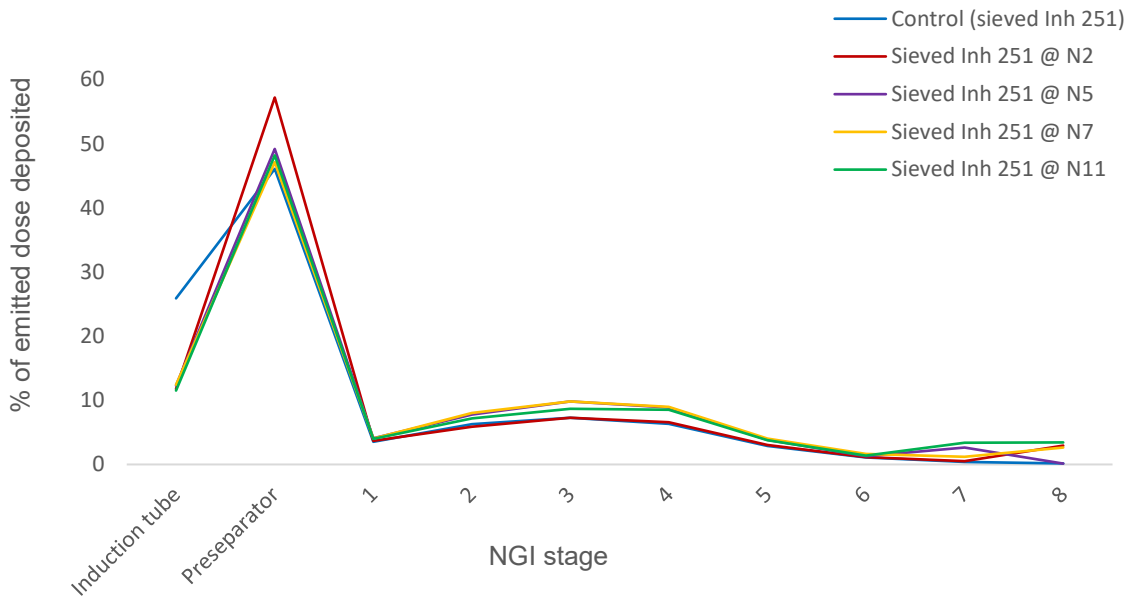

Figure 4.11 NGI profile of model DPI blends prepared with PSL carriers

From stage 6 onwards, the DPI blends prepared with PSL begin to show a different profile from the control sample. While there is a decline continues in the deposition of FP in the control sample from stage 4 up to the MOC, the blend prepared with PSL (N11) shows a continuous increase in FP deposition at stages 6 and 7 after which it plateaus until the MOC. The blend prepared with PSL(N5) shows an increase in FP deposition at stage 6 and 7 and then a decrease afterwards at the MOC, while the blends prepared with PSL (N2 and N7) show an increase in FP deposition at stage 7 and the MOC. This reveals that although the carrier pre-processing did not increase overall FPF like the addition of fines, there was a significant increase in API deposition in the latter stages of the NGI with this category of blends. In addition, the MMAD of the DPI blends shown in table 10 correspond with the API deposition patterns observed.

Table 4.10 Aerosolization performance of model DPI blends prepared with PSL carriers, expressed as fine particle fraction (FPF) and mass median aerodynamic diameter (MMAD)

Sample ID	%FPF (Emitted)	%FPF (Theoretical)	MMAD
Control (sieved Inh 251)	24.34	16.94	3.42
Sieved Inh 251 @ N2	**24.38**	**13.59**	3.06
Sieved Inh 251 @ N5	**34.25**	**17.75**	3.16
Sieved Inh 251 @ N7	**33.74**	**20.01**	3.04
Sieved Inh 251 @ N11	**32.87**	**16.18**	2.76

All the DPI blends prepared with the PSL carriers have lower MMAD than the blends prepared with the BSL carriers, which confirms better API deposition in the latter stages of the NGI. This may be attributed to the absence of fine lactose in the PSL carriers, which favours API detachment by momentum transfer. Hence, more primary particles are produced during aerosolization, which have a more favourable aerodynamic diameter to reach further in the NGI. However, this also means that API that is unable to be detached from the carrier is deposited in the throat region along with the carrier particles. This is apparent in the amount of API deposited in the preseparator for the two categories of blends. Whereas, the blends prepared with BSL carriers have API deposition in the preseparator ranging from 28.5% to 36.8%, the blends prepared with the PSL carriers have theirs ranging from 47.1% to 57.2%. In summary, the DPI blends prepared with BSL demonstrated a better overall aerodynamic performance than those prepared with PSL, while those prepared with PSL show a higher API deposition in the latter stages of the NGI. In addition, both categories demonstrate better overall aerodynamic performance than the control formulation. The better DPI formulation performance in the blends prepared with BSL may be attributed to the presence of fine lactose in BSL, which facilitated better aerodynamic performance. The mechanism of increased aerodynamic performance of the DPI blends prepared with PSL is not fully understood.

However, speculations based on surface energy distribution evidence from chapter three are that the pre-conditioning of the carrier prior to preparation of model DPI blends homogenises the lactose surface and causes a more even attachment and subsequent detachment of API from lactose surface, causing an increase in FPF. Measurement of the force required for API detachment from the control carrier and PSL carriers may be able to substantiate this claim.

4.4 Part Two – Optimisation of model DPI formulation development using a Quality by Design approach

The elements of pharmaceutical development as indicated in the ICH Q8 guidelines are as follows

4.4.1 Quality target product profile (QTPP)

This represents the quality guide for product development, and may include intended use, quality criteria of drug product based on route of administration, and should specify the intentions of the final product (ICH, 2009; Sangshetti et al., 2014). The intended formulation in this study is a DPI formulation, capable of delivering uniform and optimal API doses to the deep lung.

4.4.2 Critical quality attributes

These are the properties of the product that should be within an acceptable limit or range to ensure desired product quality. The CQAs for the DPI formulation include dose uniformity to the U.S. Pharmacopoeia standard, which is 75% to 125% of the specified target-delivered dose (USP – 29, 2009). Target fine particle fraction of 55% and easy flowing formulation to facilitate dosing and administration.

4.4.3 Risk assessment for CQAs and CPPs

Initial studies (from chapter 2) show that at the highest nitrogen flow rate of 40L/min, onset of deagglomeration of cohesive rhodamine B powder occurred at 4 minutes, faster than at an nitrogen flow rate of 25L/min. In addition, without the air-blade, the cohesive rhodamine B powder was still reduced to primary particles if centrifugal force was applied long enough. Therefore, a multi-step approach to dry coating was developed based on these findings, where the initial step employs the quick deagglomeration of fine API agglomerates by the air-blade at higher nitrogen flow rates between 50L/min to 90L/min; and the second step uses the centrifugal force without the air-blade to achieve redistribution. From the results in part 1, the addition of 9.4% fine lactose to the carrier system produced the optimal results especially in

terms of DPI performance. However, content uniformity, which is a critical product quality attribute for DPIs, was not optimised with the process parameters used. In addition, the blending duration used may have been unfavourable to achieve a homogenous blend, as API was consistently lost in all the blends prepared. There is therefore the need to determine the impact of process parameters in optimising DPI formulations to achieve all the targeted product quality attributes.

4.4.4 Design of experiments

A DoE was developed for the first dry coating step where all three variable factors of the dry coating device were present. The factors were set at 3 levels to reflect a high, medium and low settings achievable with the device. The second step, which employed high centrifugal force only for dispersion of deagglomerated API was kept constant throughout all samples at 2000rpm for 5 minutes without the nitrogen flow i.e. 0L/min. . A response surface methodology (RSM) D-optimal design was generated to evaluate the relationship between the process parameters and responses generated. The software generated seventeen runs including three replicates. Table 4.11 shows the D-optimal design worksheet with the CPP, CQA results, the total number of runs as well as the run order.

4.4.2 Results analysis and discussion

As shown in table 4.11, FPF ranges from a minimum value of 42.73% to a maximum of 59.16%. The powder flow properties, measured by angle of repose ranges from 21.97^0 to 30.03^0, all within the excellent flow region. While content uniformity measured by RSD ranges from 1.93% to 5.61%. Although, two of the 17 samples have RSD greater than 5%, all samples met the requirement of at least 9 out of the 10 doses collected from one formulation being between 75% and 125% of the target-delivered dose and none was outside the range of 65% to 135% of the target-delivered dose as specified by the U.S. Pharmacopoeia. Also, table 4.11 shows that high RSD is connected to processing at low speed of 1000rpm and the lowest nitrogen flow used, 50L/min for 1 minute duration, as revealed in N1 with RSD of 5.61, and

N12 with RSD of 5.68. This may be attributed to low blending force and short blending duration at these process parameters. Despite the presence of the nitrogen blade, which creates micro fluidization of the cohesive API, the diffusion and convective forces in operation at the low speed used and the short blending duration of 1 minute was insufficient to produce complete deagglomeration of the API, causing some API agglomerates to still exist in the blend. As blending duration is increased to 10 minutes, with the same nitrogen flow (50L/min) and speed (1000rpm) in N7, there is a decrease in RSD to 4.85. This corresponds with results from the proof of concept work in chapter two, where it was observed that if the centrifugal force was applied long enough, even without the nitrogen blade, coating is still achieved. Similarly, when nitrogen flow was increased to 90L/min with a speed of 1000rpm at 1-minute duration in N2, RSD decreased to 1.93. This suggests that the use of the nitrogen blade is critical to effective deagglomeration of cohesive API during processing in the iDPC. This also corresponds with results from chapter two, in which coating was achieved faster with higher nitrogen flow rates at shorter duration.

Table 4.11 The D-optimal design worksheet with factors, responses, total number of runs and run order

Exp No	Exp Name	Run Order	Incl/ Excl	Nitrogen flow (L/min)	Speed (rpm)	Duration (Mins)	FPF (%)	AoR (Deg)	RSD (%)
1	N1	10	Incl	50	1000	1	54.84	25.12	5.61
2	N2	6	Incl	90	1000	1	42.73	27.17	1.93
3	N3	16	Incl	70	1000	1	50.74	30.03	3.97
4	N4	8	Incl	50	2000	1	56.48	24.73	2.28
5	N5	7	Incl	90	2000	1	53.63	28.67	4.21
6	N6	4	Incl	50	1500	1	54.30	27.88	3.76
7	N7	12	Incl	50	1000	10	53.15	25.38	4.85
8	N8	3	Incl	90	1000	10	51.03	20.62	4.35
9	N9	17	Incl	50	2000	10	56.62	25.46	3.60
10	N10	2	Incl	90	2000	10	49.06	21.97	3.61
11	N11	15	Incl	70	1500	10	53.37	28.60	3.37
12	N12	11	Incl	50	1000	5	56.31	28.03	5.68
13	N13	9	Incl	70	2000	5	55.90	26.29	2.56
14	N14	1	Incl	90	1500	5	50.97	23.30	4.66
15	N15	13	Incl	70	1500	5	57.86	23.60	4.24
16	N16	5	Incl	70	1500	5	55.02	22.80	4.74
17	N17	14	Incl	70	1500	5	59.16	24.68	4.55

4.4.2.1 Reviewing the model fit and model verification

The fit of the model was reviewed in a sequential manner, as shown in figure 4.12, by removing the farthest outlier first (N11). Removing N2 and N7, which were also outliers did not improve the summary statistics, hence the next to these were removed i.e. N13 and N10 resulting in a total of 3 excluded and 14 included runs with 3 replicates. In addition, the model terms were reviewed and three quadratic terms, were the most non-significant for all three responses as shown in the coefficients plot (figure 4.13). The non-significant model terms were then excluded, leaving three single terms and three interaction terms i.e. Nitrogen flow, Speed, Duration, Nitrogen flow*Speed, Speed*Duration, and Nitrogen flow*Duration to further improve the summary statistics.

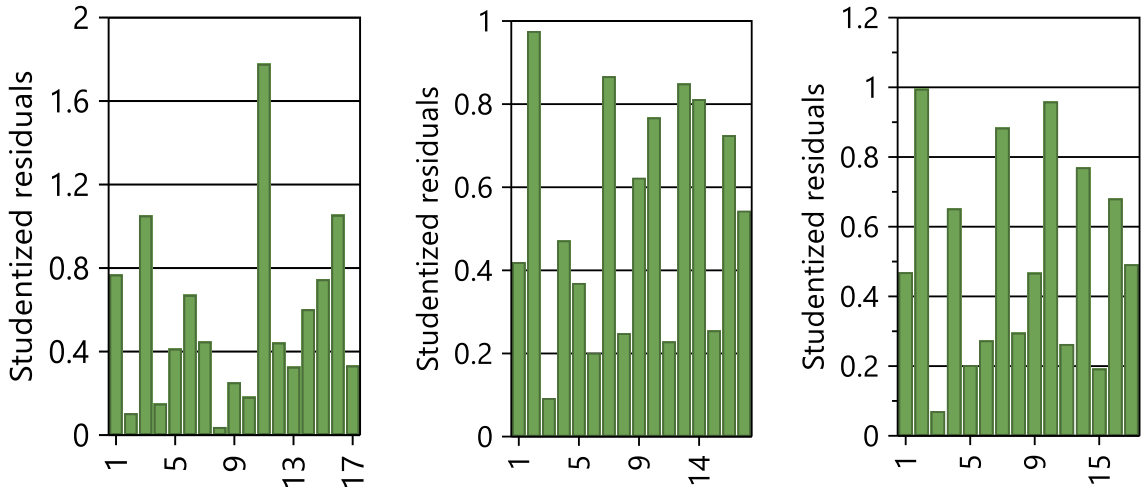

Figure 4.12 Distance to Model Plot of individual runs to identify outliers (marked with circles). N11, being the farthest on the plot was initially removed. Removal of other outliers such as N2 and N7 did not improve the summary statistics, so the next outliers were removed i.e., N13 and N10.

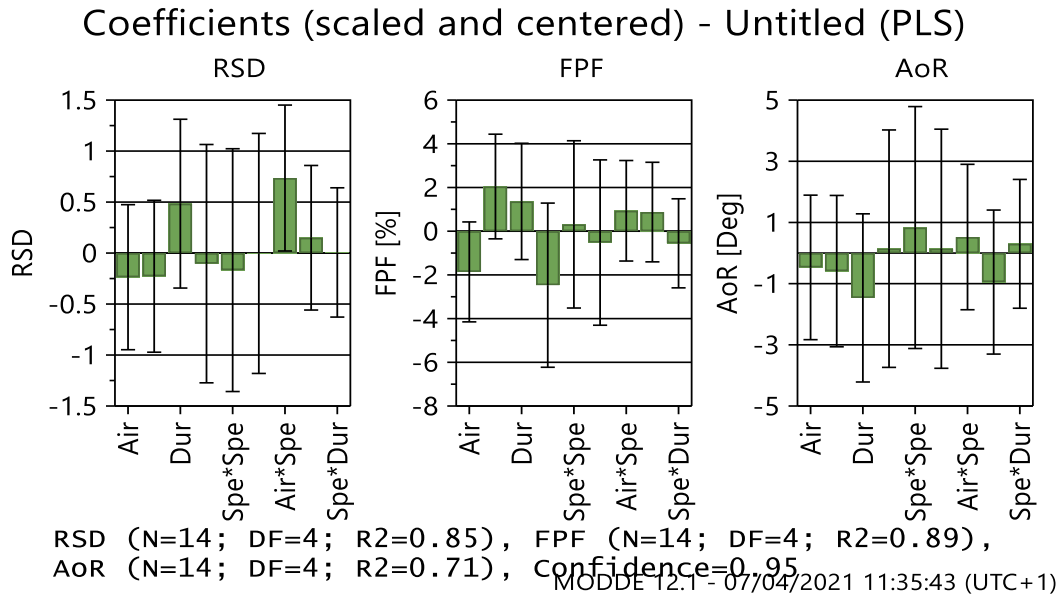

Figure 4.13 Coefficients plot of all single, quadratic and interaction terms for all the responses (RSD, FPF and AoR), showing all quadratic terms being the most non-significant throughout

After removing the outliers and non-significant model terms, the model was further verified by assessing other diagnostics. The difference between the model error sum of squares and the pure error sum of squares is referred to as the lack of fit sum of squares. For an adequate model, where the data fits the model for all the responses, the pure error variation should be significantly higher than the lack of fit variation. Figure 4.14 shows the lack of fit plot for the model generated; the first bar (SD-LoF) represents the variation of the response due to the lack of fit of the model (i.e. the model error). The second bar (SD-pe) represents the Pure error, which shows the variation due to the replicated experiments. And the third bar (SD-pe*sqrt(F(crit))) is the SD pure error (second bar) multiplied by the square root of the critical F at the 95% confidence level. Therefore, when the third bar is smaller than the first, there is a lack of fit, which is significant at the 5% level. However, for all the responses, the SD-LoF bar is smaller than the SD-pe*sqrt(F(crit)) bar, hence, there is no lack of fit and the model is valid

.

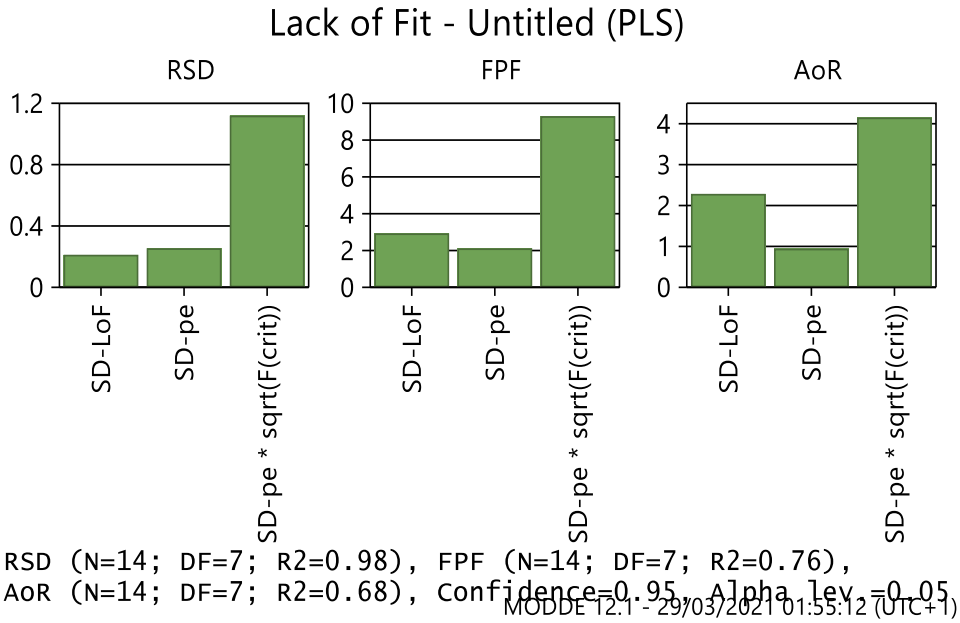

Figure 4.14 Lack of Fit plot showing standard deviation due to lack of fit, standard deviation of pure error and standard deviation of pure error critical F-value for all three responses (RSD, FPF and AoR)*

For a quick evaluation of the raw data, the replicates plot was examined. Ideally, the variability of the replicates i.e. experiments with the same factor values should be smaller than the general variability. The replicate tolerance limit set by the experiment is 10%. Figure 4.15 shows the replicates plot with all three replicates (blue squares) appearing on the same replicate index, within the 10% replicate tolerance limit. Plot also shows that no points are outside the minimum and maximum line.

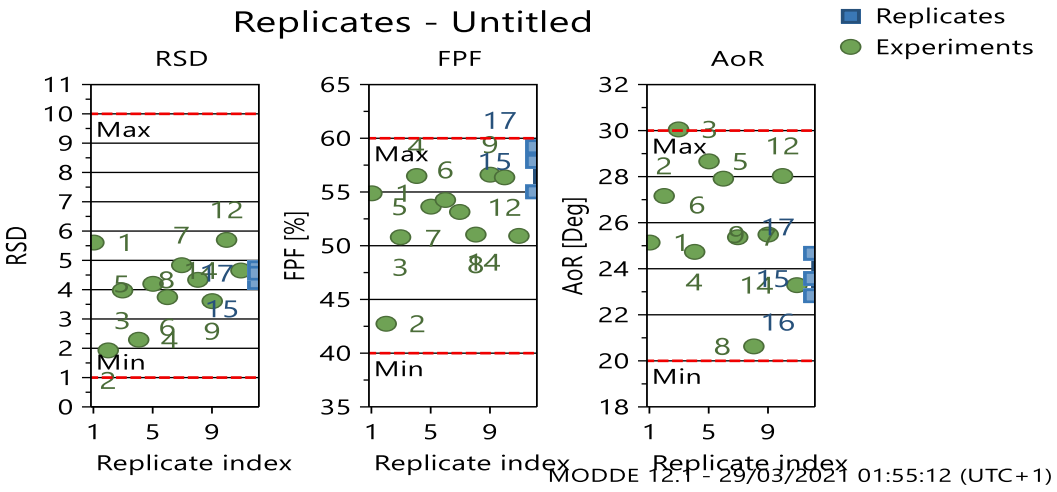

Figure 4.15 Replicates plot for all responses (RSD, FPF and AoR) with a set replicate tolerance of 10%, replicates results are shown in blue squares having close results within the 10% set limit

To assess if the deviations of the results are normally distributed and to detect the presence of any more outliers, the normal probability plot was examined. Points lying on a straight line reflects a normal distribution of the residuals, while outliers have standard deviation outside the -4 to +4 range. Figure 4.16 shows the normal probability plot for all the responses against standardised standard deviations, with most points on or near the straight line and all points with standard deviations within the -4 to +4 limit. This implies that the residuals are normally distributed and there are no outliers.

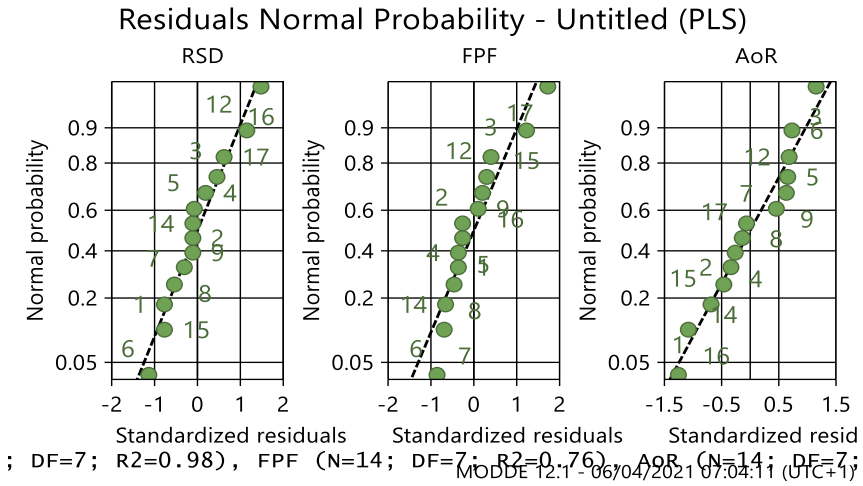

Figure 4.16 Normal probability against standardised residuals for all three responses (RSD, FPF and AoR

For a linear regression model to be valid, the variance of the residuals should be constant i.e. the residuals should not increase or decrease with the predicted values in a pattern and should have a mean of zero. Figure 4.17A shows the residual versus predicted responses plots for all responses, the points are all randomly scattered around zero without a pattern. Hence, indicating constant variance and zero mean in the error terms. Similarly, Figure 4.17B shows the residuals versus run order plot with the points randomly scattered around zero. This indicates that the residuals are independent of time of experiment.

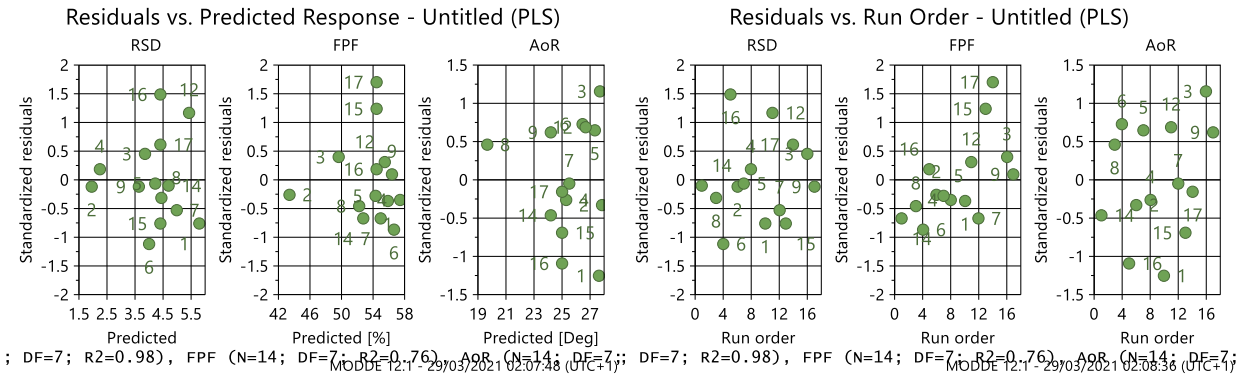

Figure 4.17 (A) Residual versus predicted responses plots for all responses (B) Residual versus run order for all responses

For an overview of the results at a glance, the observed versus predicted plot was examined. A good model will have all the points fall on the regression line, while with a less good model, the points are scattered around the regression line. The farther away from the regression line the points are the less good the model is. Figure 4.18 A, B and C show the observed versus predicted plots for all the three responses. While the RSD plot has almost all the points fit on the regression line, implying a good model, the AoR and FPF plots show a less good model with the points scattered close to the regression line.

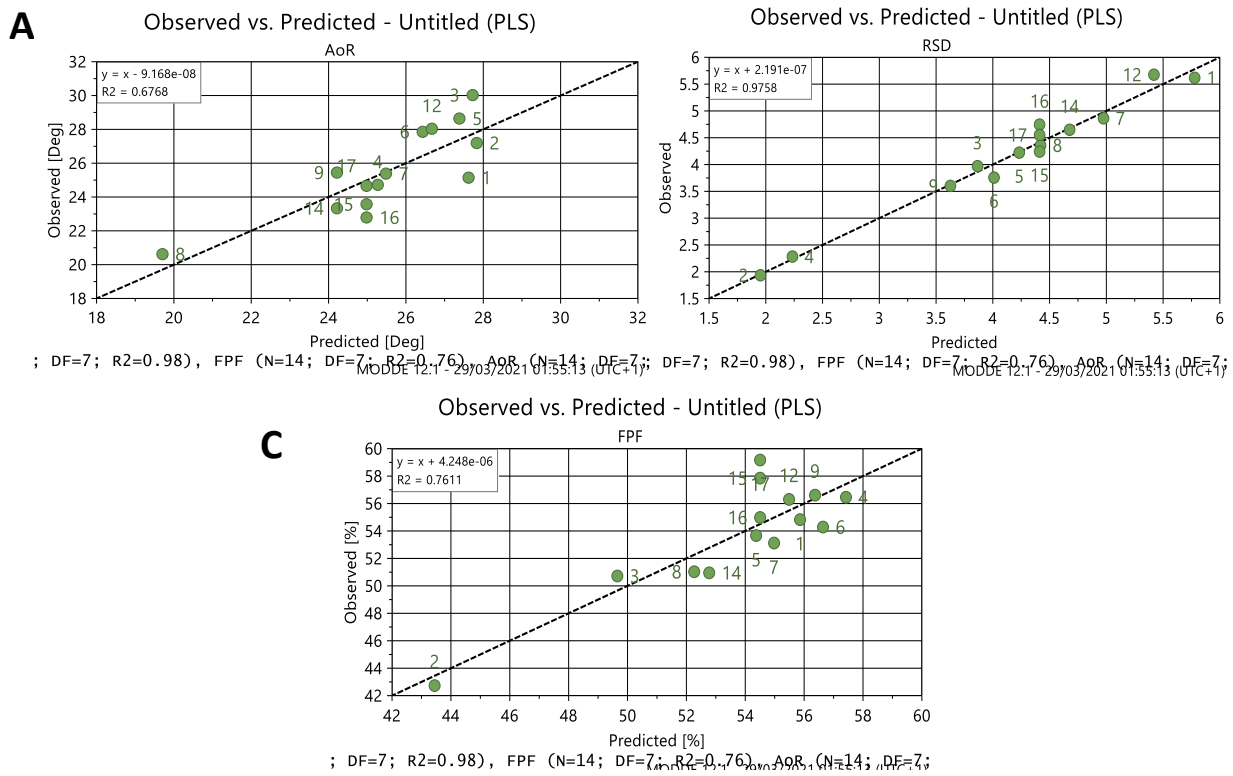

Figure 4.18 Observed versus predicted plots for all the responses (RSD, FPF and AoR)

After verifying the model and removing non-significant model terms, the model was then fitted with partial least squares (PLS). Figure 4.19 shows the summary of fit plot for all responses. This plot summarises the model in terms of R^2, which is the measure of variability of the response; Q^2, an estimate of the prediction accuracy of the model, the model validity and reproducibility. When the model fits the data perfectly, all four indices have a value of one. For a model to be considered statistically significant, the R^2 value must be greater than 0.5; a Q^2 value greater than 0.1 is a significant model while greater than 0.5 is a good model. The model validity must exceed 0.25 while the reproducibility value of a model is required to be > 0.5. Of all four indicators, Q^2 is the most sensitive and best indicator for optimisation and prediction.

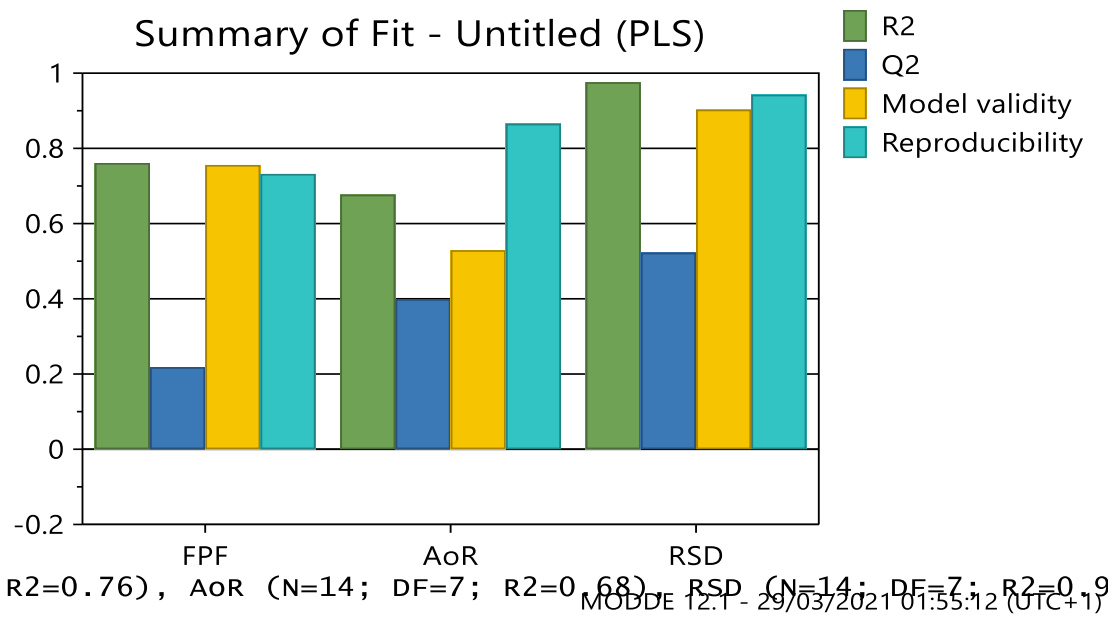

Figure 4.19 Summary of fit plot, fitted with PLS, of all three responses showing model fit (R2), predictability (Q2), model validity and reproducibility

RSD, which is a measure of the DPI blend homogeneity is the response with the best fit in the model, this was evident from the raw data as all samples except one had RSD less than 5%. The model fitted with 97.6% accuracy for RSD, 76.1% for FPF and 67.7% for AoR. The predictive ability was at the acceptable range for all three responses, although, both FPF and AoR have a low but significant predictive ability. The model validity bar is greater than 0.25, which indicates that there is no lack of fit in the model, as also shown in the lack of fit plot (figure 6). All three responses have reproducibility values of 73.2%, 86.5% and 94.3% for FPF, AoR and RSD respectively, showing that the values of the responses for the replicate experiments were significantly similar. It is important to note that the runs were randomised and the replicate runs were performed at different times, hence, reproducibility is independent of time of experiment.

4.4.2.2 Effect of model terms on DPI performance

Reviewing the model by removing outliers resulted in more significant model terms as shown in figure 4.20. Figure 4.20 shows the Regression coefficients plots of all three responses. The most significant factor that has effect on DPI blend homogeneity is the combination of nitrogen

flow and speed. When these two factors are increased, there is an increase in RSD hence, negatively impacting blend homogeneity. The same pattern is observed for duration, air and duration and speed and duration. Nitrogen flow on its own is the only factor that has a significant positive effect on RSD, as RSD is reduced with a decrease in nitrogen flow. For aerodynamic performance of the blends, measured by FPF, nitrogen flow and speed are the only factors that have a statistically significant effect. While a decrease in nitrogen flow decreases FPF, an increase in speed increased FPF to almost the same degree. When both factors are combined, they have a positive effect on FPF, although not statistically significant. None of the factors had a statistically significant effect on the powder flow properties. This is expected, as all the blends were formulated using the same carrier and active ingredient, hence; contain the same amount of fine particles. The dry coating device used has also been found not to cause particle attrition and maintain the size distribution of powders processed in it.

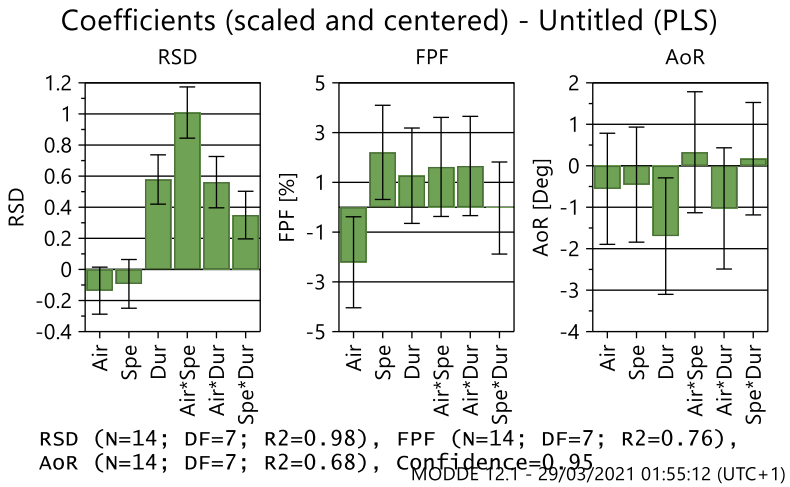

Figure 4.20 Regression coefficients plots for all the responses (RSD, FPF and AoR)

4.4.2.3 Effects of critical process parameters on responses.

The factor effects plots shown in figures 4.21, 4.22 and 4.23 show the anticipated changes in responses when the factors are varied. Ideally, DPI blends with improved performance should have good blend homogeneity, which is reflected in low RSD values; high aerodynamic

performance i.e. increase in FPF and powders with good flow properties and lower angle of repose. For fine particle fraction, the factor effects plot show a decrease in FPF as nitrogen flow increases. This can be attributed to the high force generated which breaks up the fine API agglomerates into primary particles, leading to strong attachment of API to coarse carrier surface. Similar observations were made in chapter 2 where more coverage of the coarse lactose carrier by rhodamine B particles and less rhodamine B agglomerates were visible with increased nitrogen flow. Although the strength of host – guest attachment was not measured, primary particles, presumably will attach stronger to the carrier surface than agglomerates and will be more difficult to detach when necessary. On the other hand, increase in speed and duration however have a positive effect on FPF. This may be attributed to the redistribution of API on carrier particle surface as speed and processing duration increases.

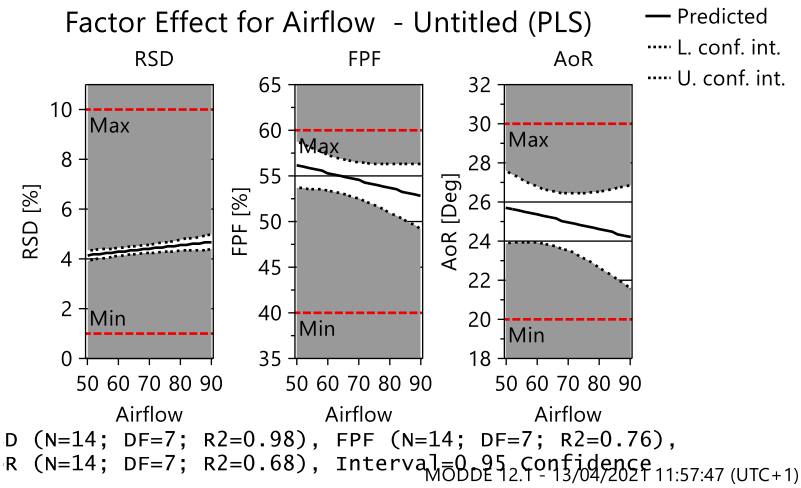

Figure 4.21 Main effect plot of nitrogen flow on RSD, FPF and AoR when speed and duration are at midpoint settings, 1500 rpm and 5 minutes respectively

The factor effects on RSD was consistent across all three factors, with a more considerable effect on RSD observed with increase in blending duration compared to nitrogen flow and speed. There is an increase in RSD, which denotes less blend homogeneity as nitrogen flow, speed and duration of mixing increases. As nitrogen flow increases from 50L/min to 90L/min, a 12% increase in RSD was observed (Figure 4.21); while an 8% increase was observed as speed increased from 1000rpm to 2000rpm (Figure 4.22). However, the effect of blending time

was more considerable with an increase in RSD of more than 50% as blending duration increases from 1 minute to 10 (figure 4.23). This may be attributed to continuous redistribution of API due to prolonged mixing, as well as possible loss of API due to triboelectric effect, causing API attached to the wall of the mixing chamber to be lost during processing.

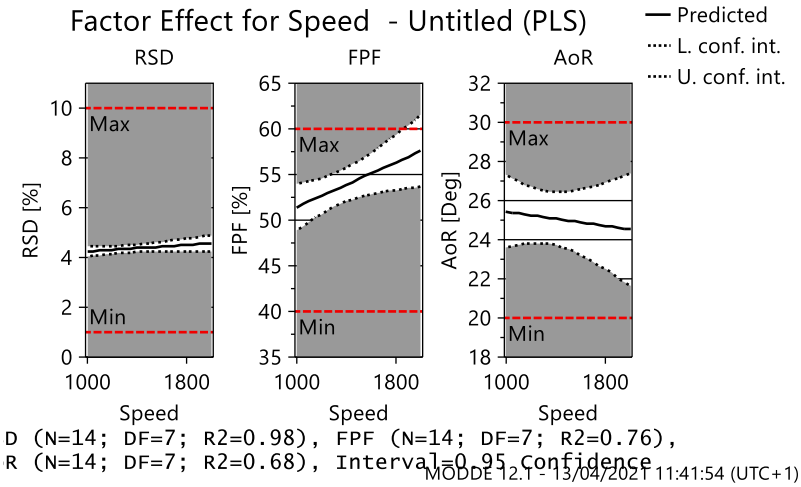

Figure 4.22 Main effect plot of speed on RSD, FPF and AoR when nitrogen flow and duration are at midpoint settings, 70 L/min and 5 minutes respectively

Despite this increase in RSD, all the blends prepared except one had RSD greater than 5% and all blends passed the content uniformity test for dry powders for inhalation as specified by the USP. Also, compared to the blend homogeneity results from part 1, where RSD values were up to 8%, the combination of parameters used in this design have produced more homogenous blends of DPI with lower RSD values.

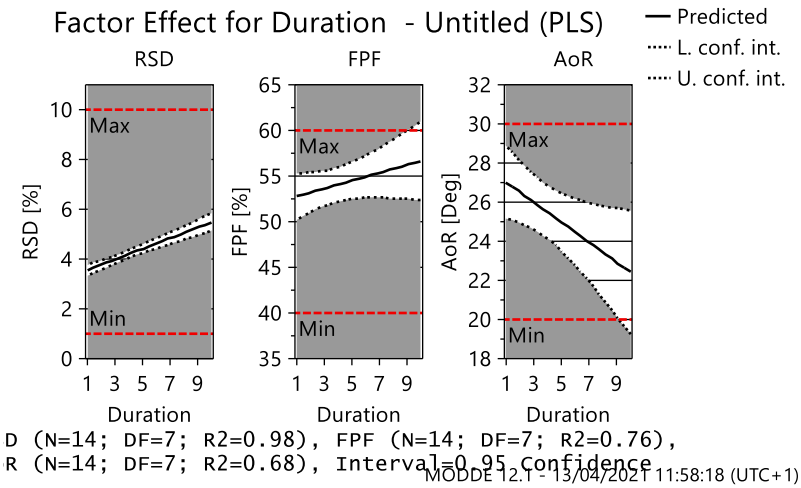

Figure 4.23 Main effect plot of duration on RSD, FPF and AoR when nitrogen flow and speed are at midpoint

4.4.2.4 Effects of interaction terms on DPI properties

So far, the effects of the three factors on the DPI blend qualities have been examined alone. In order to determine the collective effects of the three factors, and how interactions between the factors affect CQAs, the interaction plots were generated. Figure 4.24 shows the effects of nitrogen flow and speed on the three responses. Similar to the factor effects plot for nitrogen flow (figure 4.21) a decrease in FPF is predicted as nitrogen flow increases. However, as shown in the interaction plot (figure 4.24), this trend is only true at the low and medium nitrogen flow settings. In fact, there is an increase in FPF as nitrogen flow increases at 2000rpm. Therefore, high nitrogen flow is more beneficial to the DPI blend performance if accompanied by high blender speed.

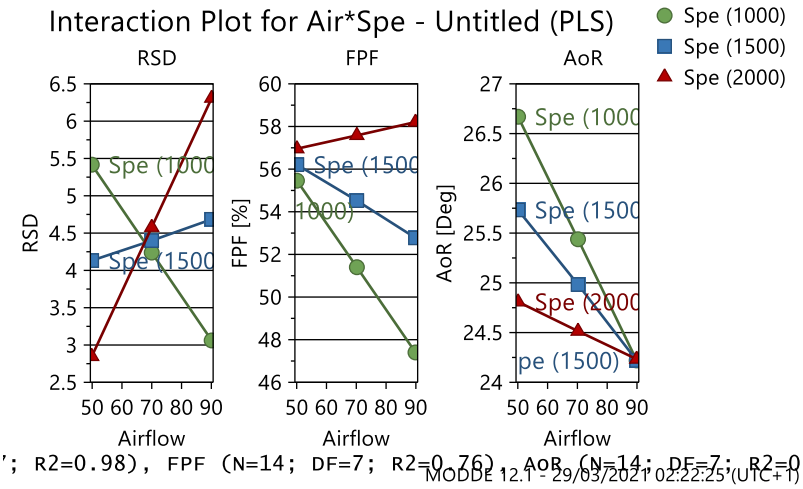

Figure 4.24 Interaction effect plot of nitrogen flow and speed on all three responses, duration at midpoint setting of 5 minutes

The same combination of factors i.e. high nitrogen flow and high speed is however detrimental to blend homogeneity, as the model predicts an increase in RSD with this combination. Likewise, at low and medium speed if nitrogen flow is increased, a decrease in FPF and decrease in RSD is predicted, suggesting that opposite trends are required for blend homogeneity and DPI aerodynamic performance. All three speed settings have similar effects on powder flow, i.e. decrease in AoR which represents better powder flow as nitrogen flow increases.

Based on these interaction effects, the response surface modelling plots establish the desirable operating conditions required for optimal response values. Figure 4.25 shows the response surface plots for the effect of nitrogen flow and speed on the three responses, while duration is kept at the midpoint value of 5 minutes.

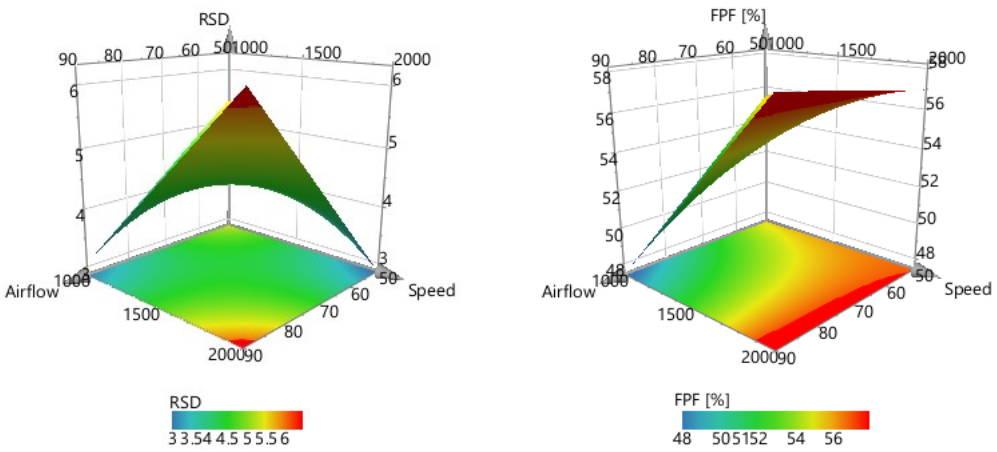

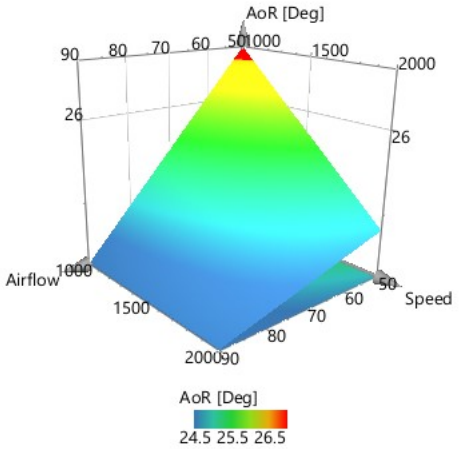

Figure 4.25 Response Surface Model (RSM) Plot of the effect of nitrogen flow and speed on FPF, RSD and AoR, with duration at midpoint setting of 5 minutes

From the graphs, it can be seen that the optimal points for RSD and FPF tend towards different sides of the surface, while the bulk of the surface is optimal for AoR.

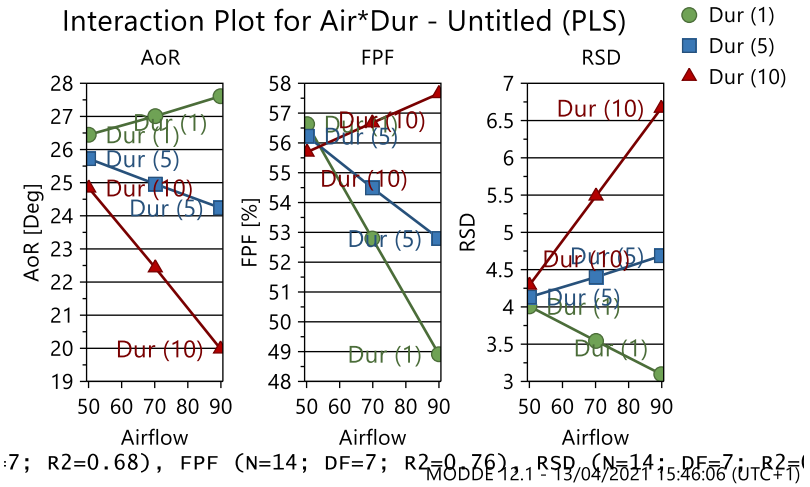

Figure 4.26 Interaction effect plot of nitrogen flow and duration on all three responses, with speed at midpoint setting of 1500rpm

Interaction between nitrogen flow and duration also has an effect on all three DPI qualities. From figure 4.26, it is observed that increase in nitrogen flow has a negative effect on blend homogeneity, as RSD increases. At the shortest duration (1 minute), an opposite trend i.e.

decrease in RSD representative of better homogeneity is predicted. Contrarily, better aerodynamic performance, measured by increase in FPF is predicted at the longest duration (10 minutes) as nitrogen flow increases. This further demonstrates that opposite trends are required for desirable blend homogeneity and DPI aerodynamic performance. The RSM plot for this interaction is shown in figure 4.27.

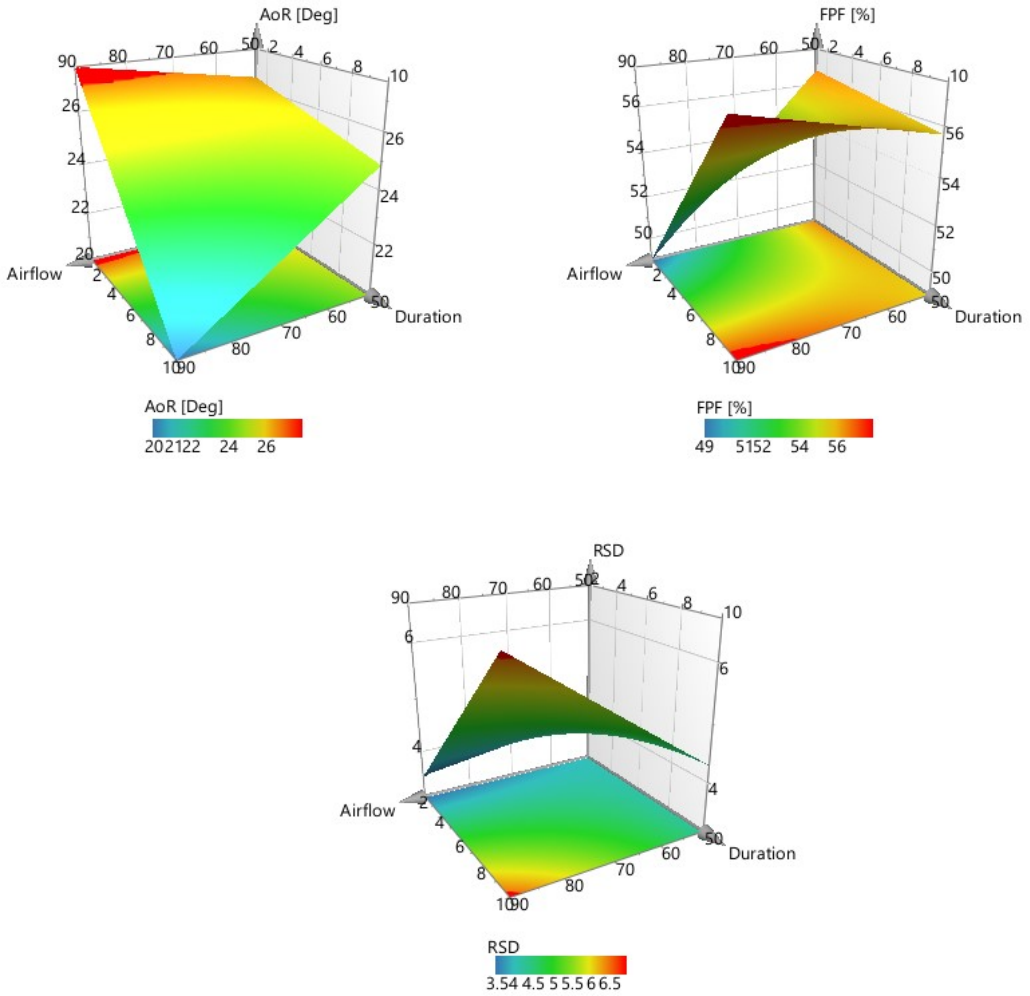

Figure 4.27 Response Surface Model (RSM) Plot of the effect of nitrogen flow and duration on FPF, RSD and AoR, with speed at midpoint setting of 1500 rpm

Similar to the effects of the interaction between nitrogen flow and speed, the optimal points for RSD and FPF can be seen to tend towards opposite directions, which further suggest that reverse operating conditions are required to optimise these two crucial CQAs.

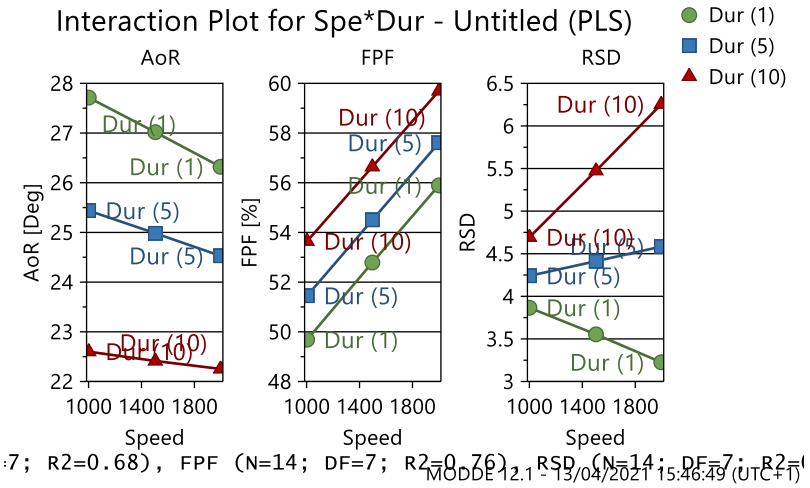

Figure 4.28 Interaction effect plot of speed and duration on all three responses, with nitrogen flow at midpoint setting of 70 L/min

Figure 4.28 shows the predicted effects of speed and duration on DPI properties. Interaction between speed and duration has no effect on FPF and AoR, as depicted by the parallel lines. This correlates with the regression coefficients plots (figure 4.20), where the speed and duration interaction was significant only for RSD. For RSD, at short duration, an increase in speed favours blend homogeneity, while blend homogeneity reduced as duration and speed increased. The RSM plot for the effect of this interaction on RSD is shown in figure 4.29, as there is no effect on FPF and AoR.

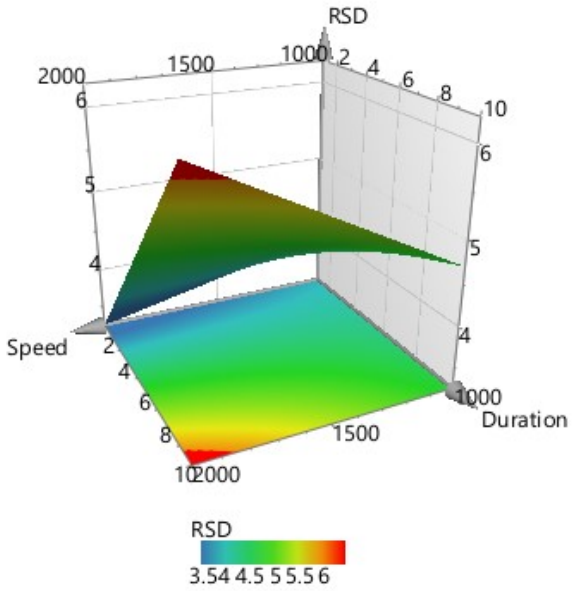

Figure 4.29 Response Surface Model (RSM) Plot of the effect of duration and speed on RSD with nitrogen flow at midpoint setting of 70 L/min

4.4.2.5 Design space generation

Based on the results obtained throughout the study, the most favourable parameters for producing DPI blends with optimal performance are highlighted in Figure 4.30 A, B and C. The green area on the plots represents the desirable operating conditions, which highlight the parameters that would produce DPI blends with optimal blend homogeneity, aerodynamic performance and powder flow. At 1 minute, maintaining the blender speed between 1314 rpm to 1595 rpm and nitrogen flow rates between 61 – 64 L/min predicts optimal formulations with 0% probability of failure. As duration increases to five minutes, the design space increases as well to a speed range between 1003 rpm to 1733 rpm and nitrogen flow rates between 62.8 – 67.6 L/min. Further increase in duration to 10 minutes results in a loss of design space with 0% probability of failure. This suggests that optimal results are obtained at mid duration of 5 minutes.

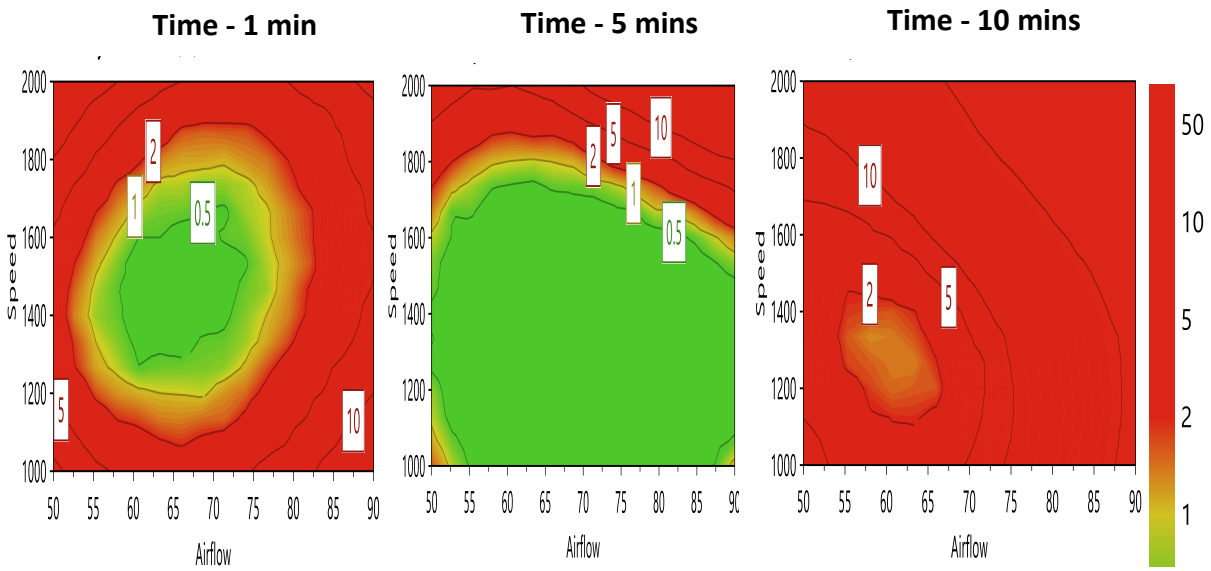

Figure 4.30 Design space plot

4.5 Conclusion

In the first part of this study, different concentrations of fine lactose were added to coarse lactose to create a carrier system for model DPI blend formulation. The blends were prepared using a fixed set of process parameters and the effect of increasing fine lactose concentration on the performance of model DPI blends was evaluated by content uniformity, fine particle fraction and powder flow. There was a direct relationship between the amount of fine particles present in formulation and powder flowablility, with increasing amount of fines producing poorer flow. SEM provided additional qualitative data to verify the increasing amount of cohesive agglomerates. The presence of carrier fines at all concentrations increased FPF with the maximum increase observed at 9.4% carrier fines concentration. The content of fine lactose present in the model DPI formulations influenced API deposition in the NGI. Similarly, in part 1 of this study, sieved lactose was pre-conditioned under different process parameters in the iDPC and used to prepare model DPI blends using the same fixed set of parameters as the fines-coarse carrier system. The effect of carrier pre-conditioning on the model DPI blends were investigated. Lactose pre-conditioning also increased FPF although, to a lesser extent than the fines-coarse carrier system. Powder flow remained consistent within this group of DPI blends due to absence of fine carrier. The mechanism of increased aerodynamic performance of the DPI blends prepared with PSL is not fully understood. However, speculations of surface energy homogenisation based on surface energy distribution evidence may be confirmed by measuring the force required for API detachment from the control carrier and PSL carriers. Content uniformity and API recovery was not optimised with the process parameters used to prepare the DPI blends.

Process optimisation by QbD was the focus of part two of this study, the optimal process parameters for DPI formulation with 9.4% fine lactose in the carrier system was investigated, and a two-step blending approach was used to minimise blending duration. The model was validated for all three responses. As expected, none of the model terms had a significant effect on powder flow (AoR), since all the blends were formulated using the same carrier and API, and the iDPC has been found not to cause particle attrition and maintain the size distribution

of powders processed in it. Nitrogen flow and speed were the most important factor that influenced RSD and FPF, and it was observed that, high nitrogen flow is more beneficial to the DPI blend performance if accompanied by high blender speed. The same combination of factors i.e. high nitrogen flow and high speed is however detrimental to blend homogeneity. In summary, the predicted space for optimal blends preparation is device speed between 1003 rpm to 1733 rpm and nitrogen flow rates between 62.8 – 67.6 L/min at 5 minutes processing time.

5. Chapter Five

Chapter 5 Redacted

6. Chapter Six

General conclusions and future work

6.1 General conclusions

Dry powder inhalers are fast becoming the first choice for inhalation therapy due to API stability, ease of dosing and device use and better lung deposition than traditional pMDIs and nebulizers. However, the pre-formulation optimisation and prediction of carrier-based DPI formulations have been stalled due to the inability to definitely quantify and link carrier physicochemical properties to resultant effects in DPI formulations. The trial and error approach currently used to optimise formulations is costly and lacks the ability to predict, as effects of optimisation processes are only determined after dosage formulation. The complex interactions between the physicochemical properties of lactose, the most commonly used carrier in DPI formulations, complicates the otherwise simple cause and effect relationship that allows for easy optimisation and prediction. The purpose of this work was to use the mechanistic understanding of the novel iDPC device to explore preparation of DPI formulations through a QbD approach, leveraging particle surface interactions.

Image analysis (CLSM) was used to observe the coating of micronized particles on lactose surface at different time points. The iDPC consistently produced composite particles at all the time points studied. The centrifugal force and micro fluidization technique were both key to achieving dry coating, although, micro fluidization accelerated the process and facilitated coating faster than the centrifugal force alone. Deagglomeration of the cohesive rhodamine B particles was attributed to shear forces generated by vortexes produced in the blender, which simulates rotating impellers in high shear mixers. The advantage of this technology over traditional high shear blenders is the absence of actual impellers, which prevents particle attrition, which was confirmed by particle size analysis through laser diffraction. SEM micrographs corroborated CLSM images. Quantitative image analysis (using image J software) was used to identify the periods when the different stages of dry particle coating i.e. deagglomeration, dispersion and redistribution occurred in the iDPC.

To determine possible changes to lactose surface caused during processing in the iDPC, sieved and unsieved lactose were exposed to different processing parameters in the iDPC,

generated by experimental design. Results showed that as with other studies, the iDPC did not cause particle attrition during processing. Fine lactose adhered to coarse lactose surface during processing, this presents the possibility of competition with API for active sites on coarse lactose during formulation. Sieved lactose samples apparently had fewer fines than the unsieved samples. Consequently, they had better flow as determined by flow factor coefficient and less attachment of fines to the coarse lactose surface as seen in the scanning electron micrographs. The solid form of the lactose samples was also retained post-processing, regardless of the processing parameters used, as no amorphous peaks were visible in both DSC thermograms and XRD patterns. The iDPC did not cause significant changes to carrier particle size, thermal properties and powder flowability, but there were some changes to the lactose surface properties such as surface rugosity, specific surface area, specific surface energy and surface energy distribution. The observed changes were related to the adsorption of fine lactose to coarse lactose surface during processing in the iDPC. In addition, the extent of changes observed may be correlated to variations in processing parameters, which reflects varying blending energy inputs of the coating process. Following the understanding of the changes to lactose surface characteristics, the next step was to understand the impact of addition of fine lactose and lactose pre-processing on process characterisation. This was done to investigate how the established method of incorporating fine lactose to a coarse lactose based formulation would turn out using the iDPC. Different concentrations of fine lactose were added to coarse lactose to create a carrier system for model DPI blend formulation, using fluticasone propionate as a model drug. The blends were prepared using a fixed set of process parameters and the effect of increasing fine lactose concentration on the performance of model DPI blends was evaluated by content uniformity, fine particle fraction and powder flow. Fine lactose was added based on theoretical surface coverage of the coarse by fine lactose. Similar to optimal fines concentration of 10% reported in literature, the addition of 9.4% fine lactose was optimal to DPI formulation performance, and the content of fine lactose in the DPI formulation influenced API deposition pattern in the NGI. There was a direct relationship between the amount of fine particles present in formulation

and powder flowablility, with increasing amount of fines producing poorer flow. SEM micrographs provided additional qualitative data to verify the increasing amount of cohesive API-carrier agglomerates, which influenced both flowablity and NGI deposition.

In parallel, sieved lactose was pre-conditioned under different process parameters in the iDPC and used to prepare model DPI blends using the same fixed set of parameters as the fines-coarse carrier system, and the effect of carrier pre-conditioning on the performance of model DPI blends were investigated. The purpose of this was to explore the possibility of a fines-free formulation with the added advantage of better flow, which is beneficial for formulation preparation, handling and dosing. Lactose pre-conditioning also increased FPF although, to a lesser extent than the fines-coarse carrier system. More primary particles were detached from lactose surface in this group of DPI blends than from the fines-coarse carrier system, which resulted in lower MMAD compared to the latter.

The next stage was to optimise the formulation process through QbD. To do this, the lactose fine concentration that produced highest increase in FPF (9.4%) was adopted, and a two-step blending approach, which was based on the mechanistic understanding of the dry coating process in the iDPC, was used to minimise blending duration. Nitrogen flow and speed were the most important factor that influenced RSD and FPF, and it was observed that, high nitrogen flow was more beneficial to the DPI blend performance when accompanied by high blender speed. The same combination of factors i.e. high nitrogen flow and high speed was detrimental to blend homogeneity. None of the factors significantly affected powder flow. The predicted space for optimal blends preparation was device speed between 1003 rpm to 1733 rpm and nitrogen flow rates between 62.8 – 67.6 L/min at 5 minutes processing time.

Finally, surface interaction dynamics determined through surface energy measurements of the lactose carrier clarified the varying DPI formulation performance demonstrated by coarse lactose-based formulations processed with different inert gases viz; helium, nitrogen and argon. Processing induced differences especially in the specific surface energy component of lactose surface energetics were revealed. This is attributed to possible reorientation of the molecules of lactose water of crystallisation, increasing interaction between polar probes and

particle surface, and resulting in increased polar surface energy. Different blending input energies generated by the different gases used also suggest that variations in the type of inert gas used to generate microfluidization of particles in the iDPC may be used to alter blending input energy and consequently DPI formulation performance.

6.2 Future work

- This work has verified the potential for creating composite particles suitable for DPI formulations using the iDPC. In addition, a quality by design approach has also been used to determine the iDPC process parameters required to develop optimal formulations using fine and coarse lactose carriers.
- The impact of surface interaction dynamics on DPI formulations especially in the absence of fine lactose still requires further investigation.
- Quantification of lactose – API adhesion strength and investigating the link with process parameters could potentially lead to surface properties being used as a CQA in DPI formulations.
- A probabilistic design of experiments approach could then be used to optimise process characterisation for desired DPI formulation performance.

List of References

ALONSO, M. & ALGUACIL, F. 1999. Dry mixing and coating of powders. *Revista de Metalurgia,* 35.

Alonso, M., Satoh, M. and Miyanami, K. (1989). Kinetic of fines transfer among carriers in Powder Coating. *Powder Technology* 59:217-224

APTE, S. 2012. Excipient-API interactions in dry powder inhalers. *Journal of excipients and food chemicals,* 3**,** 129.

Bannister, P. and Harnby, N. (1983) Colorimetric Technique for Assessing the Mixture Quality of Fine Particle Mixtures. *Powder Technology*, 36:275-270

BARLING, D., MORTON, D. & HAPGOOD, K. 2015. Pharmaceutical dry powder blending and scale-up: Maintaining equivalent mixing conditions using a coloured tracer powder. *Powder Technology,* 270**,** 461-469.

BEGAT, P., MORTON, D. A., SHUR, J., KIPPAX, P., STANIFORTH, J. N. & PRICE, R. 2009. The role of force control agents in high-dose dry powder inhaler formulations. *J Pharm Sci,* 98**,** 2770-83.

BEGAT, P., MORTON, D. A. V., STANIFORTH, J. N. & PRICE, R. 2004. The Cohesive-Adhesive Balances in Dry Powder Inhaler Formulations II: Influence on Fine Particle Delivery Characteristics. *Pharmaceutical Research,* 21**,** 1826-1833.

BENKE, E., FARKAS, Á., SZABÓ-RÉVÉSZ, P. & AMBRUS, R. 2020. Development of an Innovative, Carrier-Based Dry Powder Inhalation Formulation Containing Spray-Dried Meloxicam Potassium to Improve the In Vitro and In Silico Aerodynamic Properties. *Pharmaceutics,* 12**,** 535.

BRIDGWATER, J. 2012. Mixing of powders and granular materials by mechanical means—A perspective. *Particuology,* 10**,** 397–427.

BUCKTON, G., CHOULARTON, A., BEEZER, A. E. & CHATHAM, S. M. 1988. The effect of the comminution technique on the surface energy of a powder. *International Journal of Pharmaceutics,* 47**,** 121-128.

BUNGERT, N., KOBLER, M. & SCHERLIEß, R. 2021. In-Depth Comparison of Dry Particle Coating Processes Used in DPI Particle Engineering. 13**,** 580.

BUTTINI, F., BRAMBILLA, G., COPELLI, D., SISTI, V., BALDUCCI, A. G., BETTINI, R. & PASQUALI, I. 2016. Effect of Flow Rate on In Vitro Aerodynamic Performance of NEXThaler(®) in Comparison with Diskus(®) and Turbohaler(®) Dry Powder Inhalers. *Journal of aerosol medicine and pulmonary drug delivery,* 29**,** 167-178.

BUTLER, D. & WILLIAMS, D. R. 2000. Particulate characterization: Inverse gas chromatography. *Encyclopedia of Separation Science***,** 3609-3614.

CASTELLANOS, A. 2005. The relationship between attractive interparticle forces and bulk behaviour in dry and uncharged fine powders. *Advances in Physics,* 54**,** 263-376.

CHOW, A. H. L., TONG, H. H. Y., CHATTOPADHYAY, P. & SHEKUNOV, B. Y. 2007. Particle Engineering for Pulmonary Drug Delivery. *Pharmaceutical Research,* 24**,** 411-437.

CLINE, D. & DALBY, R. 2002. Predicting the Quality of Powders for Inhalation from Surface Energy and Area. *Pharmaceutical Research,* 19**,** 1274-1277.

CLINT, J. H. 2001. Adhesion and components of solid surface energies. *Current Opinion in Colloid & Interface Science,* 6**,** 28-33.

CUQ, B., BERTHIAUX, H. & GATUMEL, C. 2013. 9 - Powder mixing in the production of food powders. *In:* BHANDARI, B., BANSAL, N., ZHANG, M. & SCHUCK, P. (eds.) *Handbook of Food Powders.* Woodhead Publishing.

DAHMASH, E. Z. & MOHAMMED, A. R. 2015. Functionalised particles using dry powder coating in pharmaceutical drug delivery: promises and challenges. *Expert Opinion on Drug Delivery,* 12**,** 1867-1879.

Dahmash, E.Z. (2015). PhD Thesis. Development of Novel Dry Coating Device for Pharmaceutucal Applications.

Dahmash, E.Z., Al-khattawi, A., Iyire, A., Al-Yami, H., Dennison, T.J. and Mohammed, A.R. (2018) Quality by Design (QbD) based process optimisation to develop functionalised

particles with modified release properties using novel dry particle coating technique. PLoS ONE 13(11): e0206651. https://doi.org/10.1371/journal.pone.0206651

DANIHER, D. & ZHU, J. 2008. Dry powder platform for pulmonary drug delivery. *Particuology,* 6**,** 225-238.

DAS, S., LARSON, I., YOUNG, P. & STEWART, P. 2010. Understanding lactose behaviour during storage by monitoring surface energy change using inverse gas chromatography. *Dairy Science & Technology,* 90**,** 271-285.

DAS, S. & STEWART, P. 2012. Characterising surface energy of pharmaceutical powders by inverse gas chromatography at finite dilution. *The Journal of pharmacy and pharmacology,* 64**,** 1337-48.

DAS, S. C., LARSON, I., MORTON, D. A. V. & STEWART, P. J. 2011a. Determination of the Polar and Total Surface Energy Distributions of Particulates by Inverse Gas Chromatography. *Langmuir,* 27**,** 521-523.

DAS, S. C., ZHOU, Q., MORTON, D. A. V., LARSON, I. & STEWART, P. J. 2011b. Use of surface energy distributions by inverse gas chromatography to understand mechanofusion processing and functionality of lactose coated with magnesium stearate. *European Journal of Pharmaceutical Sciences,* 43**,** 325-333.

DAUMANN, B., FATH, A., ANLAUF, H. & NIRSCHL, H. 2009. Determination of the mixing time in a discontinuous powder mixer by using image analysis. *Chemical engineering science,* 64**,** 2320-2331.

DAVE, R., CHEN, W., MUJUMDAR, A., WANG, W. & PFEFFER, R. 2003. Numerical simulation of dry particle coating processes by the discrete element method. *Advanced Powder Technology,* 14**,** 449-470.

DAVIES, M., BRINDLEY, A., CHEN, X., MARLOW, M., DOUGHTY, S. W., SHRUBB, I. & ROBERTS, C. J. 2005. Characterization of Drug Particle Surface Energetics and Young's Modulus by Atomic Force Microscopy and Inverse Gas Chromatography. *Pharmaceutical Research,* 22**,** 1158-1166.

DE BOER, A. H., CHAN, H. K. & PRICE, R. 2012. A critical view on lactose-based drug formulation and device studies for dry powder inhalation: Which are relevant and what interactions to expect? *Advanced Drug Delivery Reviews,* 64**,** 257-274.

DE BOER, A. H., HAGEDOORN, P., GJALTEMA, D., GOEDE, J. & FRIJLINK, H. W. 2003a. Air classifier technology (ACT) in dry powder inhalation: Part 1. Introduction of a novel force distribution concept (FDC) explaining the performance of a basic air classifier on adhesive mixtures. *International Journal of Pharmaceutics,* 260**,** 187-200.

DE BOER, A. H., HAGEDOORN, P., GJALTEMA, D., GOEDE, J., KUSSENDRAGER, K. D. & FRIJLINK, H. W. 2003b. Air classifier technology (ACT) in dry powder inhalation Part 2. The effect of lactose carrier surface properties on the drug-to-carrier interaction in adhesive mixtures for inhalation. *International Journal of Pharmaceutics,* 260**,** 201-216.

DEMOLY, P., HAGEDOORN, P., DE BOER, A. & FRIJLINK, H. 2014. The clinical relevance of dry powder inhaler performance for drug delivery. *Respiratory medicine,* 108.

DONOVAN, M. J. & SMYTH, H. D. C. 2010. Influence of size and surface roughness of large lactose carrier particles in dry powder inhaler formulations. *International Journal of Pharmaceutics,* 402**,** 1-9.

ELSAYED, M. M. A. & SHALASH, A. O. 2018. Modeling the performance of carrier-based dry powder inhalation formulations: Where are we, and how to get there? *Journal of Controlled Release,* 279**,** 251-261.

FAN, L. T., CHEN, S. J. & WATSON, C. A. 1970. ANNUAL REVIEW Solids Mixing. *Industrial & Engineering Chemistry,* 62**,** 53-69.

GÄNZLE, M. G., HAASE, G. & JELEN, P. 2008. Lactose: Crystallization, hydrolysis and value-added derivatives. *International Dairy Journal,* 18**,** 685-694.

Gera, M., Saharan, V., Kataria, M. and Kukkar, V. (2010). "Mechanical methods for dry particle coating processes and their applications in drug delivery and development." *Recent Patents on Drug Delivery and Formulation* 4(1): 58-81

GHORI, M. U., ŠUPUK, E. & CONWAY, B. R. 2015. Tribo-electrification and Powder Adhesion Studies in the Development of Polymeric Hydrophilic Drug Matrices. *Materials (Basel, Switzerland),* 8**,** 1482-1498.

GHOROI, C., GURUMURTHY, L., MCDANIEL, D. J., JALLO, L. J. & DAVÉ, R. N. 2013. Multi-faceted characterization of pharmaceutical powders to discern the influence of surface modification. *Powder Technology,* 236**,** 63-74.

Gombás, Á ., Szabó-Révész, P., Kata, M., Regdon G. and Erős, I. (2002). Quantitative Determination of Crystallinity of alpha-Lactose Monohydrate by DSC. *Journal of Thermal Analysis and Calorimetry, 68: 503.510.*

GRASMEIJER, F., FRIJLINK, H. W. & DE BOER, A. H. 2014. A proposed definition of the 'activity' of surface sites on lactose carriers for dry powder inhalation. *European Journal of Pharmaceutical Sciences,* 56**,** 102-104.

GRIMSEY, I. M., FEELEY, J. C. & YORK, P. 2002. Analysis of the surface energy of pharmaceutical powders by inverse gas chromatography. *Journal of Pharmaceutical Sciences,* 91**,** 571-583.

GUENETTE, E., BARRETT, A., KRAUS, D., BRODY, R., HARDING, L. & MAGEE, G. 2009. Understanding the effect of lactose particle size on the properties of DPI formulations using experimental design. *International Journal of Pharmaceutics,* 380**,** 80-88.

HASSANPOUR AGHDAM, M., GHANBARZADEH, S., JAVADZADEH, Y. & HAMISHEHKAR, H. 2016. Aggregated Nanotransfersomal Dry Powder Inhalation of Itraconazole for Pulmonary Drug Delivery. *Advanced pharmaceutical bulletin,* 6**,** 57-64.

HENG, J. Y. Y., BISMARCK, A., LEE, A. F., WILSON, K. & WILLIAMS, D. R. 2006. Anisotropic Surface Energetics and Wettability of Macroscopic Form I Paracetamol Crystals. *Langmuir,* 22**,** 2760-2769.

Honda, H., Kimura M., Honda F., Matsuno T. and Koishi M. (1991). Preparation of composite and encapsulated powder particles by dry impact blending, International Journal of Chemistry and Biotechnology, 9, 21.

HOOTON, J. C., JONES, M. D. & PRICE, R. 2006. Predicting the behavior of novel sugar carriers for dry powder inhaler formulations via the use of a cohesive–adhesive force balance approach. *Journal of Pharmaceutical Sciences,* 95**,** 1288-1297.

HOPPENTOCHT, M., HAGEDOORN, P., FRIJLINK, H. W. & DE BOER, A. H. 2014. Technological and practical challenges of dry powder inhalers and formulations. *Advanced Drug Delivery Reviews,* 75**,** 18-31.

ICH (2009). International conference on harmonisation of technical requirements for registration of pharmaceuticals for human use, Pharmaceutical Development, Q8 (R2).

ISLAM, N. & GLADKI, E. 2008. Dry powder inhalers (DPIs)—A review of device reliability and innovation. *International Journal of Pharmaceutics,* 360**,** 1-11.

ISLAM, N., STEWART, P., LARSON, I. & HARTLEY, P. 2004. Effect of carrier size on the dispersion of salmeterol xinafoate from interactive mixtures. *Journal of Pharmaceutical Sciences,* 93**,** 1030-1038.

JOHNSON, K., KENDALL, K., ROBERTS, A. J. P. O. T. R. S. O. L. A. M. & SCIENCES, P. 1971. Surface energy and the contact of elastic solids. 324**,** 301 - 313.

JONES, M. D., HARRIS, H., HOOTON, J. C., SHUR, J., KING, G. S., MATHOULIN, C. A., NICHOL, K., SMITH, T. L., DAWSON, M. L., FERRIE, A. R. & PRICE, R. 2008. An investigation into the relationship between carrier-based dry powder inhalation performance and formulation cohesive–adhesive force balances. *European Journal of Pharmaceutics and Biopharmaceutics,* 69**,** 496-507.

JONES, M. D. & PRICE, R. 2006. The Influence of Fine Excipient Particles on the Performance of Carrier-Based Dry Powder Inhalation Formulations. *Pharmaceutical Research,* 23**,** 1665-1674.

KAIALY, W. 2016. A review of factors affecting electrostatic charging of pharmaceuticals and adhesive mixtures for inhalation. *International Journal of Pharmaceutics,* 503**,** 262-276.

KAIALY, W., ALHALAWEH, A., VELAGA, S. P. & NOKHODCHI, A. 2011. Effect of carrier particle shape on dry powder inhaler performance. *International Journal of Pharmaceutics,* 421**,** 12-23.

KAIALY, W., ALHALAWEH, A., VELAGA, S. P. & NOKHODCHI, A. 2012a. Influence of lactose carrier particle size on the aerosol performance of budesonide from a dry powder inhaler. *Powder Technology,* 227**,** 74-85.

KAIALY, W., TICEHURST, M. & NOKHODCHI, A. 2012b. Dry powder inhalers: Mechanistic evaluation of lactose formulations containing salbutamol sulphate. *International Journal of Pharmaceutics,* 423**,** 184-194.

KARDE, V. & GHOROI, C. 2015. Fine powder flow under humid environmental conditions from the perspective of surface energy. *International Journal of Pharmaceutics,* 485**,** 192-201.

KAWASHIMA, Y., SERIGANO, T., HINO, T., YAMAMOTO, H. & TAKEUCHI, H. 1998. Effect of surface morphology of carrier lactose on dry powder inhalation property of pranlukast hydrate. *International Journal of Pharmaceutics,* 172**,** 179-188.

KHO, K. & HADINOTO, K. 2013. Dry powder inhaler delivery of amorphous drug nanoparticles: Effects of the lactose carrier particle shape and size. *Powder Technology,* 233**,** 303-311.

Khoo, J.; Naderi, M.; Burnett, D. 2012. Surface Energetic Heterogeneity Profiles by iGC Surface Energy Analyser: iGC SEA Application Note 224. Available online: https://www.surfacemeasurementsystems.com/downloads/seaapplication-notes/ (accessed on 01-02-2022).

INNUNEN, H., HEBBINK, G., PETERS, H., SHUR, J. & PRICE, R. 2014. An Investigation into the Effect of Fine Lactose Particles on the Fluidization Behaviour and

Aerosolization Performance of Carrier-Based Dry Powder Inhaler Formulations. *AAPS PharmSciTech,* 15**,** 898-909.

Koner, JS, Dahmash, EZ, Wyatt, DA & Mohammed, A 2018, 'Dry particle coating-a unique solution for pharmaceutical formulation', *Pharmaceutical Technology*, vol. 42, no. 3, pp. 26-30. Available on http://www.pharmtech.com/dry-particle-coating-unique-solution-pharmaceutical-formulation accessed on 28-04-2018

KOU, X., CHAN, L. W., STECKEL, H. & HENG, P. W. S. 2012. Physico-chemical aspects of lactose for inhalation. *Advanced Drug Delivery Reviews,* 64**,** 220-232.

KUMON, M., SUZUKI, M., KUSAI, A., YONEMOCHI, E. & TERADA, K. 2006. Novel Approach to DPI Carrier Lactose with Mechanofusion Process with Additives and Evaluation by IGC. *Chemical and Pharmaceutical Bulletin,* 54**,** 1508-1514.

KUO, C.-Y., ROLLINGS, R. S. & LYNCH, L. N. 1998. Morphological Study of Coarse Aggregates Using Image Analysis. 10**,** 135-142.

Lam, K. and Newton, J. (1991). Investigation of applied compression on the adhesion of powders to a substrate surface. *Powder Technology*, 65(1–3):167-17https://doi.org/10.1016/0032-5910(91)80179-M. accessed 21-08-2021

LABIRIS, N. R. & DOLOVICH, M. B. 2003. Pulmonary drug delivery. Part II: the role of inhalant delivery devices and drug formulations in therapeutic effectiveness of aerosolized medications. *British journal of clinical pharmacology,* 56**,** 600-612.

LARHRIB, H., ZENG, X. M., MARTIN, G. P., MARRIOTT, C. & PRITCHARD, J. 1999. The use of different grades of lactose as a carrier for aerosolized salbutamol sulphate. *International Journal of Pharmaceutics,* 191**,** 1-14.

LE, V. N. P., ROBINS, E. & FLAMENT, M. P. 2012. Agglomerate behaviour of fluticasone propionate within dry powder inhaler formulations. *European Journal of Pharmaceutics and Biopharmaceutics, 80, 596-603.*

LISTIOHADI, Y., HOURIGAN, J. A., SLEIGH, R. W. & STEELE, R. J. 2009. Thermal analysis of amorphous lactose and α-lactose monohydrate. *Dairy Science & Technology,* 89**,** 43-67.

LITTRINGER, E. M., MESCHER, A., SCHROETTNER, H., ACHELIS, L., WALZEL, P. & URBANETZ, N. A. 2012. Spray dried mannitol carrier particles with tailored surface properties – The influence of carrier surface roughness and shape. *European Journal of Pharmaceutics and Biopharmaceutics,* 82**,** 194-204.

LOH, Z. H., SAMANTA, A. K. & SIA HENG, P. W. 2015. Overview of milling techniques for improving the solubility of poorly water-soluble drugs. *Asian Journal of Pharmaceutical Sciences,* 10**,** 255-274.

LOUEY, M. D., RAZIA, S. & STEWART, P. J. 2003. Influence of physico-chemical carrier properties on the in vitro aerosol deposition from interactive mixtures. *International Journal of Pharmaceutics,* 252**,** 87-98.

LOUEY, M. D. & STEWART, P. J. 2002. Particle Interactions Involved in Aerosol Dispersion of Ternary Interactive Mixtures. *Pharmaceutical Research,* 19**,** 1524-1531.

LUCAS, P., ANDERSON, K. & STANIFORTH, J. N. 1998. Protein Deposition from Dry Powder Inhalers: Fine Particle Multiplets as Performance Modifiers. *Pharmaceutical Research,* 15**,** 562-569.

MANGAL, S., MEISER, F., TAN, G., GENGENBACH, T., MORTON, D. A. V. & LARSON, I. 2016. Applying surface energy derived cohesive–adhesive balance model in predicting the mixing, flow and compaction behaviour of interactive mixtures. *European Journal of Pharmaceutics and Biopharmaceutics,* 104**,** 110-116.

MARRIOTT, C. & FRIJLINK, H. W. 2012. Lactose as a carrier for inhalation products: breathing new life into an old carrier. *Advanced Drug Delivery Reviews,* 64**,** 217-219.

MEI, R., SHANG, H., KLAUSNER, J., KALLMAN, E. J. K. P. & JOURNAL, P. 1997. A Contact Model for the Effect of Particle Coating on Improving the Flowability of Cohesive Powders. 15**,** 132-141.

NAIK, S. & CHAUDHURI, B. 2015. Quantifying Dry Milling in Pharmaceutical Processing: A Review on Experimental and Modeling Approaches. *Journal of Pharmaceutical Sciences,* 104**,** 2401-2413.

NEWELL, H. E., BUCKTON, G., BUTLER, D. A., THIELMANN, F. & WILLIAMS, D. R. 2001. The Use of Inverse Phase Gas Chromatography to Measure the Surface Energy of Crystalline, Amorphous, and Recently Milled Lactose. *Pharmaceutical Research,* 18**,** 662-666.

NOKHODCHI, A. & MARTIN, G. P. 2015. *Pulmonary Drug Delivery: Advances and Challenges*, Wiley.

NOWAK-WEGRZYN, A., SHAPIRO, G. G., BEYER, K., BARDINA, L. & SAMPSON, H. A. 2004. Contamination of dry powder inhalers for asthma with milk proteins containing lactose. *Journal of Allergy and Clinical Immunology,* 113**,** 558-560.

OHTA, M. & BUCKTON, G. 2004. Determination of the changes in surface energetics of cefditoren pivoxil as a consequence of processing induced disorder and equilibration to different relative humidities. *International Journal of Pharmaceutics,* 269**,** 81-88.

OOI, J., TRAINI, D., HOE, S., WONG, W. & YOUNG, P. M. 2011. Does carrier size matter? A fundamental study of drug aerosolization from carrier based dry powder inhalation systems. *International Journal of Pharmaceutics,* 413**,** 1-9.

PARIMALADEVI, P. & SRINIVASAN, K. 2014. Influence of supersaturation level on the morphology of α-lactose monohydrate crystals. *International Dairy Journal,* 39**,** 301-311.

PATERA, J., ZAMOSTNY, P., LITVA, D., BEROVA, Z. & BELOHLAV, Z. 2012. Evaluation of Functional Characteristics of Lactose by Inverse Gas Chromatography. *Procedia Engineering,* 42**,** 644–650.

PATERSON, A. H. J. 2017. Lactose processing: From fundamental understanding to industrial application. *International Dairy Journal,* 67**,** 80-90.

PENG, T., LIN, S., NIU, B., WANG, X., HUANG, Y., ZHANG, X., LI, G., PAN, X. & WU, C. 2016. Influence of physical properties of carrier on the performance of dry powder inhalers. *Acta Pharmaceutica Sinica B,* 6**,** 308-318.

PFEFFER, R., DAVE, R. N., WEI, D. & RAMLAKHAN, M. 2001. Synthesis of engineered particulates with tailored properties using dry particle coating. *Powder Technology,* 117**,** 40-67.

PILCER, G. & AMIGHI, K. 2010. Formulation strategy and use of excipients in pulmonary drug delivery. *International journal of pharmaceutics,* 392**,** 1-19.

PILCER, G., WAUTHOZ, N. & AMIGHI, K. 2012. Lactose characteristics and the generation of the aerosol. *Advanced Drug Delivery Reviews,* 64**,** 233-256.

PITCHAYAJITTIPONG, C., PRICE, R., SHUR, J., KAERGER, J. & EDGE, S. J. I. J. O. P. 2010. Characterisation and functionality of inhalation anhydrous lactose. 390 2**,** 134-41.

RAMLAKHAN, M., WU, C.-Y., WATANO, S., DAVE, R. & PFEFFER, R. 2000. Dry Particle Coating Using Magnetically Assisted Impaction Coating: Modification of Surface Properties and Optimization of System and Operating Parameters. *Powder Technology,* 112**,** 137-148.

RIETEMA, K. 2012. *The Dynamics of Fine Powders*, Springer Netherlands.

ROWE, R. C., SHESKEY, P. J., QUINN, M. E. & ASSOCIATION, A. P. 2009. *Handbook of Pharmaceutical Excipients*, Pharmaceutical Press.

SAHARAN, V. A., V, K., KATARIA, M., KHARB, V. & CHOUDHURY, P. 2008. Ordered Mixing: Mechanism, Process and Applications in Pharmaceutical Formulations. *Asian J. Pharm. Sci.,* 3**,** 240-259.

SANGSHETTI, J. N., DESHPANDE, M., ZAHEER, Z., SHINDE, D. B. & AROTE, R. 2017. Quality by design approach: Regulatory need. *Arabian Journal of Chemistry,* 10**,** S3412-S3425.

SATO, A., SERRIS, E., GROSSEAU, P., THOMAS, G., CHAMAYOU, A., GALET, L. & BARON, M. 2012. Effect of operating conditions on dry particle coating in a high shear mixer. *Powder Technology,* 229**,** 97-103.

SATO, A., SERRIS, E., GROSSEAU, P., THOMAS, G., GALET, L., CHAMAYOU, A. & BARON, M. 2013. Experiment and simulation of dry particle coating. *Chemical Engineering Science,* 86**,** 164-172.

SHALASH, A. O., MOLOKHIA, A. M. & ELSAYED, M. M. A. 2015. Insights into the roles of carrier microstructure in adhesive/carrier-based dry powder inhalation mixtures: Carrier porosity and fine particle content. *European Journal of Pharmaceutics and Biopharmaceutics,* 96**,** 291-303.

SHUR, J., HARRIS, H., JONES, M. D., KAERGER, J. S. & PRICE, R. 2008. The Role of Fines in the Modification of the Fluidization and Dispersion Mechanism Within Dry Powder Inhaler Formulations. *Pharmaceutical Research,* 25**,** 1631-1640.

SHUR, J., PRICE, R., LEWIS, D., YOUNG, P. M., WOOLLAM, G., SINGH, D. & EDGE, S. 2016. From single excipients to dual excipient platforms in dry powder inhaler products. *International Journal of Pharmaceutics,* 514**,** 374-383.

SINGH, R. K., ATA, A., FITZ-GERALD, J., RABINOVICH, Y. & HENDRICKSON, W. 1997. Dry Coating Method Using Magnetically Assisted Impaction in a Randomly Turbulent Fluidized Bed. *KONA Powder and Particle Journal,* 15**,** 121-131.

SOU, T. & BERGSTRÖM, C. A. S. 2021. Contemporary Formulation Development for Inhaled Pharmaceuticals. *Journal of Pharmaceutical Sciences,* 110**,** 66-86.

Staniforth, J. N. (1997) Improvement in dry powder inhaler performance:surface passivation effects. *Proc*. *Drug Deliv*. *Lung* 8:85- 86.

STECKEL, H., MARKEFKA, P., TEWIERIK, H. & KAMMELAR, R. 2004. Functionality testing of inhalation grade lactose. *European Journal of Pharmaceutics and Biopharmaceutics,* 57**,** 495-505.

STECKEL, H. & MÜLLER, B. J. I. J. O. P. 1997. In vitro evaluation of dry powder inhalers I: drug deposition of commonly used devices. 154**,** 19-29.

Surface Measurement Systems Ltd. 2013. An overview of iGC SEA – A new Instrumental Technique for Characterising the Phyisco-chemical Properties of Pharmaceutical Materials: iGC SEA Application Note 301. Available online: https://www.surfacemeasurementsystems.com/downloads/seaapplication-notes/ (accessed on 01-02-2022).

TICEHURST, M. D., YORK, P., ROWE, R. C. & DWIVEDI, S. K. 1996. Characterisation of the surface properties of α-lactose monohydrate with inverse gas chromatography, used to detect batch variation. *International Journal of Pharmaceutics,* 141**,** 93-99.

TRAINI, D., ROGUEDA, P., YOUNG, P. & PRICE, R. 2005. Surface Energy and Interparticle Force Correlation in Model pMDI Formulations. *Pharmaceutical research,* 22**,** 816-25.

TRAINI, D., YOUNG, P. M., THIELMANN, F. & ACHARYA, M. 2008. The Influence of Lactose Pseudopolymorphic Form on Salbutamol Sulfate–Lactose Interactions in DPI Formulations. *Drug Development and Industrial Pharmacy,* 34**,** 992-1001.

TRAINI, D., SCALIA, S., ADI, H., MARANGONI, E. & YOUNG, P. M. 2012. Polymer coating of carrier excipients modify aerosol performance of adhered drugs used in dry powder inhalation therapy. *International Journal of Pharmaceutics,* 438**,** 150-159.

Visser, J. (1995) Particle Adhesion and Removal: A Review, *Particulate Science and Technology*, 13:3-4,169-196, DOI: 10.1080/02726359508906677

WANG, Y., KOYNOV, S., GLASSER, B. & MUZZIO, F. 2016. A method to analyze shear cell data of powders measured under different initial consolidation stresses. *Powder Technology,* 294.

WEERS, J. & MILLER, D. 2015. Formulation Design of Dry Powders for Inhalation. *Journal of pharmaceutical sciences,* 104.

WEERS, J. & CLARK, A. 2017. The Impact of Inspiratory Flow Rate on Drug Delivery to the Lungs with Dry Powder Inhalers. *Pharmaceutical Research,* 34**,** 507-528.

WEI, D., DAVE, R. & PFEFFER, R. 2002. Mixing and Characterization of Nanosized Powders: An Assessment of Different Techniques. *Journal of Nanoparticle Research,* 4**,** 21-41.

WILLIAMS, D. R. 2015. Particle engineering in pharmaceutical solids processing: surface energy considerations. *Current pharmaceutical design,* 21**,** 2677-2694.

XU, Z., MANSOUR, H. M., MULDER, T., MCLEAN, R., LANGRIDGE, J. & HICKEY, A. J. 2010. Heterogeneous Particle Deaggregation and Its Implication for Therapeutic Aerosol Performance. *Journal of Pharmaceutical Sciences,* 99**,** 3442-3461.

YANG, J., SLIVA, A., BANERJEE, A., DAVE, R. N. & PFEFFER, R. 2005. Dry particle coating for improving the flowability of cohesive powders. *Powder Technology,* 158**,** 21-33.

YANG, M. Y., CHAN, J. G. Y. & CHAN, H.-K. 2014. Pulmonary drug delivery by powder aerosols. *Journal of Controlled Release,* 193**,** 228-240.

YOKOYAMA, T., URAYAMA, K., NAITO, M., KATO, M. & YOKOYAMA, T. 1987. The Angmill Mechanofusion System and its Applications. *KONA Powder and Particle Journal,* 5**,** 59-68.

YOUNG, P. M., COCCONI, D., COLOMBO, P., BETTINI, R., PRICE, R., STEELE, D. F. & TOBYN, M. J. 2010. Characterization of a surface modified dry powder inhalation carrier prepared by “particle smoothing”. *Journal of Pharmacy and Pharmacology,* 54**,** 1339-1344.

ZENG, X., MARTIN, G. & MARRIOTT, C. 2000. *Particulate Interactions in Dry Powder Formulation for Inhalation*.

ZENG, X. M., MARTIN, G. P., TEE, S.-K., GHOUSH, A. A. & MARRIOTT, C. 1999. Effects of particle size and adding sequence of fine lactose on the deposition of salbutamol sulphate from a dry powder formulation. *International Journal of Pharmaceutics,* 182**,** 133-144.

ZENG, X. M., MARTIN, G. P., TEE, S.-K. & MARRIOTT, C. 1998. The role of fine particle lactose on the dispersion and deaggregation of salbutamol sulphate in an air stream in vitro. *International Journal of Pharmaceutics,* 176**,** 99-110.

ZHANG, J., EBBENS, S., CHEN, X., JIN, Z., LUK, S., MADDEN, C., PATEL, N. & ROBERTS, C. 2006. Determination of the Surface Free Energy of Crystalline and Amorphous Lactose by Atomic Force Microscopy Adhesion Measurement. *Pharmaceutical research,* 23**,** 401-7.

ZHENG, J. 2009. *Formulation and Analytical Development for Low-Dose Oral Drug Products*, Wiley.

ZHOU, Q. & MORTON, D. A. V. 2012. Drug–lactose binding aspects in adhesive mixtures: Controlling performance in dry powder inhaler formulations by altering lactose carrier surfaces. *Advanced Drug Delivery Reviews,* 64**,** 275-284.

ZHOU, Q., QU, L., GENGENBACH, T., DENMAN, J. A., LARSON, I., STEWART, P. J. & MORTON, D. A. V. 2011. Investigation of the extent of surface coating via mechanofusion with varying additive levels and the influences on bulk powder flow properties. *International Journal of Pharmaceutics,* 413**,** 36-43.

ZHOU, Q. T., ARMSTRONG, B., LARSON, I., STEWART, P. J. & MORTON, D. A. V. 2010a. Understanding the influence of powder flowability, fluidization and de-agglomeration characteristics on the aerosolization of pharmaceutical model powders. *European Journal of Pharmaceutical Sciences,* 40**,** 412-421.

ZHOU, Q. T., QU, L., LARSON, I., STEWART, P. J. & MORTON, D. A. V. 2010b. Improving aerosolization of drug powders by reducing powder intrinsic cohesion via a mechanical dry coating approach. *International Journal of Pharmaceutics,* 394**,** 50-59.